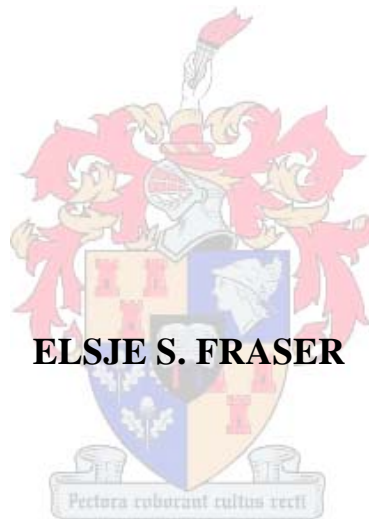# COMPUTATIONAL MODELLING OF CONCRETE FOOTING ROTATIONAL RIGIDITY

by

ELSJE S. FRASER

THESIS PRESENTED IN PARTIAL FULFILMENT OF THE
REQUIREMENTS FOR THE DEGREE OF MASTER OF SCIENCE OF
ENGINEERING AT THE UNIVERSITY OF STELLENBOSCH

STUDY LEADER

PROF G.P.A.G. VAN ZIJL

DECLARATION

By submitting this thesis electronically, I declare that the entirety of the work contained therein is my own, original work, that I am the owner of the copyright thereof (unless to the extent explicitly stated) and that I have previously in its entirety or in part submitted it for obtaining any qualification.

SIGNED: ……………………….

DATE: ……………………….

SYNOPSIS

In many buildings we rely on large footings to offer structural stability by preventing failure deformation patterns. This is particularly evident in industrial buildings where large open spans and little lateral support are a regular occurrence. Designers often compensate for the lack of knowledge available with regard to foundation-soil interaction by furnishing structures with overly large footings. This may lead to a significant increase in building costs if many large foundations are present. Also, in absence of an objective modelling and computational method, errors may be made, leading to instability of such structures.

This study chronicles the interface material law that governs the behaviour along the contact surface of adjacent materials and the behaviour of large foundations under ultimate limit loading.

Various approaches to defining the material law along the concrete-soil interface are investigated. Their differences and similarities are discussed and illustrated using both simple single element tests and by applying each interface model type to the finite element model defining the case study.

A case study is chosen that represents a common foundation-soil system frequently used in general practice and therefore relevant to other structures. Two contrary structures are investigated; a structure subjected to vertical downward wind forces which compound the gravity actions on the structure (termed the *heavy structure* in this document) and a structure subjected to uplifting wind forces alleviating the gravity action on the structure (termed the *light structure* in this document). Further investigations include alterations to the foundation size and subgrade compositions, the role of the slab stiffness and presence and the effect of commonly used structural joints and connections.

Modelling strategies are developed to represent a complex three-dimensional model by means of a considerably simpler and more economical two-dimensional model. In the final chapter the use of two-dimensional linear springs in place of the soil mass is investigated in an attempt to predict certain foundation behaviour by means of the simplest finite element model possible using software available in most engineering offices. Hereby a simple, but reasonably accurate analysis and design method is developed and verified in this study, equipping the practicing engineer with computational tools for design of such foundation systems.

Elsje S. Fraser   University of Stellenbosch

OPSOMMING

In baie geboue maak ons staat op groot fondamente om strukturele stabiliteit te lewer deur falings deformasiepatrone te voorkom. Dit kom veral voor in industriële geboue waar groot oop ruimtes en min laterale ondersteuning op 'n gereelde basis voorkom. Ontwerpers kompenseer vir die tekort aan beskikbare kennis met betrekking tot fondasie-grond wisselwerking (interaksie) deur strukture met oormatige groot fondament afmetings voor te skryf. Dit mag lei tot 'n merkwaardige toename in bou koste as baie groot fondasies teenwoordig is. Aan die ander kant kan, in afwesigheid van objektiewe modellerings- en berekeningsmetodes, foute begaan word wat tot onstabiliteit van hierdie soort strukture kan lei.

Hierdie studie boekstaaf die koppelvlak materiaalwet wat die gedrag langs die kontak oppervlak van aangrensende materiale beheer, en die gedrag van 'n groot fondasie onder swiglaste.

Verskeie benaderings om die materiaalwet langs die beton-grond koppelvlak te definieer is ondersoek. Hul verskille en ooreenkomste word bespreek en ge-illustreer deur gebruik te maak van beide eenvoudige enkelelement toetse en deur die koppelvlak tipe op die eindige element model wat in die gevalle studie definieer word, aan te wend.

'n Gevalle-studie is gekies wat 'n algemene fondasie-grond sisteem verteenwoordig en gereeld van gebruik gemaak word in die algemene praktyk en daarom toepaslik is op ander strukture. Twee strukture met teenoorgestelde laspatrone is ondersoek; 'n struktuur onderhewig aan vertikaal afwaartse windlaste, wat saam met die gravitasie aksie inwerk ('n *swaar struktuur* genoem in hierdie dokument) en 'n struktuur waar die vertikale windlaste opwaarts inwerk en die gravitasie aksie verlig ('n *lig struktuur* genoem in hierdie dokument). Verdere ondersoeke sluit in veranderinge aan die fondasie grootte en onderligende grondmateriaal se samestellings, die rol van die vloerstyfheid en die teenwoordigheid en uitwerking van algemene strukturele uitsettingsvoë en aansluitings.

Modelering stategiëe is ontwikkel om 'n komplekse drie-dimensionele model met 'n aansienlik eenvoudiger en meer ekonomiese twee-dimensionele model te verteenwoordig. In die finale hoofstuk word die gebruik van twee-dimensionele lineêre vere ondersoek om die grond massas voor te stel. Dit word gedoen in 'n poging om sekere fondasie gedrag te voorspel deur die gebruik van die eenvoudigste moontlike eindige element model wat met sagteware wat in meeste

ingeneurs kantore beskikbaar is, geanaliseer kan word. Hierdeur word 'n eenvoudige, maar redelik akkurate analise- en ontwerpmetode ontwikkel en geverifieer in hierdie studie, wat berekeningsgereedskap vir die ontwerp van sulke fondasie sisteme bied aan die praktiserende ingenieur.

ACKNOWLEDGEMENTS

TABLE OF CONTENTS

LIST OF FIGURES

LIST OF TABLES

1.   INTRODUCTION

Structural characteristics of concrete column-foundation systems embedded in compacted soils or gravels and various subgrades, and the interaction between them, such as load distribution characteristics, inelastic response, and ultimate strength; cannot be calculated realistically with simple procedures currently used in design and evaluation. Experimental tests are at times time consuming and expensive, depending on the number of specimens and parameters required for an investigation. If properly conducted, comprehensive numerical studies can provide reliable estimates of response of such structures, eliminating the necessity for extensive physical experimental tests for these systems. Nonlinear finite element analysis is thus used in this study to predict and detail the behaviour of large foundations under loading and the interaction with its soil surroundings.

1.1   Background

In order to create a study that has relevance to its field of practice, the design of an aluminium foil finishing plant received from Mr Gerrit Bastiaanse of BKS (Rosochacki, 2007) was used to determine initial geometrical dimensions, loading and soil structure of a typical industrial building. The writer undertook investigations of this specific light structure which experiences uplifting wind loads and that of a geometrically identical heavy structure under the application of compressing loads. This is done in order to broaden the relevance of the study to foundations experiencing different failure conditions. Uplifting forces could cause the "popping out" of a foundation while the same foundation under compressive forces could cause failure of the subgrade materials by exceeding its bearing capacity. In both cases failure could be as result of slip lines forming in the subgrade due to moments causing rotation. It would therefore be more inclusive to consider both structures in a study concerning foundation design.

1.1.1   Case Study

Typical of the requirements of an industrial structure, the foil finishing plant has large open spaces and large spans between slender reinforced concrete columns. There are thirteen spans of six metres, giving a structure footprint of eighty by one hundred metres. To provide for

Elsje S. Fraser   University of Stellenbosch

unrestricted movement of overhead cranes along the lengths of the building, every second span is supported by outer columns alone, allowing for more floor space (see figure 1.1). The section of roof between every other supported span is carried by universal beam rafters.
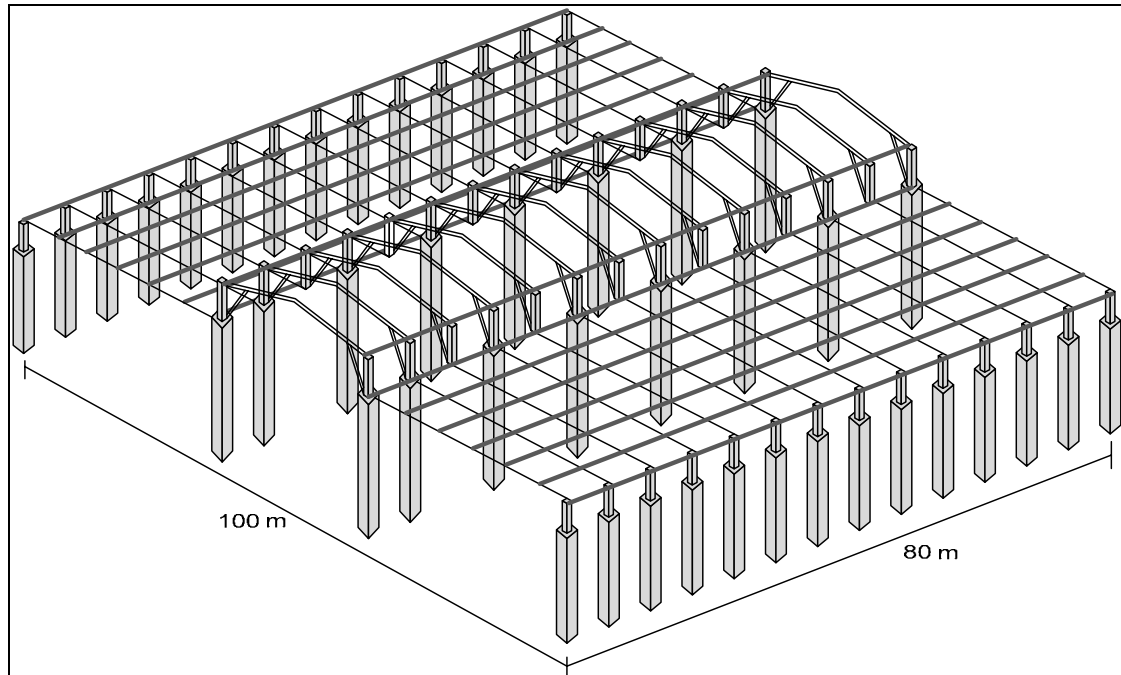
Figure 1.1: Floor layout of foil finishing plant.

The roof is supported by light steel truss frames that are connected to the concrete columns via UB rafters. The large distance between the slender columns requires an alternative to lateral bracing members to withstand typical loading on this structure. This bracing is provided in the form of large column foundations able to resist bending moments and toppling forces from wind loads (see figure 1.2). In the design of this structure it is assumed that the structure is fixed to these large foundations. If they are unable to withstand their ultimate limit state in a worse case scenario, the entire structure will fail.
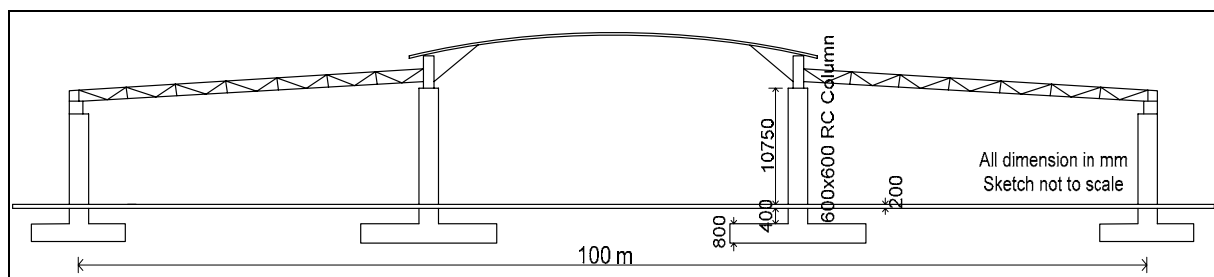
Figure 1.2: The layout of the span of the foil finishing plant.

This particular case is an example of a commonly used structure and allows the investigation to be relevant to similar industrial buildings. By considering a representative column-foundation system allows for the easy adaptation of a finite element model to new dimensions, loads and material parameters.

Elsje S. Fraser   University of Stellenbosch

1.1.2   The Light Structure

Worst case scenarios are assumed in determining the loads on the structure. This scenario occurs when openings are present at the windward side of the structure while the rest of the structure is effectively sealed. The light structure experiences uplifting forces under the application of the wind load. Values are rounded to the nearest fifty and are given in table 1.1. The dead load given is weight of the structure above and includes the self weight of the column. The weight of the foundation is not included as the foundation dimensions will vary in later investigations and is therefore added separately. Global axes and directions are given in figure 1.3.

Table 1.1: Ultimate limit loads on the light structure.

	V(x) (kN)	F(y) (kN)	M(z) (kNm)
Deadload	0	-500	0
Windload	200	850	500
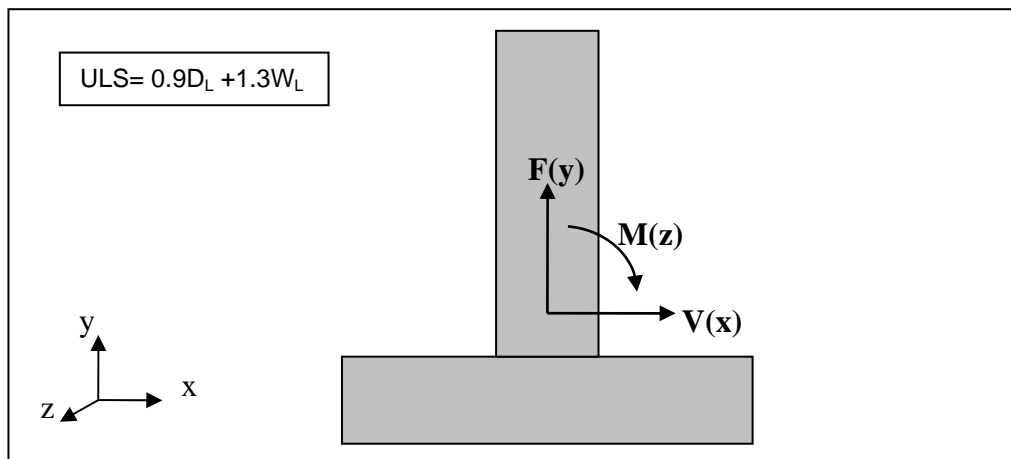
Figure 1.3: The layout of ultimate limit state column reaction forces and moments.

1.1.3   The Heavy Structure

As for the light structure, the worst case scenario is considered in determining the loading (see table 1.2). The difference between the heavy and light structures is the size of the dead load and the direction of the wind load. A heavier structure naturally has a high amount of self weight. The wind load is found for a situation of an impermeable structure in a part of the building experiencing downward pressures. The values are chosen to have a size that makes behaviour of the structure comparable to that of the lighter version. To generalise the loading conditions, the given sets of load cases are varied proportionally in later investigations in this thesis in order to study the behaviour at a range of loads.

Table 1.2: Ultimate limit loads on the heavy structure.

	V(x) (kN)	F(y) (kN)	M(z) (kNm)
Deadload	0	-1000	0
Windload	200	-850	500

1.2   Scope and Limitations of this Study

This study investigates a foundation-soil system typically found in industrial buildings with slender columns and large open spans. The study broadens its scope to include foundations under uplifting and compressing wind forces. It explores the impact of varying subgrade materials covering a range of high to low stiffness types. The foundation size is increased and decreased, the grade of concrete used for the slab is lowered and the effect of commonly used movement joints and a joint filler material is considered.

Settlement of a foundation is a primary threat to structural instability. This is however not the focal point of this study, which rather studies instant rotational rigidity due to wind loads.

Three typical failure possibilities are not included in this study and are considered the responsibility of the design engineer to provide for these possible failure patterns. The first requirement of the designer is to be sure that the self weight of the structure and foundation is larger than an uplifting wind load. The foundation should therefore be sufficiently heavy to prevent itself from separating from the subgrade directly beneath it. The point of uplift under increasing load increments will be indicated by the delamination of the interface elements along the base of the foundation. The designer should therefore not rely on the slab to offer any resistance against overall foundation uplift as this event will in this study represent a failure mode (see figure 1.4).
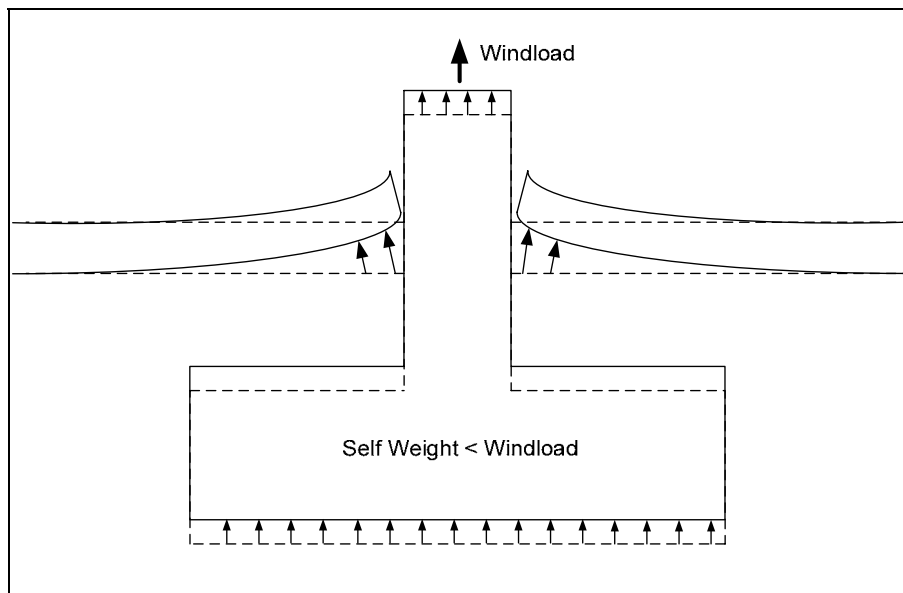
Figure 1.4: Uplifting of foundation causing failure of the structure.

A second condition the designer needs to take into account prior to considering the outcomes of this study is to verify the overturning stability of the foundation (see figure 1.5). The foundation needs to be deep enough and have a width capable of withstanding overturning forces and moments.
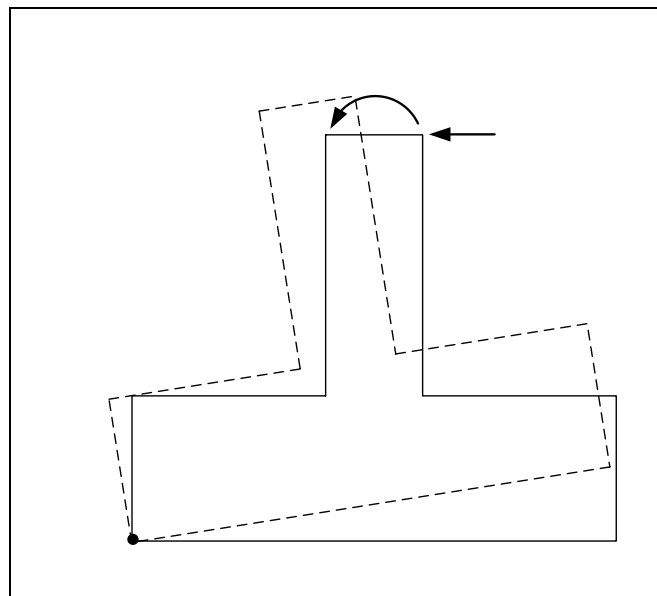
Figure 1.5: Inefficient overturning stability of the foundation causing failure.

A third a final failure criterion the designer needs to account for is the cracking of the column or foundation (see figure 1.6). These cracks would cause a hinge effect and has the potential of greatly increasing displacements and rotations and may overshadow the outcomes of this study. It is therefore assumed in all investigations in this study that column will not tear off from the foundation under large moments or that the foundation will split under the same loading.
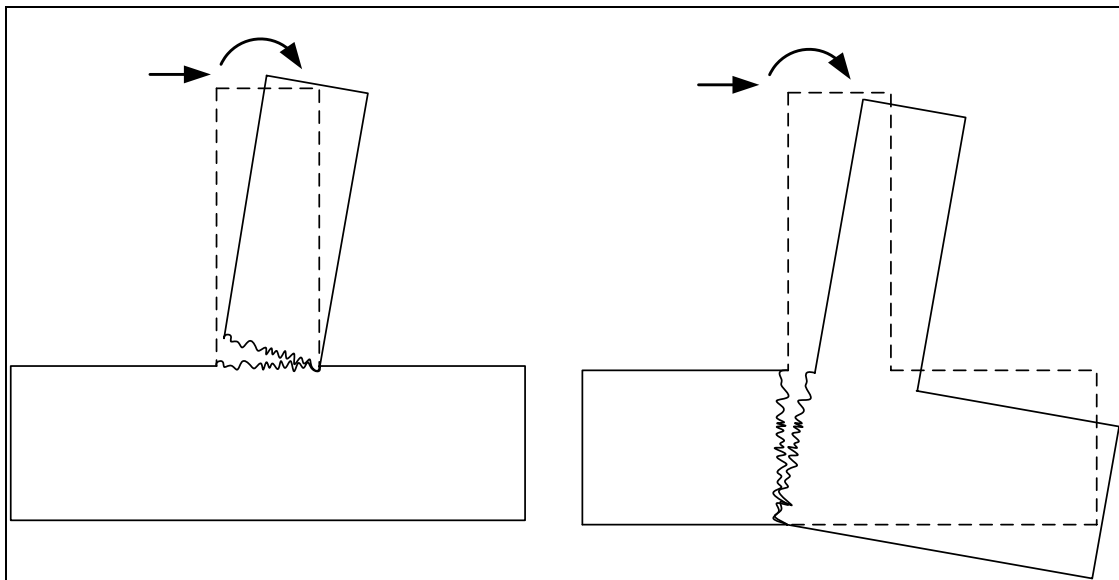
Figure 1.6: Cracking of foundation or column causing severe displacements and rotations.

1.3   Objectives of this Study

The overall objective of this investigation is to gain a better understanding of the behaviour of fixed concrete foundations and their interaction with their surrounding material under various realistic and critical loading situations. Finite element modelling strategies are to be developed that can be used in engineering practices when applied to similar cases. Alterations to the various models studied are done in a specific manner to clearly see changes in foundation behaviour and in order to compare the various modelling techniques. Specific focus is placed on calculating the rotation of foundations in all of the models investigated. This interest is due to the potential failure caused by lateral displacement at the top of the column resulting from a tilting action of the foundation when rotating. Combined with compressive axial loads, increased moments can be experienced within the column and thus the foundation. This can in turn result in overturning moments causing an even more severe case of overturning of the column, leading to failure.

Finite element strategies include the development of a conversion method for simplifying a three-dimensional model into an accurate two-dimensional model. Once this method has been established and proven, a feasible spring model is developed in which the soil action is represented by nonlinear and later by linear springs. The aim is to given the designer a simple and inexpensive yet reliable method to model foundations using common design software available in most design offices. The rotations of the foundation will be used as a criterion in determining the accuracy of simplified finite element models.

Elsje S. Fraser   University of Stellenbosch

Conclusions are drawn about the findings of the various analyses regarding the behaviour of the structure and recommendations are made for the use of the finite element modelling strategies.

1.4   Method of Investigation

Nonlinear finite element models are evaluated and subsequently used to examine the structural behaviour of a foundation under loading and to create interfacial bond elements that depict the interaction of the foundation with its surrounding materials. A sensitivity study is performed varying foundation geometry, loading, strength of concrete, and stiffness of the subgrades to establish a pattern of behaviour applicable to a broad range of foundation types. The contact problem between a concrete foundation and soil is approached by means of a DIANA interface model with multi-surface plasticity (DIANA, 2008). The foundation-soil interface has a very low tensile bond/adhesive strength and high compressive strengths. The model has the capability to simulate these phenomena and is also capable of simulating gradual reduction in resistance, or softening, after the maximum bond strength has been exceeded. Furthermore the model also takes into account friction forces which arise on the contact surface between soil and concrete.

Nonlinear analyses of an embedded concrete foundation, based on a finite element model capable of simulating evolving behaviour of the foundation and soil, as well as the evaluation of ultimate limit state loads, are proposed.

2. THE FINITE ELEMENT MODEL

As physical experiments fall beyond the scope of the thesis, it is decided in this study to create a three-dimensional model of the structure to be used as a reference for a simplified two-dimensional model. This is because the three-dimensional model is considered to be a more holistic representation of the structure and will therefore more accurately represent its behaviour. The reason for the differing level of accuracy of the models will be discussed in chapter four.

The surface between the concrete of the foundation and column, and the soil with which it comes into contact, is of particular interest. The specific characteristics of this surface will determine the response of the structure to any and all forms of loading. An interface element is assembled to capture the behaviour of this boundary. Interface elements are also placed along the contact surface between the slab and column and the option is kept to alternate the material properties between that of the interface element or the 40 MPa concrete, as illustrated in figure 2.1. No interface elements are positioned between the contact surface of the slab and soil. This is done to simplify the model and thus reduce analysis time as fewer complex nonlinear interface elements will lead to more rapid convergence of load increments applied to the model. This design is considered to be acceptably representative of the column-foundation system as the focal point of this study lies with the displacements and rotations of the foundation and column. For the uplift and separation of the slab from the soil to occur, foundation displacements will be of the nature to cause serious concern and will receive urgent interest, leaving the slab comparatively overlooked due to its less severe qualities. A layer of interface elements surrounding the foundation and column are therefore sufficient for the purposes of this study and elements between the slab and soil deemed unnecessary.

The possibility of a crack forming in the foundation starting at the corner between the column and foundation, causing a hinge-effect, is not considered. It was decided that it would be the responsibility of the designing engineer to provide sufficient steel reinforcement to accommodate this phenomenon as this is a typical consideration made by the designer and this study does not make provision for miscalculations made the engineer. Rather, the purpose of this study is to investigate the intricate interaction between the foundation and the soil as to present the design engineer with information and guidelines how to establish the foundation

rotation with reasonable accuracy. It is then the responsibility of the designer to superimpose the column deflection.
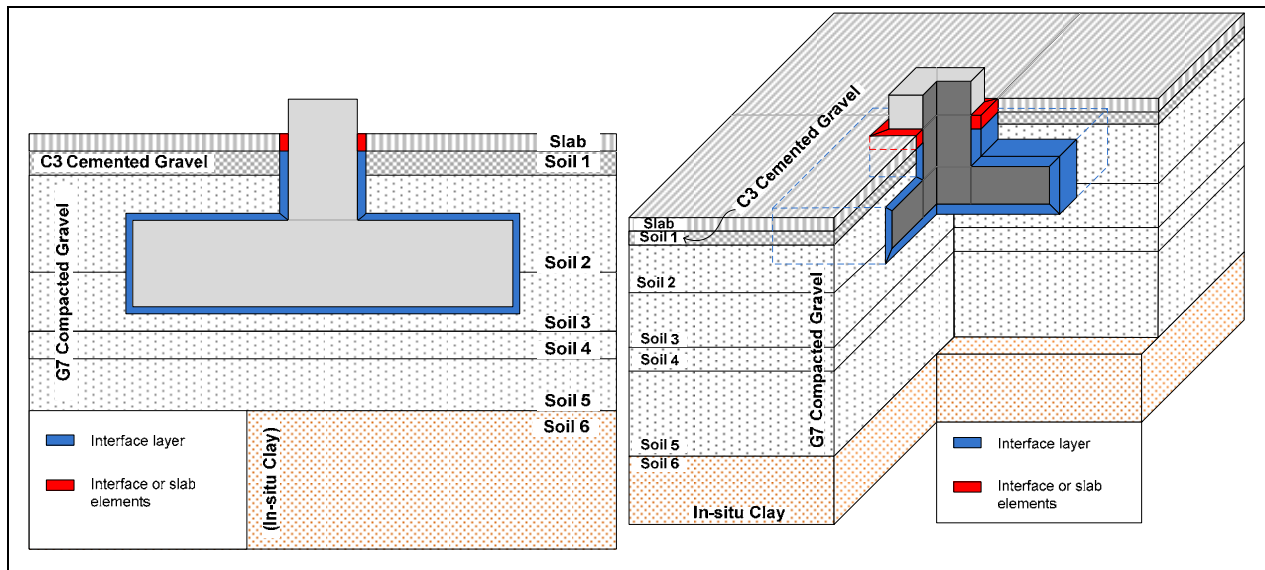
Figure 2.1: The column, foundation, soil and interface surface for the 2D and 3D models.

2.1 Dimensions

A particular structural design is taken as the starting point for the study, in order to use relevant geometrical sizes and loading conditions. Subsequently, parameter studies include variation of foundation size and load size to derive a generic approach to modelling the foundation-soil interaction. The dimensions of the reference column, foundation and subgrades are obtained from drawings provided by Mr Gerrit Bastiaanse of BKS (Rosochacki, 2007). The challenge however is in determining the outer boundaries of the model; that is, it had to be decided how far around and below the foundation the soil would react against pressures from the structure. It has to be ensured that the foundation behaviour is not subjected to boundary conditions in an unrealistic way. These boundaries depend on several material properties of the soil and the dimensions of the foundation. This entails the bearing capacity of the soil and the type of failure most probable to the type of soil at hand. A brief elucidation of the topic follows in the next section.

2.1.1 Ultimate Bearing Capacity

The ultimate bearing capacity q_f is defined as the pressure that would cause shear failure of the supporting soil directly beneath and adjacent to a foundation. In addition to the properties

of the soil, both the settlement and the resistance to shear failure depend on the shape and size of the foundation and its depth below the surface. There are three modes of failure, namely: local shear failure, punching shear failure, and general shear failure. In general the failure mode depends on the compressibility of the soil and the depth of the foundation relative to its breadth. In the case of general shear failure, continuous failure surfaces develop between the edges of the ground surface and the footing, as can be seen in figure 2.2:
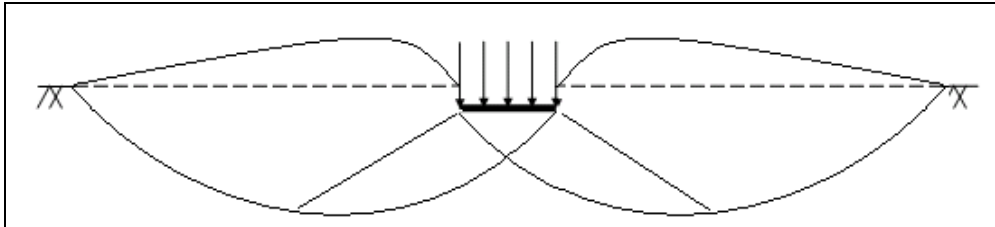
Figure 2.2: General shear failure.

As the pressure increases towards the value q_f the state of equilibrium is initially reached in the soil around the edges of the footing and gradually spreads downwards and out away from the foundation structure. Heaving of the earth surface occurs on both sides of the foundation even though final slip movement will occur only on one side, and is accompanied by tilting of the footing. This mode of failure is typical of soils of low compressibility, i.e. dense or stiff soils such as sand or compacted gravel. A suitable failure mechanism for a strip footing is shown in figure 2.3.
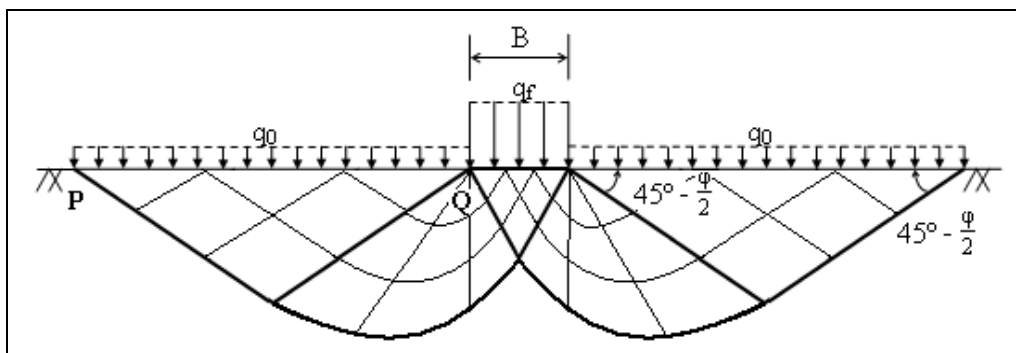
Figure 2.3: Typical patterns of slip-lines in the soil beneath a foundation.

The distance from points P to Q for a known frictional angle φ' of the soil and for a foundation breadth B, can be calculated as follows:

$$PQ = B \exp[\frac{\pi}{2}\tan\varphi]\tan(\pi/4 + \varphi/2) \qquad\qquad 2.1$$

For a known breadth B, a depth beyond which no further exertions upon the soil are present, can also be found as shown in figure 2.4 below.
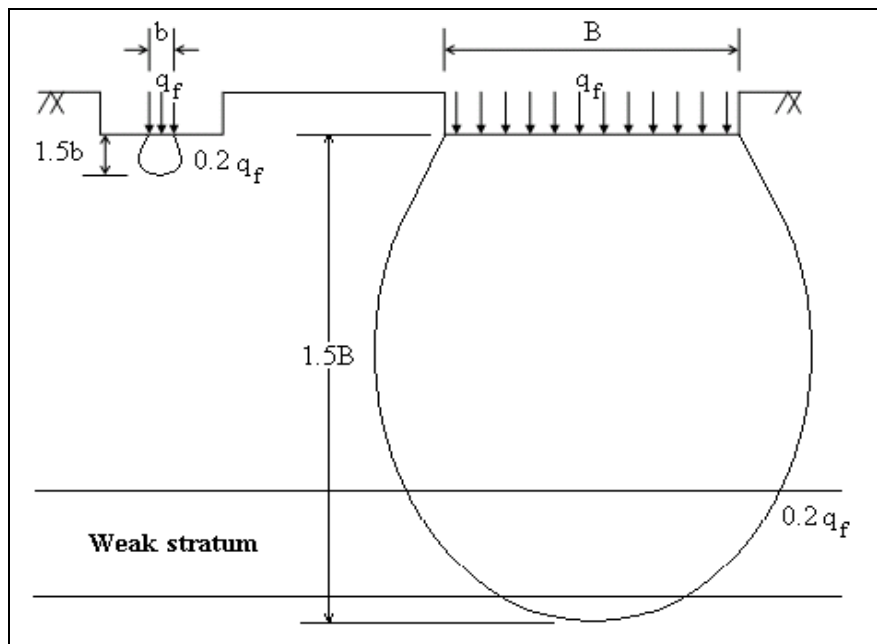
Figure 2.4: Typical patterns of stress distribution in the soil beneath a foundation (Craig).

The geometrical soil boundaries for the numerical investigation of any foundation can therefore be determined for a known foundation breadth and angle of shear resistance.

2.1.2   Conclusion on Model Dimensions Adopted

For a known foundation breadth and angle of shearing resistance, a perimeter can be calculated that forms the boundary of soil affected by the deformations and displacements of the column-foundation system. The dimensions that follow this particular system are shown in figure 2.5 below. These dimensions apply to the three-dimensional model in both width and depth. The material properties used to determine these dimensions are provided in a section to follow. Later investigations in chapter four will confirm that the bearing capacities of the subgrade materials are not exceeded and that the model dimensions used are sufficient for the purpose of this study. The layer of interface elements modelled along the contact surface between the column-foundation system and the soil is 1 mm thick. Ideally the interface element would be infinitely thin as it represents only a surface of contact, thus a plane of elements. This is however not possible to model and a compromise of an insignificantly thin element, compared to other dimensions in the model, is made instead. The contact surface between the column and slab is also 1 mm thick. Note that in a parameter study, the latter interface size is varied, to consider the influence of a larger joint.
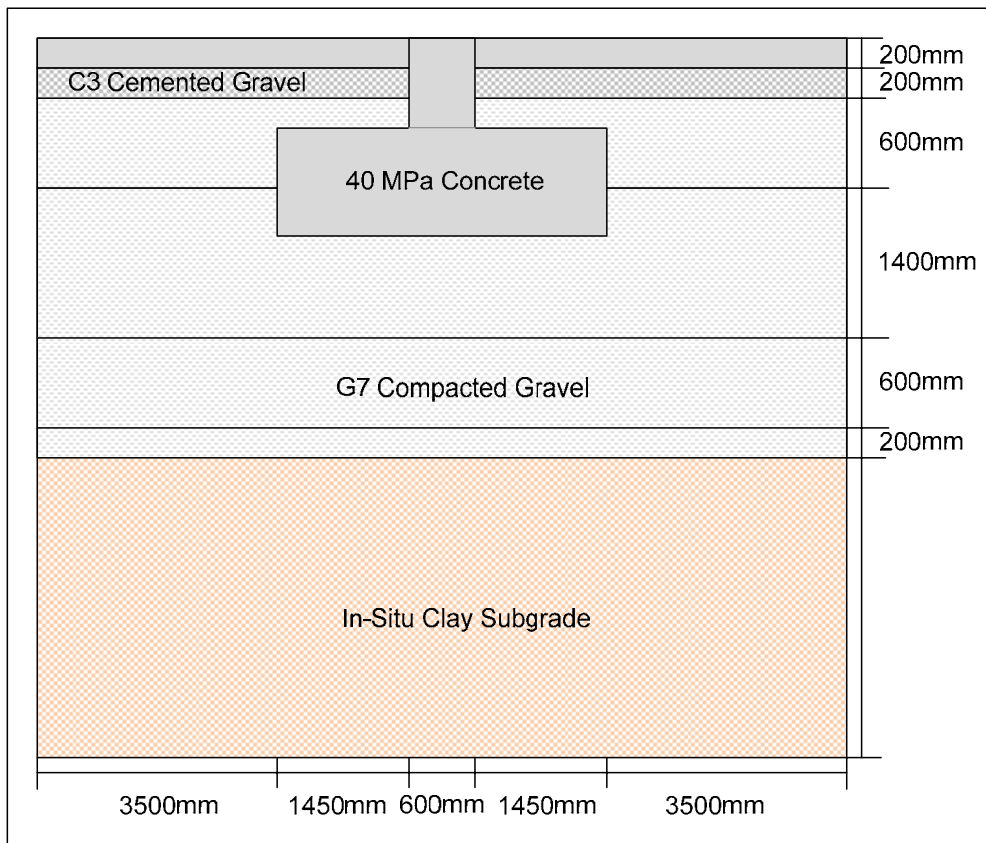
Figure 2.5: The geometrical dimensions of the Finite Element model.

2.2 Model Elements

All concrete and soil materials in the structure are modelled with isoparametric continuum elements for both two- and three-dimensional investigations. The boundary where these materials meet is modelled with structural interface elements. The geometrical configuration of all elements used is discussed in this section. The nonlinear material behaviour of the interface, which is key to this study, is discussed in detail in the following chapter.

2.2.1 Interface Elements

A structural interface element with basic variables being the nodal displacements Δu_e, and derived values the relative displacements Δu, and tractions t, is needed for the purpose of this study. The structural interface element describes a relation between t and Δu across the boundary of adjacent materials. The actual set of variables will depend on the particular dimensions of the interface element resulting from the mesh density of the models. Interface elements with the qualities prescribed are available in the element library of DIANA (Diana,

2008) and were used to construct the finite element models. DIANA allows the option to output the computed values (displacement and tractions) in the integration points. Both elements used are based on linear interpolation and a two-point Lobatto integration scheme was used. For the two-dimensional model, L8IF interface elements were used along the contact surfaces between concrete and soil while Q24IF elements served the same purpose in the three-dimensional analysis.

In the two-dimensional model the structural interface element is of the configuration of a two-by-two line between two lines, that is, the interface element is aligned between neighboring four noded elements. The local xy axes for the displacements are evaluated in the first node with x from node 1 to node 2. The configuration of the DIANA L8IF element, the element used in this case, is shown in see figure 2.6.
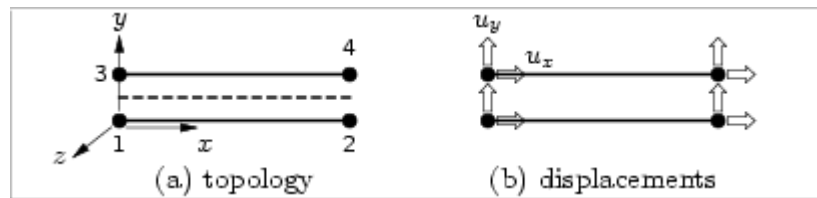
Figure 2.6: A L8IF element from the DIANA Element Library (Diana, 2008).

Variables are oriented in the xy axes and can be briefly described as follows:

$$\boldsymbol{u}_e = \begin{Bmatrix} u_x \\ u_y \end{Bmatrix}, \quad \Delta\boldsymbol{u} = \begin{Bmatrix} \Delta u_x \\ \Delta u_y \end{Bmatrix}, \quad \boldsymbol{t} = \begin{Bmatrix} t_x \\ t_y \end{Bmatrix} \qquad 2.2$$

The normal traction t_y of the required element is normal to the interface and the shear traction t_x tangential to the interface, as illustrated in figure 2.7.
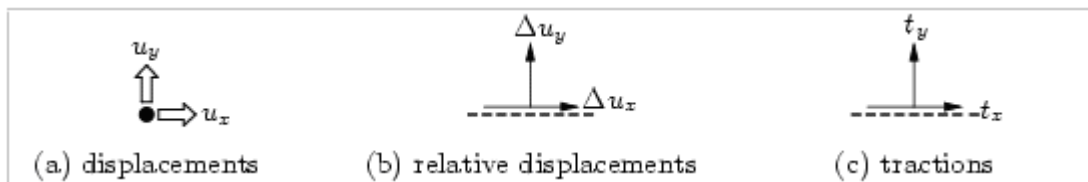
Figure 2.7: Variables of two-dimensional structural interfaces (following Diana, 2008).

In the three-dimensional model the structural interface element is of the configuration of a four-by-four quadrilateral plane between two planes, that is, the interface element is aligned between neighboring eight noded elements. The local xyz axes for the displacements are evaluated in the first node with x from node 1 to node 2 and z perpendicular to the plane. The configuration of the DIANA Q24IF element, the element used in this case, is shown in figure 2.8.
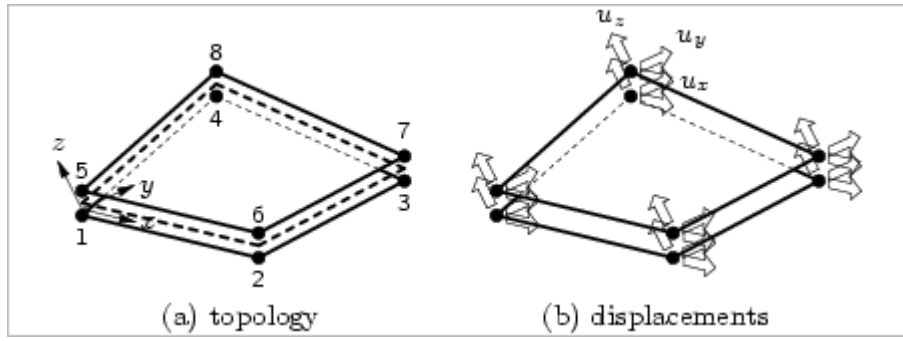
Figure 2.8: A Q24IF element from the DIANA Element Library (Diana, 2008).

Variables are oriented in the local *xyz* axes and are, in brief, defined as follows:

$$\boldsymbol{u}_e = \begin{Bmatrix} u_x \\ u_y \\ u_z \end{Bmatrix}, \quad \Delta\boldsymbol{u} = \begin{Bmatrix} \Delta u_x \\ \Delta u_y \\ \Delta u_z \end{Bmatrix}, \quad \boldsymbol{t} = \begin{Bmatrix} t_x \\ t_y \\ t_z \end{Bmatrix} \qquad 2.3$$

The normal traction t_x of the required element is perpendicular to the interface and the shear tractions t_y and t_z are tangential to the interface, as illustrated in figure 2.9.
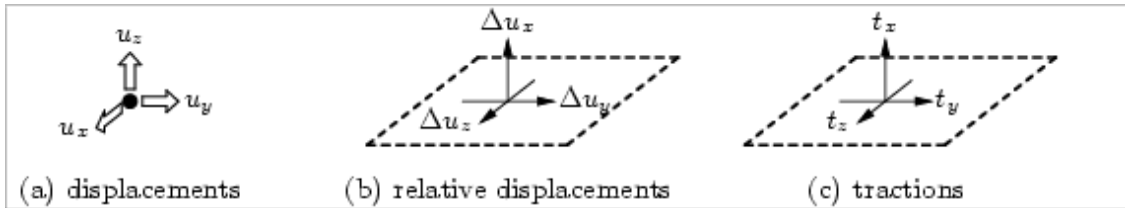
Figure 2.9: Variables of three-dimensional structural interfaces (Diana, 2008).

2.2.2   Continuum Elements

For the purpose of this study an isoparametric element, with translation its basic variable, is sufficient to model all concrete and subgrade materials. The derived variables of the translations are Green-Lagrange strains, Cauchy stresses and generalized forces. Elements with these basic prescriptions are available in the element library of DIANA and are used to create the finite element models. Both elements used are based on linear interpolation and Gauss integration. For the two-dimensional model, Q8MEM plane stress elements are used for the concrete and soil components of the model while brick-type HX24L elements served the same purpose in the three-dimensional analysis.

The four-node quadrilateral isoparametric plane stress element used in the two-dimensional model is illustrated in figure 2.10a. The configuration of the DIANA Q8MEM element, the element used in this case, is shown in figure 2.10b.
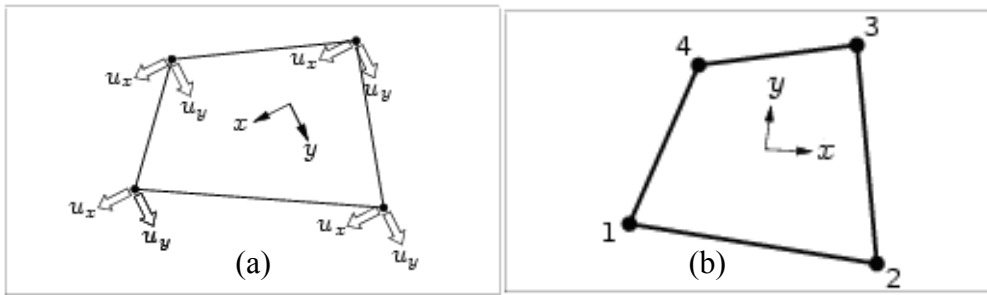
Figure 2.10(a): Displacement orientation of a regular plane stress element.
(b): A Q8MEM element from the DIANA Element Library (Diana, 2008).

The translation variables u_x and u_y of the plane stress element are oriented in the *xy* direction (see figure 2.10) and can be briefly expressed as follows:

$$\boldsymbol{u}_e = \begin{Bmatrix} u_x \\ u_y \end{Bmatrix}$$

2.4

The displacement field yields the deformations du_x and du_y of an infinitesimal part $dx\, dy$ of the element (see figure 2.11).
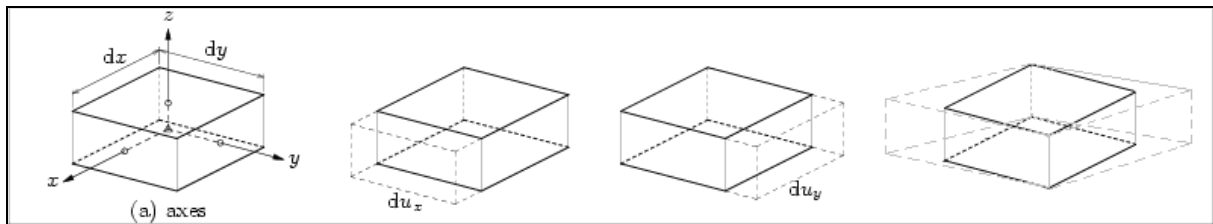
Figure 2.11: Deformation on a unit cube (Diana, 2008).

From these deformations the Green-Lagrange strains can be derived and the Cauchy stresses calculated as follows:

$$\boldsymbol{\varepsilon} = \begin{Bmatrix} \varepsilon_{xx} \\ \varepsilon_{yy} \\ \varepsilon_{zz} \\ \gamma_{xy} \end{Bmatrix}, \qquad \boldsymbol{\sigma} = \begin{Bmatrix} \sigma_{xx} \\ \sigma_{yy} \\ \sigma_{zz} = 0 \\ \sigma_{xy} = \sigma_{yx} \end{Bmatrix}$$

2.5

The Cauchy stresses are illustrated in figure 2.12.
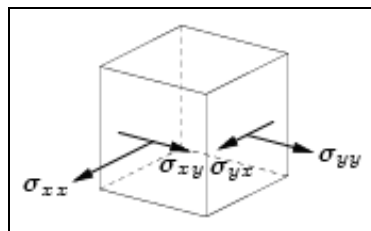
Figure 2.12 Tensional stresses on a unit cube in their positive direction (Diana, 2008).

The eight-node isoparametric solid brick element used in the three-dimensional model is illustrated in figure 2.13a. The configuration of the DIANA HX24L element, the element used in this case, is shown in see figure 2.13b.
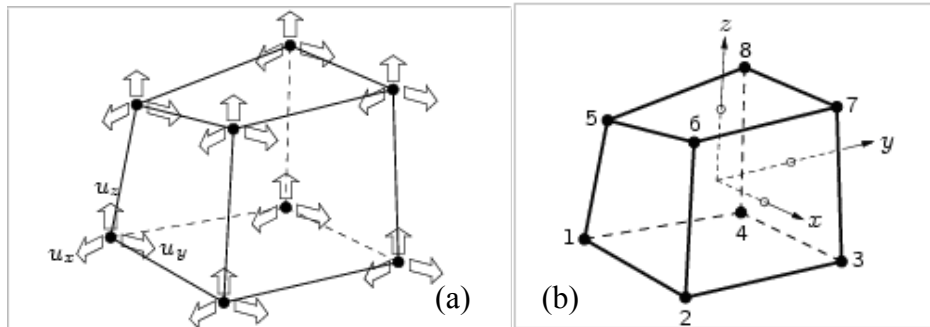
*Figure 2.13 (a): Displacement orientation of a regular solid stress element.
(b): An HX24L element from the DIANA Element Library (Diana, 2008).*

The translation variables u_x, u_y and u_z in the nodes of solid elements are oriented in the local element directions (see figure 2.13) and can be expressed in brief as follows:

$$\boldsymbol{u}_e = \begin{Bmatrix} u_x \\ u_y \\ u_z \end{Bmatrix} \qquad 2.6$$

The displacements in the nodes yield the deformations du_x, du_y and du_z of an infinitesimal part $dx\ dy\ dz$ of the element (see figure 2.14).
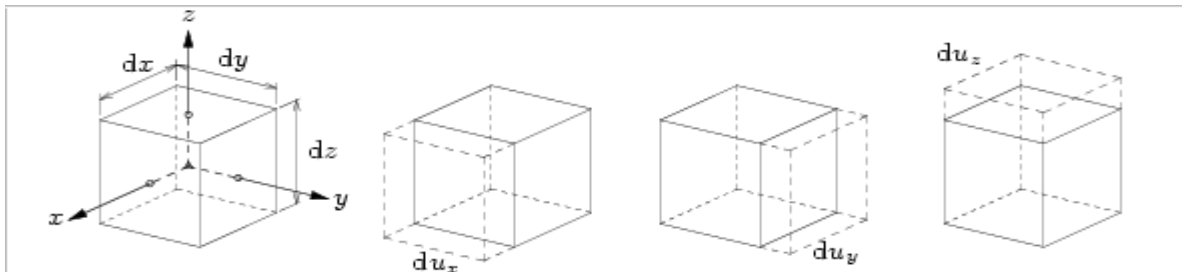
Figure 2.14: Deformation on a unit cube (Diana, 2008).

From these deformations described the Green-Lagrange strains are derived from which the Cauchy stresses can then be calculated, as illustrated in figure 2.15. These can be defined as follows:

$$\boldsymbol{\varepsilon} = \begin{Bmatrix} \varepsilon_{xx} \\ \varepsilon_{yy} \\ \varepsilon_{zz} \\ \gamma_{xy} \\ \gamma_{yz} \\ \gamma_{zx} \end{Bmatrix}, \qquad \boldsymbol{\sigma} = \begin{Bmatrix} \sigma_{xx} \\ \sigma_{yy} \\ \sigma_{zz} \\ \sigma_{xy} = \sigma_{yx} \\ \sigma_{yz} = \sigma_{zy} \\ \sigma_{zx} = \sigma_{xz} \end{Bmatrix} \qquad 2.7$$
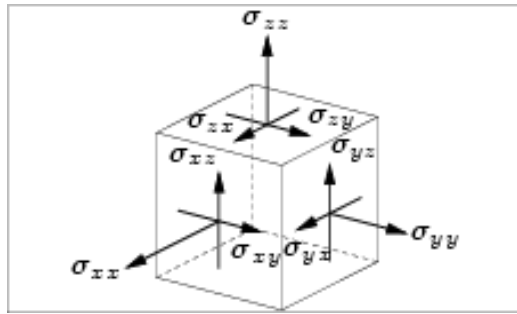
Figure 2.15: Tensional stresses on a unit cube in their positive direction (Diana, 2008).

2.3   Loading

To determine the uplifting and toppling effect of wind loads separately from the settling action caused by the dead load of the structure and its subgrades, these forces are applied in individual load cases with the option to impose either or both load cases in analyses.

Given the loading pattern described in the previous chapter, a dead load of 1000 kN is applied upon the column by the structure, and a horizontal force of 200 kN accompanied by an overturning moment force of 500 kNm, as shown in figure 1.3. The division of these loads on models that differ in dimensional and mesh density aspects is explained below.

2.3.1   Loading Division on Two-Dimensional Mesh

It is decided for simplicity reasons to impose wind loads and moment forces only on the edges of the column. In a two-dimensional case, this means that the loads are merely halved and applied to the edge nodes of the model. Gravitational loads are evenly distributed across the elements with the outer nodes carrying half the load of the inner nodes. This method is true for all mesh densities. The moment is converted to a couple-force as the elements used in this model cannot depict the effect from a pure moment. The division is illustrated in figure 2.16. Applying the loads on only the edge nodes does however mean that local deformations will be more severe. This is however not of concern as part of the column base above the slab is modelled to absorb this deformation and attention is not paid to this particular area, this part being the same height as the width of the column.
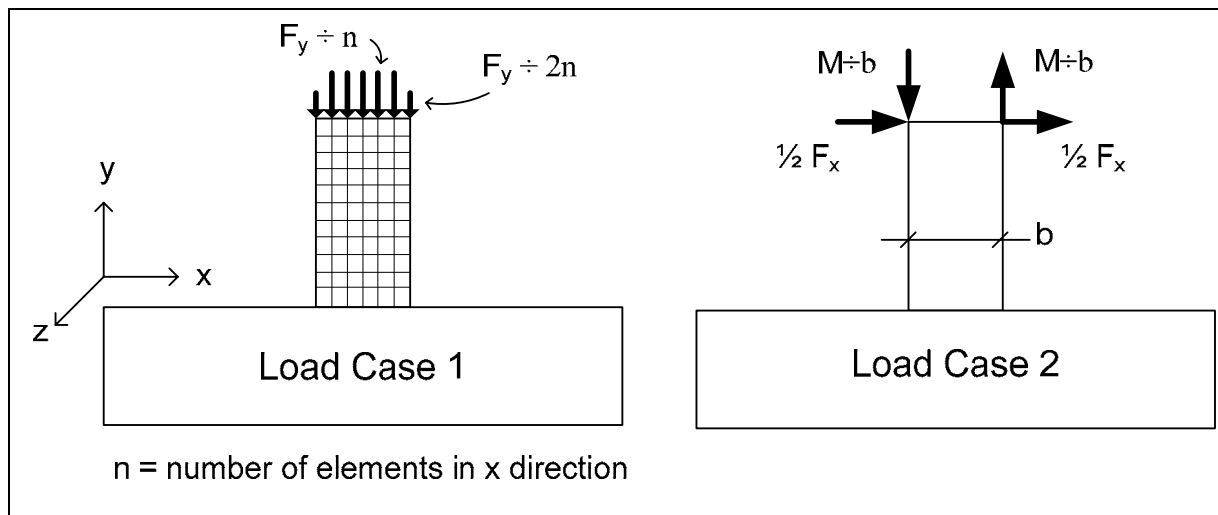
Figure 2.16: Division of loads on the two-dimensional model on column edges.

2.3.2   Loading Division on Three-Dimensional Mesh

In the three-dimensional case, load case one is divided by the number of elements on the top of the column, therefore by thirty-six for the fine mesh. Corners nodes received this resulting load, edge nodes twice the amount calculated and inner nodes four times the amount. Load case two is applied to nodes along the edge of the column in the z-direction. The results from a two-dimensional load division, as described in the above section, are now subdivided proportional to the number of elements in the z-direction. Corner nodes carry half the load of inner nodes. An illustration of this method is given in figure 2.17 where the force shown refers to that found in the two-dimensional division and applies to loads in all directions for all load case two.
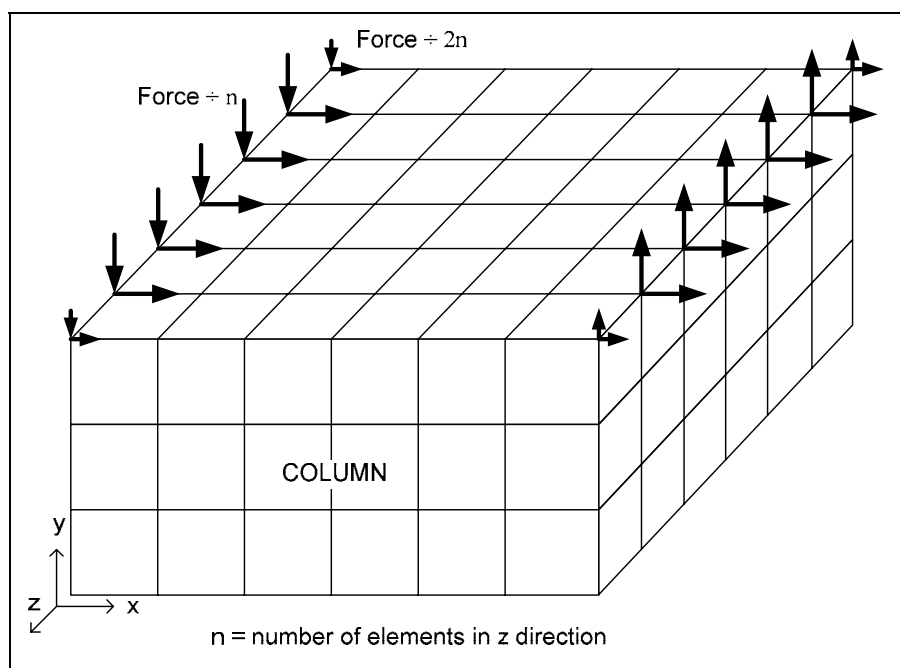
Figure 2.17: Division of load case two on the three-dimensional model on column edges.

2.4 Material Properties

A foundation is the component of a structure which transmits loads directly to the underlying soils. If a soil stratum near the surface is able to adequately bear the structural loading, it is possible to use shallow foundations for the transfer of these loads, as is the case in this study. It is therefore essential that the soil conditions are known within the significant depth of any foundation.

The resistance of a soil to failure in shear is required in analysis of the stability of soil masses. Failure will occur when at a point on any plane within a soil mass the shear stress becomes equal to the shear strength of the soil at that point. The shear strength τ_f of a soil is expressed by Coulomb as a linear function of the effective normal stress at failure (σ'_f), as shown in figure 2.18 and described as follows:

$$\tau_f = c' - \sigma'_f \tan \phi' \qquad\qquad 2.8$$

Here φ' and c' are the shear strength parameters referred to as the angle of shearing resistance and the cohesion intercept respectively. If at a point on a plane within the soil mass the shear stress equals the shear strength of the soil, failure will occur at that point. Failure will thus occur anywhere in the soil where a critical combination of effective normal stress and shear stress develops.
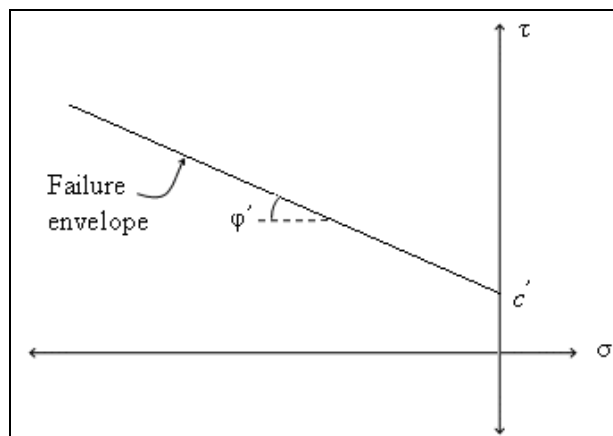
Figure 2.18: Coulomb's expression of shear strength as a linear function.

The column, foundation and slab are comprised of concrete with strength of 40 MPa. The scope of this study does not include the failure possibility of crushing concrete. As only the linear elastic behaviour of the concrete material is considered, the material properties given in table 2.1 are sufficient for modelling the concrete components of the structure. Although soils 1 to 5 are various forms of G7 compacted gravels, they have similar material properties (figure 2.1). The values of this material model were found in the TRH4 manual for highway

construction (TRH4, 1996). The clay measurement of the subgrade is considered to be drained as sufficient time would have elapsed for the process to occur during the compaction of the above lying gravels and erection of the structure. Typical values for drained clay are obtained from Craig's Soil Mechanics (Craig, 2004). All values of above mentioned materials are available in table 2.1. The material properties of the interface models follow in the next chapter.

Table 2.1: Material properties of the foundation-subgrade system.

	Concrete	Cemented Gravel (C3)	Compacted Gravel (G7)	In-situ Clay
Elasticity Modulus (E)	30 GPa	2 GPa	100 MPa	10 MPa
Poisson (μ)	0.2	0.2	0.35	0.3
Density (kg/m^3)	2400	2000	1650	1900
Friction Angle (φ)	-	0	0	35º
Shear Strength (kPa)	-	-	20	10

2.5   Boundary Conditions

Given the numerical investigations done and the geometrical boundaries determined in section 2.1, wherein it is found that exertions beyond the dimensions of the finite element model caused by the foundation will not be felt in the soil, it is concluded that the edges of the model will be fixed against translations in all directions. Edge numbers one to three in figure 2.19 are therefore pinned against any horizontal and vertical displacements.
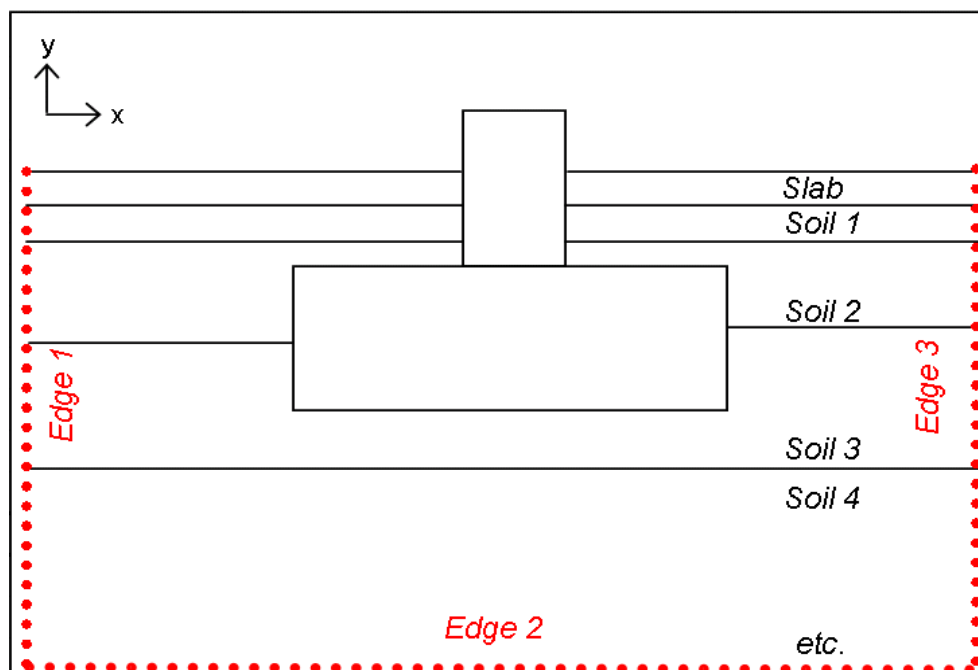
Figure 2.19: Edges one to three of the finite elements models pinned against any translations.

Elsje S. Fraser   University of Stellenbosch

These conditions will vary in later investigations as phenomena such as the settlement of the subgrades are considered by means of phased analyses to determine the potential effect on the structure.

2.6   Mesh Density

The geometrical layout given in figure 2.5 is divided into three regions according to areas of interest, as shown in figure 2.20. The mesh density decreases from region 1 to 2, and from region 2 to 3. This is done to economise analysis time of the model. The mesh is more refined directly around the foundation and column areas and less so towards the model boundaries. The layer of clay below the compacted materials is also coarser, comprised of larger and more rectangular elements. For the elements to have reasonable deformation behaviour, the ratio of the sides of an element was kept within a one to four relationship. These rectangular shaped elements allow the use of larger and thus fewer elements towards the edges of the model and in areas of less interest. Refinement of the mesh is done to find a model with suitable accuracy for a given computational time.
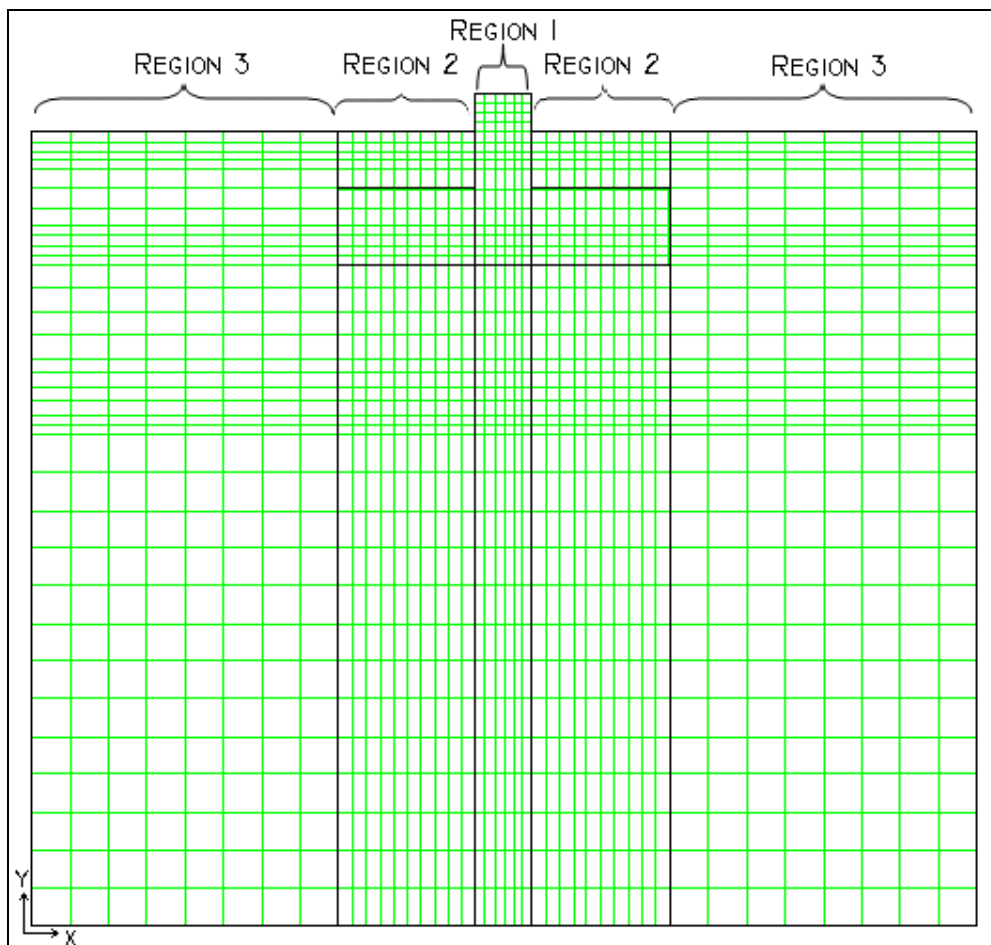
Figure 2.20: Division of model into areas of particular interest.

2.6.1   Motivation for Refinement

The deliberate geometrical distortion of elements can be beneficial if used with care and understanding, as when the sides of an element are kept within a specific ratio. By reducing the number of elements in a model by a given factor, the computational time reduces by the square of that factor. Therefore, if the number of elements of a two-dimensional model is halved, the computation time reduces four times while the three-dimensional model will run nine to sixteen times faster, depending on the specific area of refinement in the two-dimensional version. As will be seen in table 2.3 below, this can reduce the computational time for a three-dimensional model from seventy-two hours to only three or four. A finely meshed three-dimensional model can thus be very time consuming and expensive. When multiple loading combinations, boundary constraints, foundation size or material properties are to be investigated, as will be done in this study, a highly demanding model becomes unreasonable and a simpler yet sufficiently accurate alternative needs to be found.

2.6.2   Refinement of Mesh

A single geometrical model is prescribed various mesh sizes to determine the effect on the accuracy and computation time of the model. This is done in order to find a mesh with the most reliable results for a practical analysis period. Four intensities are chosen and are illustrated in a two-dimensional view in figure 2.21. The same division applies for the three-dimensional models in the x- and z-directions. The means that the same division applies to the depth of the model as does to its width.
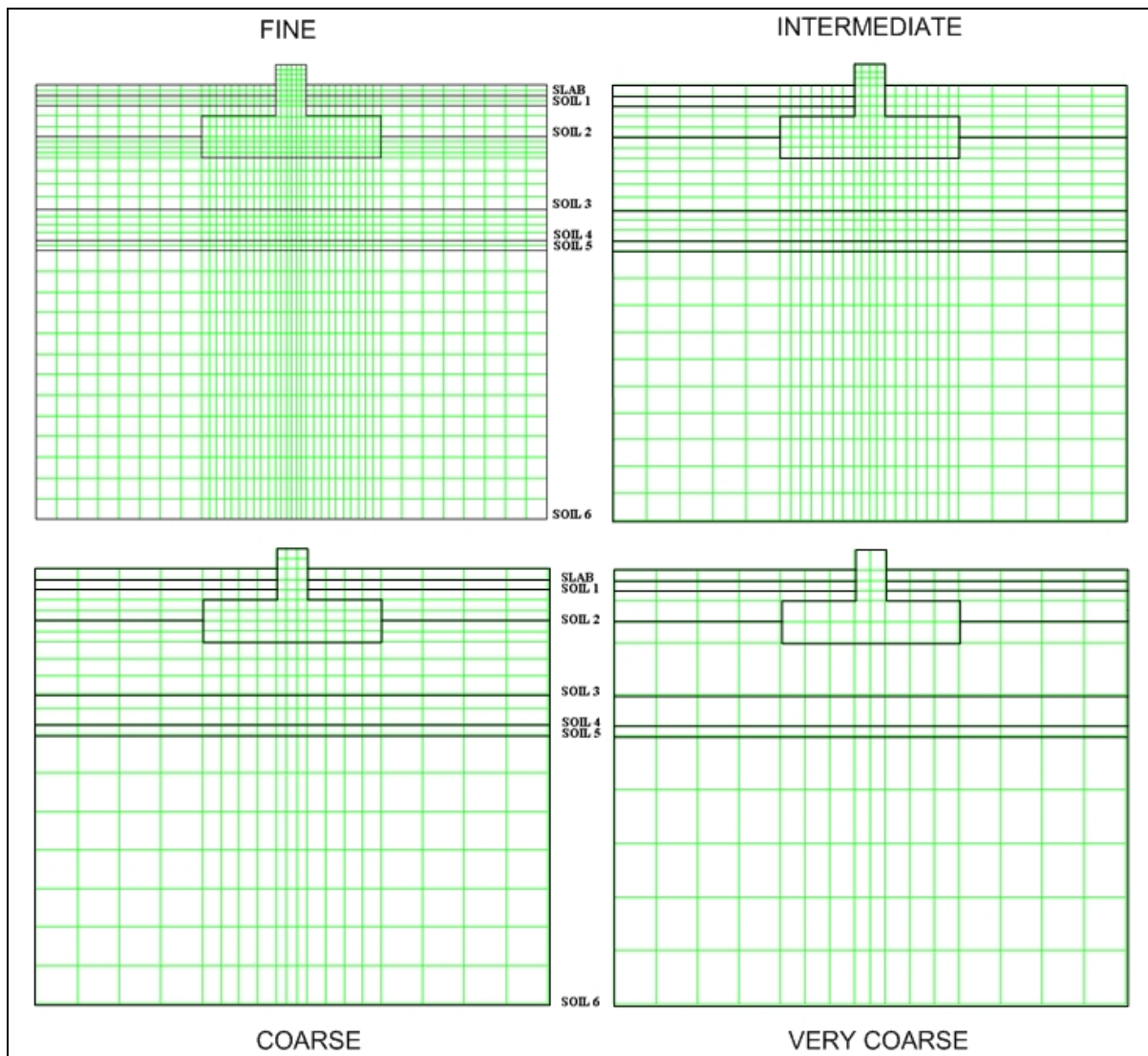
Figure 2.21: A two-dimensional layout of the mesh for the complete model of different mesh densities.

The number of elements of the four mesh densities is given in table 2.2 and the amount of time each took to converge for a dozen load increments, is given in table 2.3. Three-dimensional models of intermediate and very coarse densities are created but are never analysed as the fine and coarse alternatives are deemed sufficiently informative in bridging results from three- to two-dimensional analyses. Further effort to find convergence for additional complex models is considered unnecessary. The conversion from three- to two-dimensional investigations is discussed in detail in the sections to follow.

Table 2.2: Number of elements for model of various mesh densities for different dimensions.

	Fine	Intermediate	Coarse	Very Coarse
Two-dimensional	1520	758	419	234
Three-dimensional	62284	20616	7683	3544

Table 2.3: Amount of time for models of various mesh densities to converge.

	Fine	Intermediate	Coarse	Very Coarse
Two-dimensional	188 seconds	78 seconds	47 seconds	34 seconds
Three-dimensional	72 hours	-	4 hours	-

A tremendous reduction in computation time can be seen in table 2.3 from the fine to coarse three-dimensional mesh. The same is true for two-dimensional analyses and despite the analysis time of the coarse mesh being a fraction of the finer option, the little over three minutes is a satisfactory amount of time to yield a more accurate end result.

2.6.3   Comparison of Results

As results can be produced rapidly in two-dimensional analyses, the comparison of results between the mesh density alternatives is done with the use of the two-dimensional models only. This is justifiable as all two-dimensional models are calibrated to accurately represent the three-dimensional reference models. This calibration method is described in a later section. As a result it can be accepted that the three-dimensional models will yield good correlation with results of the two-dimensional models.

Models of different density are inspected for changes in deformations and rotations at various points, particularly those of interest for this study, for several load increments, boundary conditions and material properties.   The finest mesh is considered to be the most accurate having more and better shaped elements in the model and is found to have the highest deformations of the models. The differences in results from the most to the least dense model change at strict increments with very little alteration in these increments for changing variables. The variation in results is accumulated from all the cases and points investigated and an average deviation from the fine mesh is determined for each of the other mesh densities. These points and calculation can be seen in further detail in Appendix A. A graph illustrating the average percentage of deviation of each mesh from the fine mesh is shown in figure 2.22. With the magnitude of displacements decreasing along with the number of elements in a model, is can be concluded that the fine mesh is the most conservative of the investigated options and should therefore be used in further two-dimensional analyses.
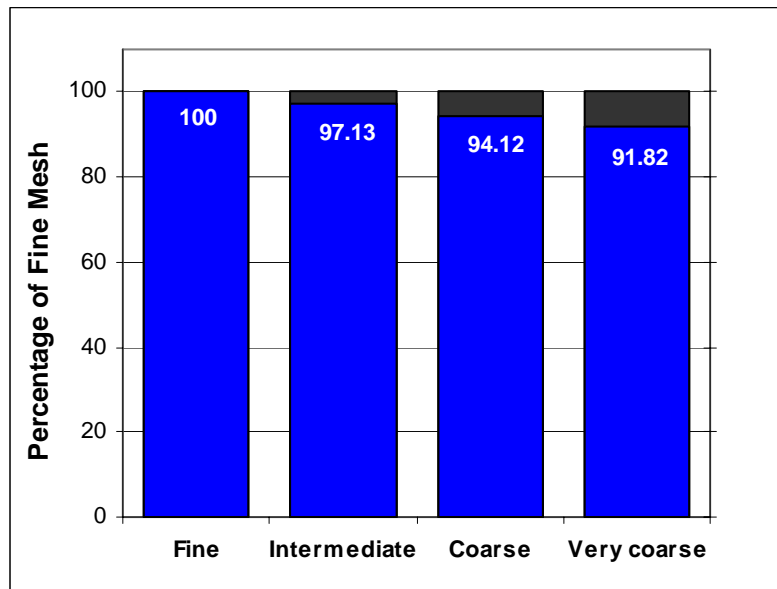
Figure 2.22: The average percentage of each mesh of the fine mesh displacement results.

The fine mesh is decided to be sufficiently fine judging from the flattening curve shown in figure 2.23, indicating that further refinement would make little or no significant difference to the results found and would unnecessarily increase the computation time required for analyses. It is therefore concluded that the fine mesh is amply conservative and accurate for further use in this study.
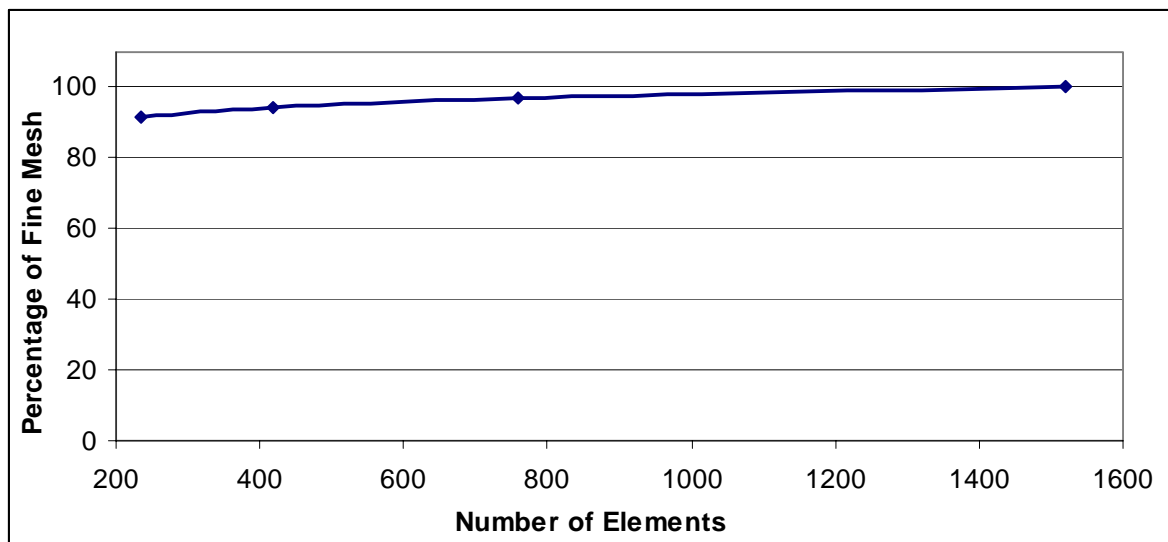
Figure 2.23: The effect of the number of elements in a model on the results obtained.

2.7 The Background and Planning to a Finite Element Analysis

Up until this point in this chapter, only the actual finite element model has been described. All physical aspects and input gone into creating the model have been discussed and

illustrated. In this final section of this chapter, the thought process and typical hurdles that have to be overcome in the analysis of the finite element model are explained and a basic background is given to some issues that arose during the process.

2.7.1   Modelling Strategy

In contrast to a linear problem the character of a nonlinear problem may become apparent only after trying to solve it. At the beginning, the types and degree of the nonlinearity may not be clear, and even if they are, the appropriate elements, load steps, mesh layout and solution algorithm may not be. Attempting to solve a nonlinear problem in "one go" is likely to fail and produces confusion and frustration to the inexperienced analyst. It is advantageous to anticipate finite element results by doing a simplified preliminary analysis. A linear analysis should precede more complex nonlinear analyses. Linear analyses can identify modelling errors that would also cause problems in a nonlinear analysis and can test the adequacy of the preliminary discretization. The initial use of a linear analysis can also suggest the location and degree of yielding, what gaps are probable to open or close, or estimated load and deformation states at actual collapse. Nonlinearities produced by different sources can be added one at a time, as in a phased analysis, so as to better understand their effects on the model and how to treat them.

Trial models in progress to refinement may use a comparatively coarser mesh, larger load steps and liberal convergence tolerances. All of these will be refined in later investigations. In most cases a final load must be approached in several small steps. An overly large step can slow convergence or produce an abrupt change in a displacement versus load diagram and can be mistaken for actual physical behaviour. Convergence failure can be a result of a numerical difficulty provoked by large load increments or indicate that a condition of collapse has been reached and that the structure has failed.

Once past the preliminary trial stages, the remainder of the analysis should be considered in specific detail as to optimise time expenditure. Each load step in a nonlinear investigation can produce as much or more output than an entire linear analysis. It is therefore essential to anticipate which output to request and to consider the process with which it will be examined.

2.7.2 Nonlinear problems

To recognize behaviour as nonlinear is only to realise what the behaviour is not. The term "nonlinearity" by definition implies that a response is not directly proportional to the action that produced it. In reality nonlinearity is always present; in most common problems however these nonlinearities are small enough to be ignored. Software can unfortunately not detect when nonlinearity is important and to consequently take it into account. It is therefore up to the analyst to recognise important nonlinearities and intelligently supply additional data and activate the nonlinear processes.

In linear structural analyses deformations are small compared to the overall dimensions of the structure. Equilibrium equations are written with respect to undeformed configurations and deflections calculated are regarded to not affect the equilibrium of the structure. This is referred to as an elementary or a first-order analysis. Linear models provide reasonable approximations for many problems of practical interest, although the substantial removal from linearity is common.

Nonlinearity admits a wide range of phenomena, each potentially difficult to formulate and possibly interacting with one another. Materials can creep, fracture or yield, local buckling could occur and gaps may open or close. Under ultimate or abnormal loading conditions, linear analysis is unable to reflect the real behaviour of a structure. Under large deflections nonlinear behaviour changes the stiffness of a structure even when the material shows a purely linear elastic behaviour. An analysis taking these deformations into account is termed a geometric nonlinear or a second-order elastic analysis. The nonlinear nature of second-order inelastic analyses requires an incremental-iterative numerical method to be used to map the load-deflection behaviour of the structure. The implementation of second-order inelastic analysis therefore requires major computational effort.

In structural mechanics different types of nonlinearity can be categorised as material, contact or geometrical nonlinearities. Yielding, nonlinear elasticity, plasticity, fracture and creep are included in material nonlinearity in which material properties are a function of the state of stress or strain. In contact nonlinearity a gap between adjacent parts may open or close, the contact area between components changes as contact forces change, or sliding contact with frictional forces may occur. The calculation of contact forces gained or lost is needed in order to determine structural behaviour. In the case of geometrical nonlinearity deformation is of

the proportion that equilibrium equations need to be revised and written with respect to the deformed structural geometry. Another example of geometrical nonlinearity is a load changing direction as it increases as in the case of pressure inflating a membrane. Problems in these categories are nonlinear because stiffness, and occasional loads, become functions of deformation or displacement.

In the sections following brief explanations of the solution procedures for nonlinear analysis that economizes the computation of finite element models, such as the Newton-Raphson Method, are discussed (Cook, 2002).

2.7.3   Newton-Raphson Method

In finite element methods the nonlinear global displacement stiffness equations are solved using an array of incremental-iterative methods. Incremental methods solve global equations by treating them as a set of ordinary differential equations, using a series of linear steps. Iterative schemes treat the principal relations as nonlinear equations and iterate within each load increment until a predetermined tolerance is larger than the unbalanced forces, incremental dissipated energy variation, and/or incremental displacement variation.

The Newton–Raphson method solves the global equations by applying the unbalanced forces, calculating the consequent displacements and then iterating until the deviation from equilibrium is tolerably small. Advantages of this method are its accuracy and speedy convergence. A disadvantage is that it may not always converge, particularly when the problem or material is strongly nonlinear. To conquer this drawback, various techniques have been developed to steady and accelerate the convergence of Newton-Raphson methods. Such techniques include line search or arc length control procedures (see figure 2.24).

Line search methods attempt to steady Newton-Raphson iterations by expanding or shrinking current displacement increment, minimizing the resulting unbalanced forces. When the search direction is poor or when the unbalanced forces are unsmooth displacement function line searches may however be of limited use.

Arc length methods attempt to force the Newton-Raphson iterations to stay within the vicinity of the last converged equilibrium point. The applied load must be thus reduced as the iterations proceed, greatly reducing the risk of divergence for strongly nonlinear problems.
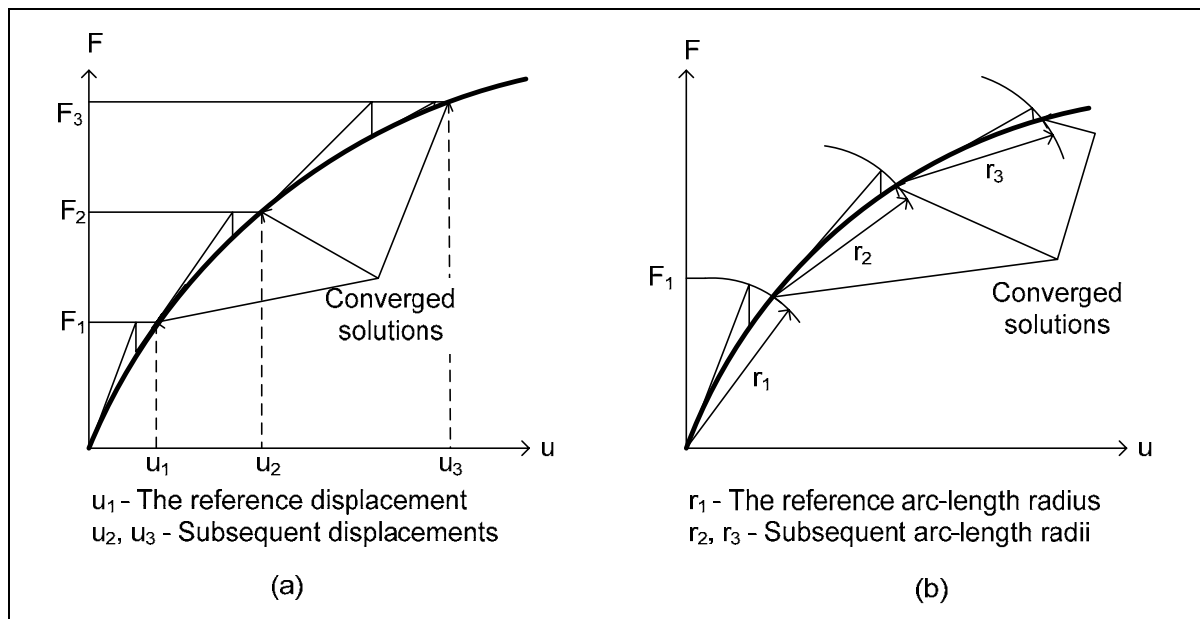
Figure 2.24 (a): Newton-Raphson line search approach for incremental load-steps;
(b): Newton-Raphson iterations to convergence for incremental arc-lengths.

2.7.4   Convergence

Equilibrium conditions become satisfied only once convergence is reached. Sluggish convergence or failure to converge may have various roots. In an attempt to resolve these conditions, the algorithm may use many iterations, a waste if the area of interest lies elsewhere. Convergence failure may also indicate that loading on the structure has reached its capacity due to the exhaustion of the strain-hardening capacity in plasticity, buckling, or a gap that opens permanently allowing part of the structure to "float away" or undergo a significant displacement without significant increase in resistance, or with reduced resistance. When approaching such a state of collapse or a limit point, displacement becomes large. During these states, and for some distance beyond it, the tangent stiffness matrix is negative definite, provoking software to halt execution and issue an error message unless appropriate numerical procedures are invoked. The use of arc-length controlled steps can find the solution despite negative pivots. Also, if there is no snap-back, displacement control can prevent the load step process from terminating.

A range of tactics are possible when convergence fails. The amount of iterations allowed per load step or for a gap or contact problem can be increased. The load increment size can be reduced. An examination for poorly shaped elements can be carried out or the convergence tolerance can be relaxed.

If convergence is eventually achieved, results must be examined to determine that the given problem has not been altered by the computational tactics. Convergence may not be a physically realistic solution. For a single load, several equilibrium configurations may exist and a numerical solution may converge to any of them, even if the configuration is unstable (Cook, 2002).

3. THE MATERIAL LAW OF THE INTERFACE ELEMENT

Associated with computational investigations of the interaction between a soil mass and components of engineering structures, are the modelling of non-linear processes such as slip or separation, on the interface between the structure and soil. The analysis of a soil-concrete system is complicated by the interface between the structure and soil. To simulate the interaction between the soil and foundation under the application of various loads, the appropriate characteristics of an interface element needed to be captured. Three types of interface elements are available in DIANA and are considered before being chosen to meet with specified criteria discussed below. A plasticity based multi-surface interface model, also known as the 'Composite Interface model' or combined cracking-shearing-crushing interface model, the Friction interface model and the Nonlinear Elastic interface model are studied and tested in this chapter.

3.1 Background

The forces carried from the column due to wind and self weight cause downward or upward pressures and overturning moments on the foundation and soils below. This will in turn result in deflections, stresses and strains due to compression, shearing and tension.
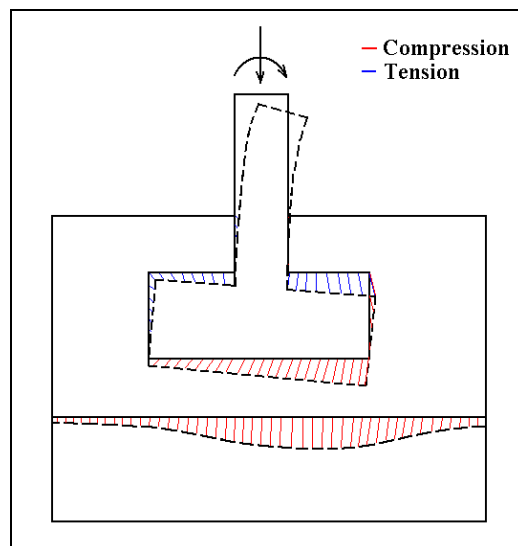
Figure 3.1: The deformation pattern of a column-foundation structure under typical loading.

Processes and mechanisms of contact interaction are modelled numerically, approximating the interface with finite elements of a minimal thickness. Since these elements should define the

shear and normal stresses on the boundary of the dissimilar materials, their mechanical and strength characteristics should reflect the properties along the slip boundary and not necessarily correspond to those of the adjacent materials.

3.2   Shear-slipping of Concrete and Soil

Residual deformations of the concrete and soil mass of the structure along the contact boundary are expressed by the effect of two processes, namely compaction, the closure of cracks and pores, caused by hydrostatic pressure, and plastic deformations which accumulate during slip along the contact surface due to shear stresses. Modelling of these deformations will make it possible to obtain results of the interaction between a soil mass and structure form a computed prediction of processes that approximate actual phenomena more closely.
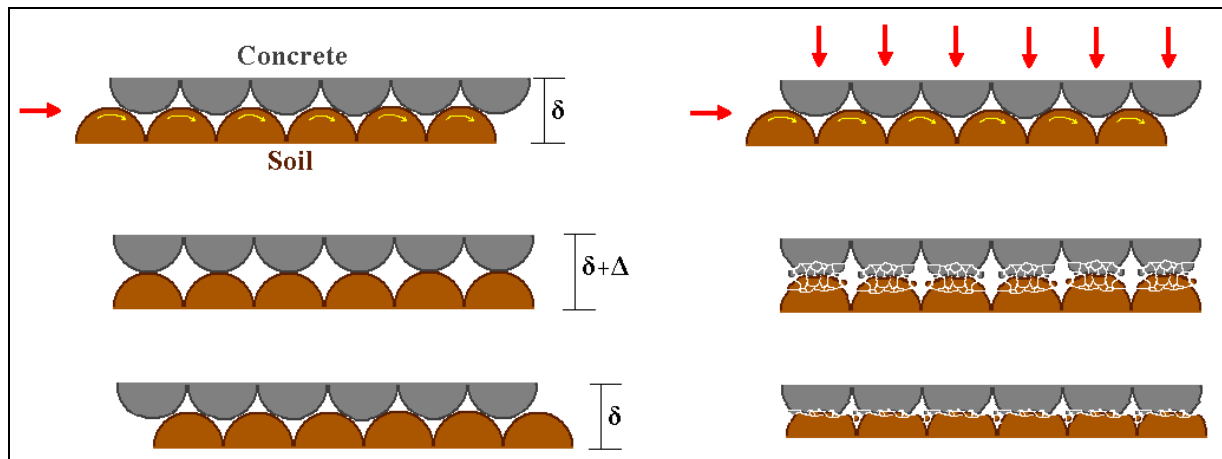
Figure 3.2: The plastic deformation and compaction that occur during shear forces.

Concrete and soil particles in contact with one another may need an initial force to induce slipping, after which only a small amount of force is needed to maintain slipping. Upon the application of an additional critical compressive force, the particles may first crush before continuing to slip/grind. An interface model appropriate to simulate fracture, frictional slip as well as crushing along interfaces is needed.

3.3   The Cohesive Crack Model and Softening Curve

In the interface model types to follow, an exponential softening curve depicts many parts of their material laws. A brief explanation to the source of this curve is explained in this section by the help of a cohesive crack model.

The formulation of a cohesive crack model is characterised by the use of linear elasticity to determine the response of the structure on either side of the crack, while nonlinearity describes the boundary conditions along the crack line. The load-elongation curve for a tensile specimen in which a stable crack has evolved, including the post-peak region known as the softening curve, is illustrated in figure 3.3. G_f is called the specific fracture energy, or fracture energy for short. It is the critical energy release-rate referring to the cracked surface area due to a material property not dependant on the cracking history. The tensile, or cohesive, fracture energy G_f^I geometrically coincides with the area under the softening curve (see figure 3.3).
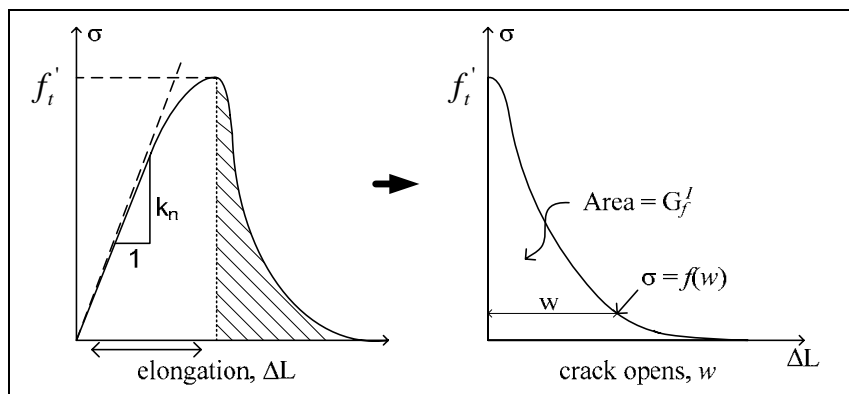
Figure 3.3: The stress elongation curve and softening curve for a stable tensile test (Bažant, 1998).

The softening curve $\sigma = f(w)$ is the fundamental component of the cohesive crack model. The two properties of greatest importance to the softening curve are the tensile strength f_t' and the tensile fracture energy G_f^I. For the tensile strength being the stress at which a crack starts to open, it can be written for the softening curve that

$$f(0) = f_t'. \qquad\qquad 3.1$$

The tensile fracture energy G_f^I is the external energy required to first create a cohesive crack and then fully break free the unit surface area. Consider a thin element of initial length h located at the cohesive crack, and stress σ acting on the faces of this thin element transmitted by rest of the specimen (see figure 3.4).
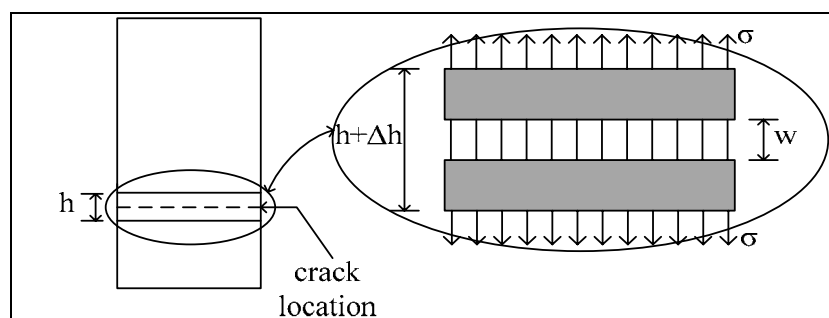
Figure 3.4: Thin strip containing the cohesive crack (Bažant, 1998).

The total work on this thin element of length h with specimen cross section S, is then formulated as the following:

$$W = hS \int \sigma d\varepsilon + S \int \sigma dw \qquad 3.2$$

The energy required to deform the bulk material inelastically is expressed by the first term while the second term describes the energy required to open the crack. If the element thickness was of the nature that h → 0, the first term, the bulk energy, becomes infinitely small and only the second term remains. By dividing this remaining term by the crack surface it is found that

$$G_f = \int_0^\infty \sigma\, dw = \int_0^\infty f(w) dw. \qquad 3.3$$

From an analytical perspective, exponential softening is of the simpler softening types. The general expression for exponential softening is $\sigma = c_1 \exp(-c_2 w)$, with material constants c_1 and c_2. These constants are related to $f_t^{'}$ and G_f. It follows directly from equation 3.1 that $c_1 = f_t^{'}$, and equation 3.3 can be rewritten as shown in equation 3.4 below.

$$G_f = f_t \int_0^\infty \exp(-c_2 w)dw = \frac{f_t^{'}}{c_2} \qquad 3.4$$

Therefore with $c_2 = f_t^{'}/G_f$, the exponential softening can be rewritten in the form shown in equation 3.5, revealing that the exponential softening is completely determined by $f_t^{'}$ and G_f.

$$\sigma = f_t^{'} \exp\left(-\frac{f_t^{'}}{G_f} w \right) \qquad 3.5$$

3.4   Interface Models

Each interface model available in the DIANA Material Library (Diana, 2008) captures features unique to its own material law. Among these features there is the ability to define tensile bond failure and shear-slipping along the contact areas, while enforcing a compressive limit function. The abilities of each of the three individual interface material models used in investigations in this study are discussed in this section. Plane stress is assumed for the two-dimensional interface models employed for analysis of in-plane behaviour of the dissimilar adjacent materials. Plane interaction is assumed for three-dimensional analysis. The element types used are described in the previous chapter (see figure 2.6 and figure 2.8).

3.4.1 Multi-surface Plasticity

This plane stress interface model was developed and formulated by Lourenço and Rots (1997). It is based on multi-surface plasticity, consisting of a Coulomb friction model combined with a tension cut-off and an elliptical compression cap (see figure 3.5). The elastic domain is bounded by a composite yield surface that includes compression, tension and shear failure. Softening acts in all three modes. This softening is governed by tensile fracture energy G_f^I, shearing fracture energy G_f^{II}, and compressive fracture energy G_f^{III}. Hardening of the cap precedes softening degradation.
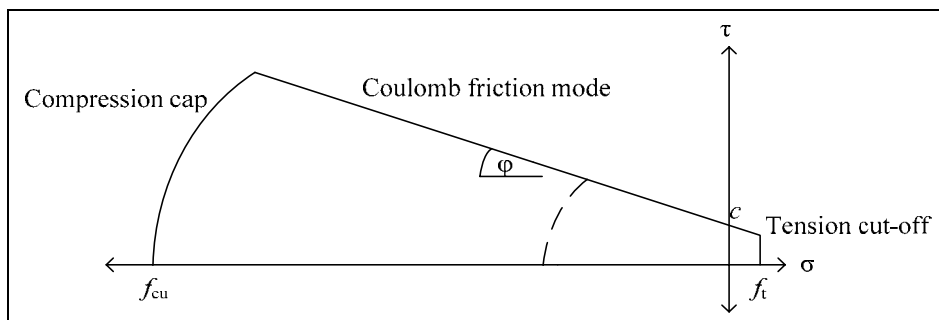
Figure 3.5: Composite yield surface.

Exponential tension and shear softening curves with a Mode I fracture energy G_f^I and Mode II fracture energy G_f^{II} respectively, depict the material law described. For compression, the fracture energy is the geometrical area found under the softening curve. It is only the area illustrated by plastic deformation and does not include the elastic deformation. The same applies for shear. If there is however a confining pressure on the element, there will be a peak resistance of $c - \varphi\sigma$ and a residual resistance equal to $-\varphi\sigma$. The fracture energy will exclude this residual stress level. Both fracture energies are shown in figure 3.6 below. Note that, for computational convenience, DIANA uses a small residual compressive resistance, as shown in figure 3.6. Also in this case the energy excludes the residual value. The tensile fracture energy G_f^I is as illustrated in figure 3.3 in the previous section.
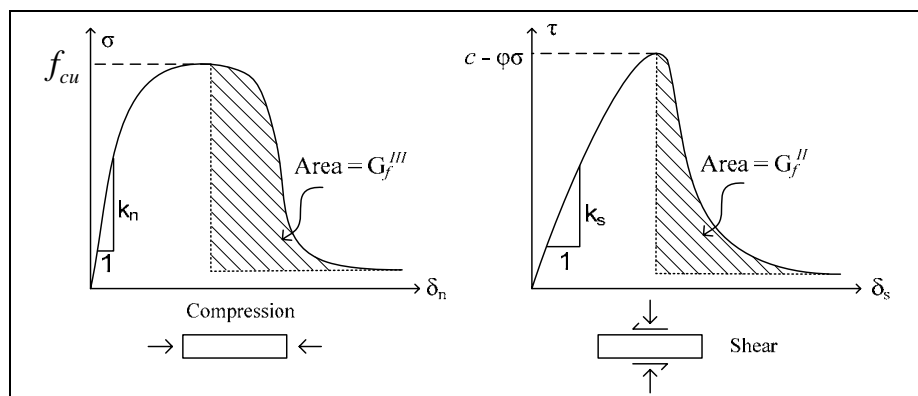
Figure 3.6: Interface traction-displacement behaviour in various stress states.

3.4.2   Nonlinear Elasticity

The available nonlinear elastic interface model allows the user to create multi-linear diagrams of tension-compression and shear behaviours. The relation between normal traction t_y and normal relative displacement Δu_y, illustrated in figure 2.7, or between the tangential traction t_x and the tangential relative displacement Δu_x (shear slip), can be defined as coordinates on these multi-linear diagrams. DIANA then interpolates for values between assigned coordinates. Exponential softening curves and a high compressive strength can therefore be assigned to this model by allocating the appropriate coordinates to each graph. A shortcoming of this model type is however that it is not able to represent the effect of friction on the structure. This means that if a normal pressure were to be experienced by an interface element, it would not behave any differently from that of no normal pressure, or that of normal tension. This inability to differentiate between the possible loading conditions is an inaccuracy that must be taken note of as a significant variation from the more accurate multi-surface plasticity material law, which considers Coulomb-friction type behaviour as described in the previous section. This interface model does have the advantage of easy convergence versus that of the combined cracking-shearing-crushing or friction models. It is therefore used largely as a tool in this study to indicate the behavioural tendencies of a model which can after initial trials be subjected to more accurate investigations.

3.4.3   Friction

The friction interface model available incorporates Coulomb-friction type behaviour, similar to the multi-surface plasticity model of section 3.4.1. However, it has no compression limit, as shown in figure 3.7. Another difference with the multi-surface plasticity model lies in the coupled shear-tension behaviour. The user has the option to simulate brittle cracking where once the tensile strength of the interface is exceeded, the tensile strength drops to zero. For this phenomenon the shear stiffness can then be adjusted to a condition of zero shear retention or constant shear retention. An option to alter the shear retention according to aggregate interlocking is available but is very specific relation of Walraven and Reinhardt (1981) and is not discussed in any detail in this study. A multi-linear cohesion hardening diagram can be assigned to the model. Once tensile normal forces that exceed a prescribed tensile resistance are applied, the behaviour is governed by the user prescribed condition of shear retention. The specific behaviour of the model developed for this study will be described by means of verification tests in the next section.
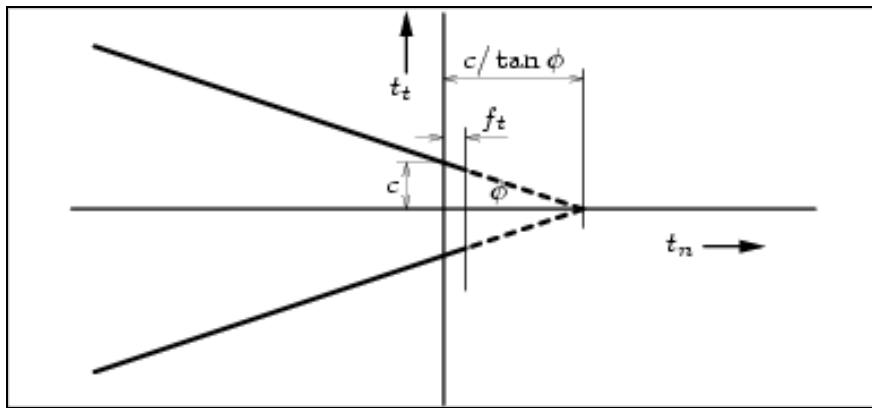
Figure 3.7: The Coulomb friction criterion of the friction interface model (Diana, 2008).

3.5   Verification of Interface Element Model Parameters

In typical concrete-soil interaction, and especially when the soil is of a sandy or gravel composition as in this case study, the soil will separate from the concrete under a very low tensile force, resulting in de-bonding and consequently, under lateral loading, shear-slipping. The material properties of the interface model are chosen in a manner in which the tensile forces the structures can exert on one another are negligible compared to their compressive strengths. This means that a low amount of fracture energy is required and would be characterised by an exponential softening curve with a sudden drop after the tensile strength is reached. As illustration, the effect of several fracture energies is shown in figure 3.8, as found in simple, single element tests. For lack of experimental data, a suitable fracture energy value is chosen from these for the purpose of modelling the soil-structure interaction in footings.
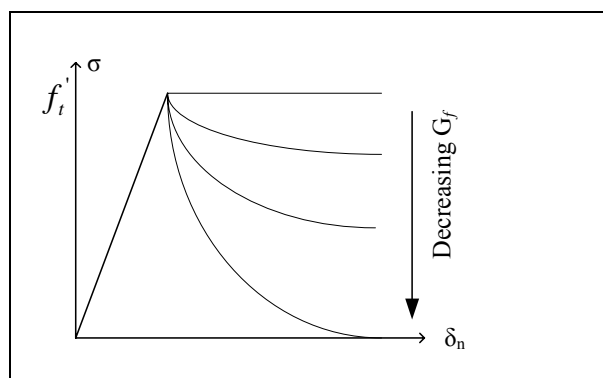
Figure 3.8: The effect of decreasing fracture energy on the softening curve.

Elementary tests are carried out on the two- and three-dimensional interface elements. Simulations of ten-by-ten-by-ten millimetre specimens under compressive, tensile and shear loads are created in order to provide insight into the behaviour of the proposed model for all material descriptions.

3.5.1 Combined Cracking-Shearing-Crushing

To allow the numerical overlapping of neighbouring particles to be negligible, high stiffness values of for the normal modulus k_n and shear modulus k_s are chosen (refer to figures 3.3 and 3.6). The inelastic properties of the interface are shown in table 3.1 and the tensile and shear fracture energies, G_f^I and G_f^{II} respectively, are chosen by observing the effect on the softening curve through an iterative process.

Table 3.1: Inelastic properties of the interface model.

Values determined through simulations on a single interface element		
Normal modulus	k_n	2×10^5 N/mm^3
Shear modulus	k_s	2×10^4 N/mm^3
Compressive strength	f_{cu}	1.0×10^{10} N/mm^2
Tensile strength	f_t	0.01 N/mm^2
Cohesion	c	0.02 N/mm^2
Friction coefficient	φ	0.5

As a very low tensile strength is expected in a soil-concrete system, especially when sand or gravel is present as in this case, a small amount of fracture energy will be required for failure, or separation. The appropriate stress-displacement plot is chosen for a tensile fracture energy value of 0.1 N/mm. Values ten times more or less than this amount showed the behaviour of the softening curve to be too stiff or too limp respectively. These behaviours can be seen in figure 3.9.
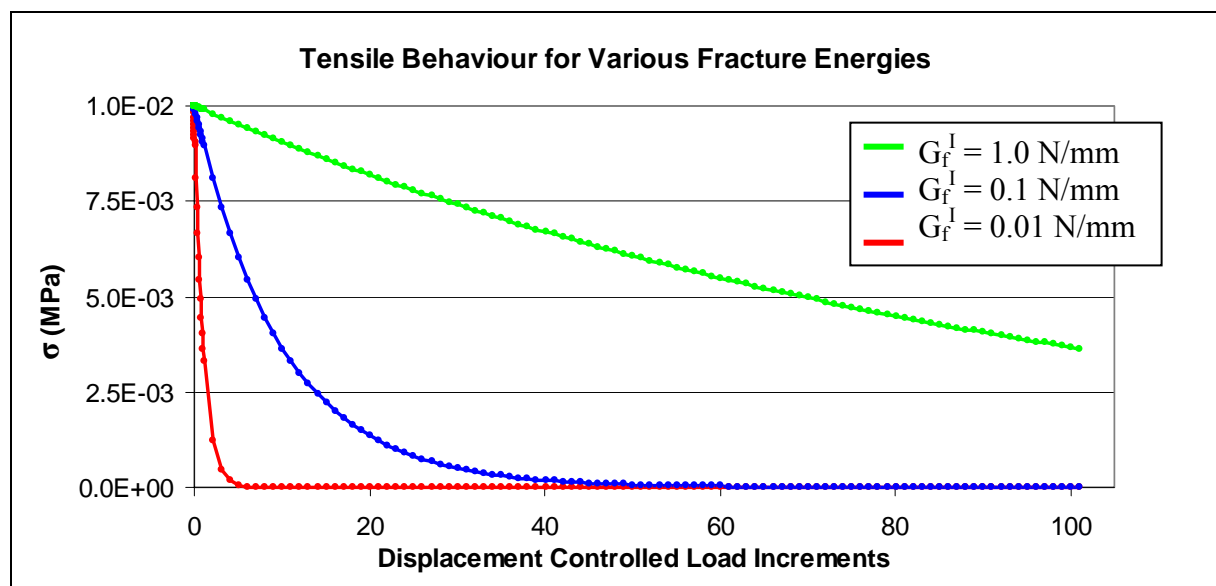
Figure 3.9: Stress-displacement plots of a single element test for tension.

As in the case of tensile strength, for a soil-concrete system with sand or gravel present, a low amount of shear resistance is expected to be characteristic of the system and should be represented in the interface model. From the single element test a shear fracture energy of 0.1 N/mm reveals a softening curve as desired. This can be seen in figure 3.10. Again values ten times more or less this amount showed the behaviour of the softening curve to be too stiff or too limp respectively.
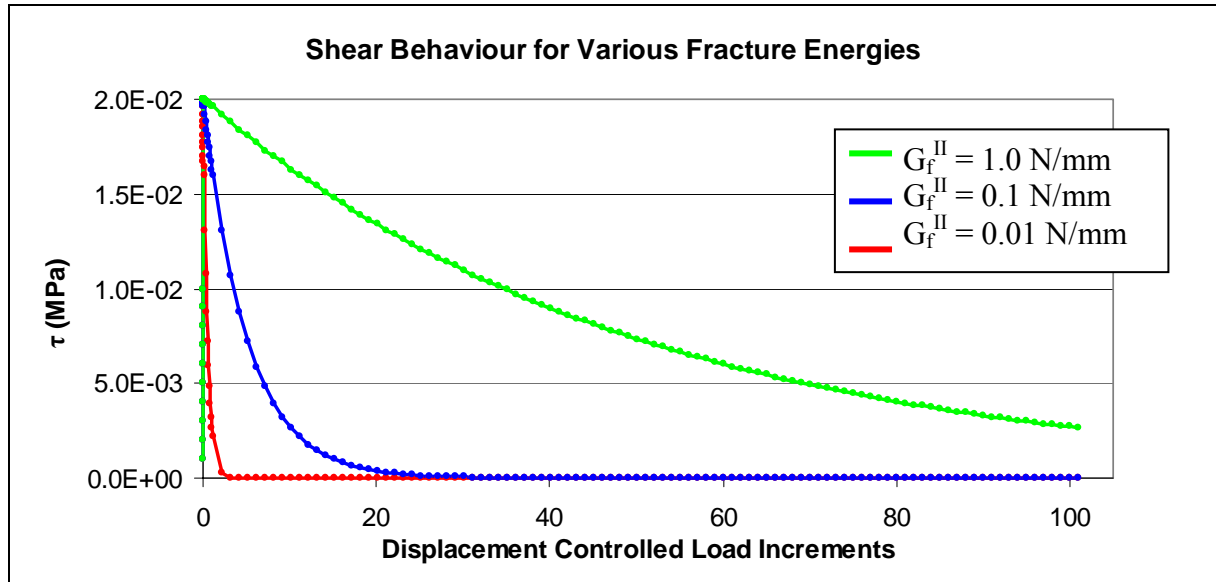
Figure 3.10: Stress-displacement plots of a single element test for shear.

These plots resulted in the decision to use the following fracture energies shown in table 3.2.

Table 3.2: Fracture energies of the Crushing-Shearing-Cracking interface model.

Values determined through simulations on a single interface element		
Mode I fracture energy	G_f^I	0.1 N/mm
Mode II fracture energy	G_f^{II}	0.1 N/mm

In the presence of a normal pressure, a peak shear resistance equal to $c - \varphi\sigma$ is expected as discussed in section 3.3. The shape of the softening curve should remain the same. The effect of a 1 MPa and 2 MPa normal pressure is tested on a single element and it is found that the element behaved accordingly. Identical tests are done on a three-dimensional model and indistinguishable plots are found for these tests. It is therefore concluded that the numerical interface model is capable of predicting the response required based on the response of its basic constituents.
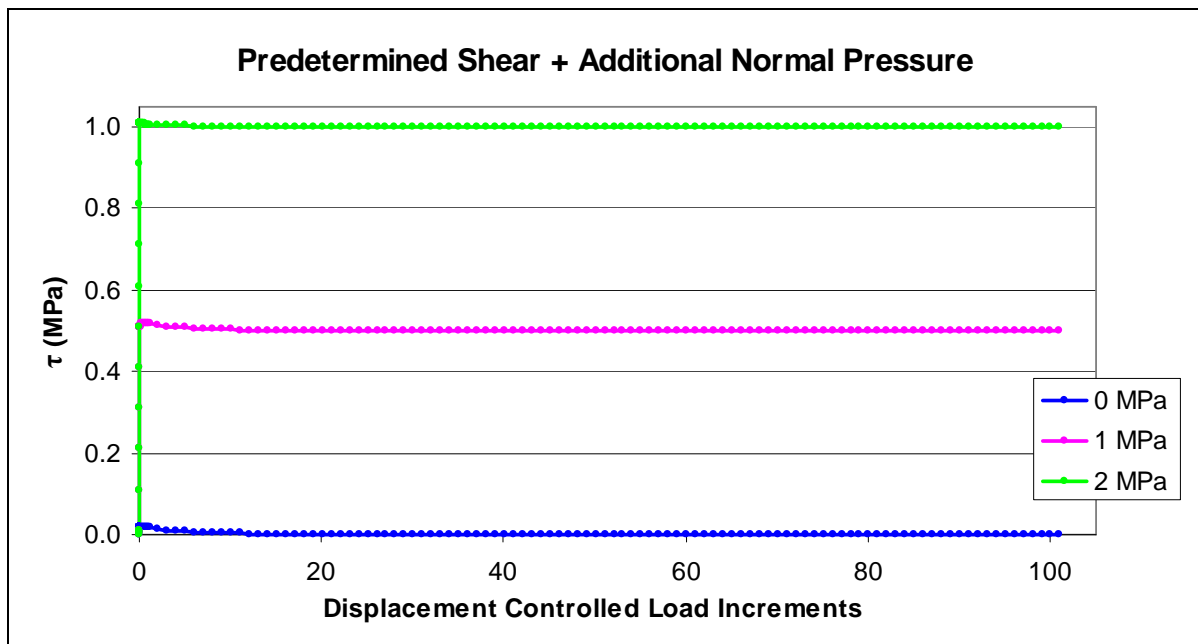
Figure 3.11: Stress-displacement plots for shear in the presence of a confining pressure.

3.5.2 Nonlinear Elastic

To construct the diagrams for compression-tension and shear behaviour, values are taken from the softening curves of corresponding graphs from the cracking-shearing-crushing model illustrated in figures 3.9 and 3.10. These graphs are therefore not as smooth as those above due to the piece-wise linear interpolation between softening coordinate points. The same tests are performed on a single element as described above and the tensile and shear softening curves are shown in figures 3.12 and 3.13 respectively.
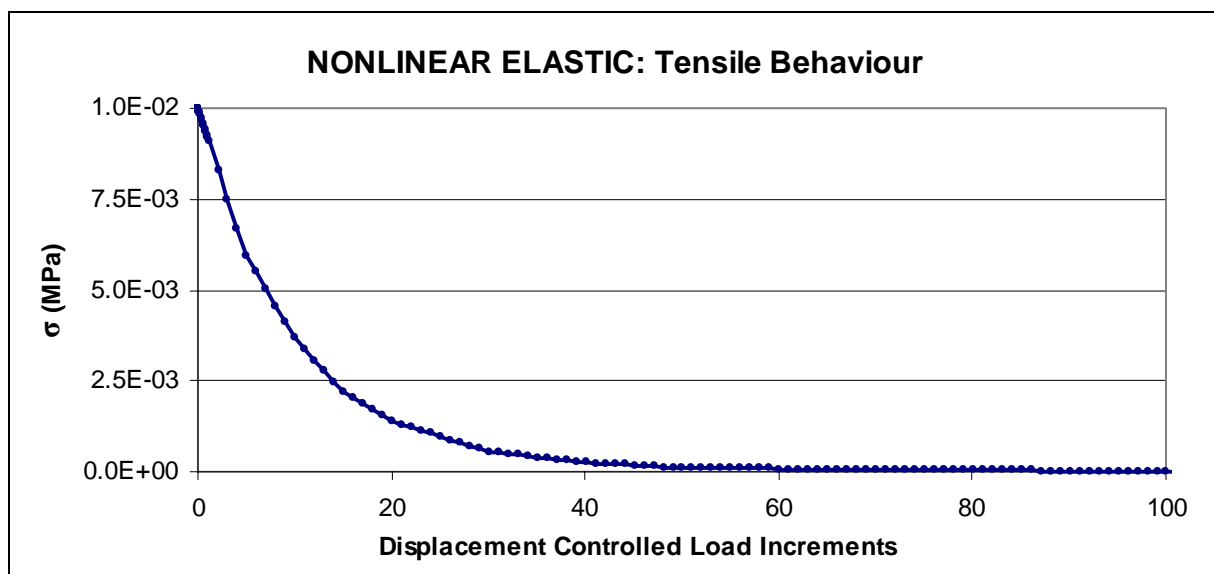
Figure 3.12: Stress-displacement plots of a single element test for tension.
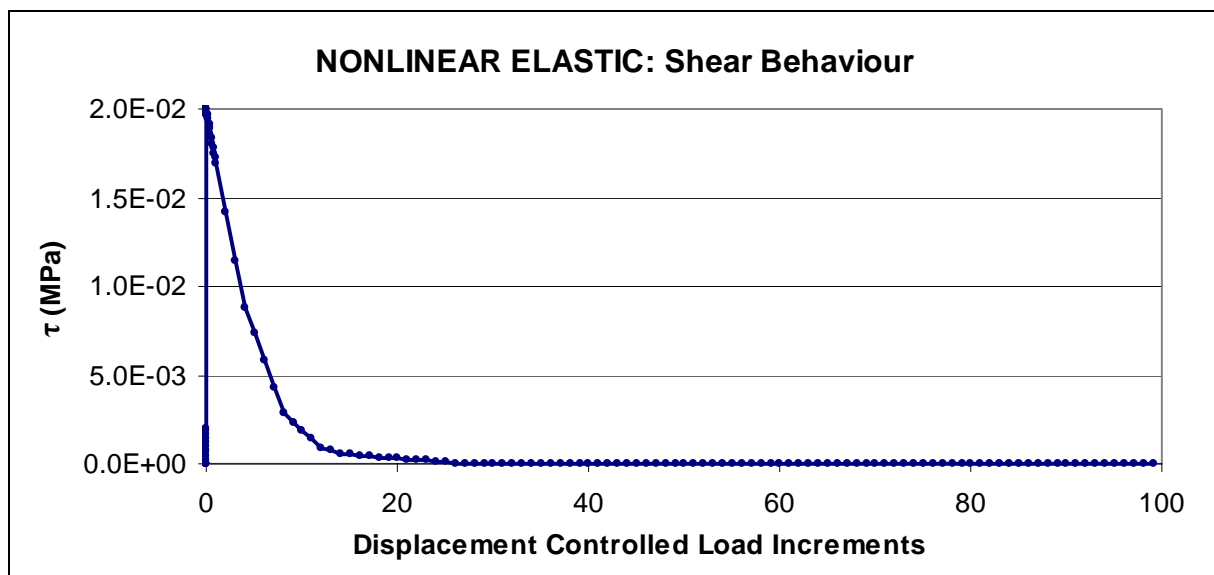
Figure 3.13: Stress-displacement plots of a single element test for shear.

The addition of a normal force to the single element does not change the shear response as in the other models. Instead, the softening curve for shear will remain exactly as seen in figure 3.13. Provision is made for negative shear and a high compression strength is prescribed for this model (see figure 3.14). The latter simulates a contact problem, but incorporates the limited tensile resistance. Three-dimensional tests give identical results.
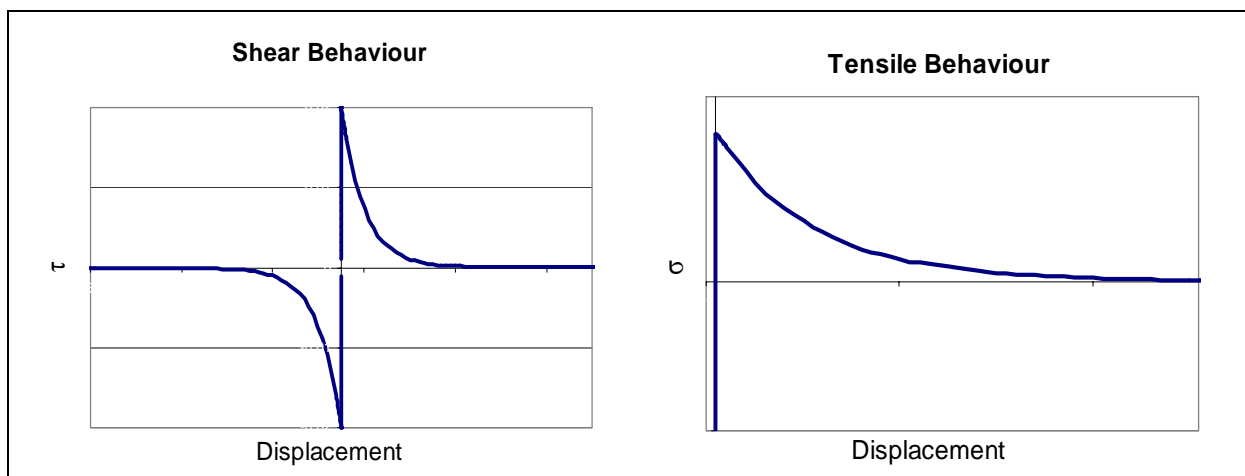
Figure 3.14: Complete stress-displacement plots to incorporate negative shear and compression.

3.5.3   Friction

The inelastic properties of the friction interface model are shown in table 3.3.

Table 3.3: Inelastic properties of the friction interface model.

Normal modulus	k_n	2×10^5 N/mm^3
Shear modulus	k_s	2×10^4 N/mm^3
Cohesion	c_0	0.02 N/mm^2
Friction coefficient	φ	0.5
Dilatancy angle	ψ	0
Tensile strength	f_t	0.01 N/mm^2

The cohesion hardening diagram is described by equation 3.5 and has been rewritten in the form found in equation 3.6. This equation will describe softening of the cohesion. The term "hardening" used in DIANA to name the diagram does not necessarily imply that only the option of cohesion hardening exists, but indeed softening, or reduced resistance can also be prescribed. This model therefore behaves in pure shear as do the two previous models that were described. For an initial cohesion c_0 prescribed in table 3.1 and shear fracture energy G_f^{II} determined through a single element test described in a section above and given in table 2.2, a value of cohesion can be found for increments of displacement u. A diagram of corresponding values is shown in figure 3.15 and is therefore also the plot found when subjecting a single element friction model to a pure shearing force.

$$c = c_0 \exp\left(-\frac{c_0}{G_f^{II}}u\right) \qquad\qquad 3.6$$
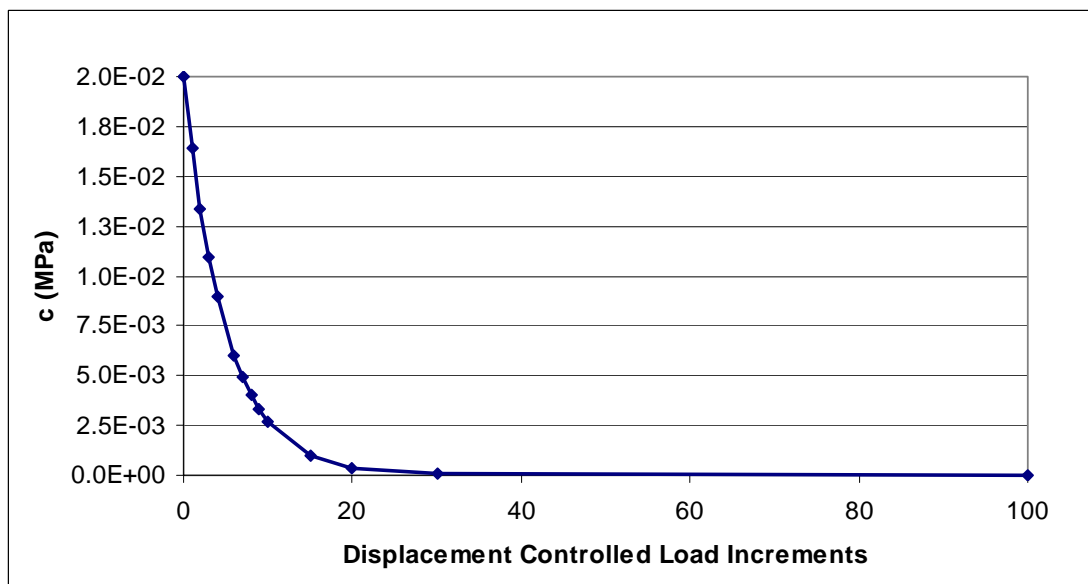
Figure 3.15: The cohesion hardening diagram of the Friction interface model.

In this particular interface model, the option exists to create a brittle material. This means that once the tensile strength of the material is exceeded the tensile strength drops immediately to

zero, as shown in figure 3.16. This tensile behaviour is prescribed to the friction model in the absence of a softening curve alternative. Once such brittle behaviour in tension has been activated, the user must prescribe what the shearing resistance is. Physically, once two bodies previously in contact have been moved far enough away from each other, zero friction/shearing resistance exists between them. However, if the bodies have not been moved far enough apart, some shearing resistance may remain. This can be simulated by the user prescribing a reduced shear, or shear retention value. Figure 3.17 shows the effect of this factor on shear behaviour after the tensile strength of the interface element has been exceeded. A tensile force was applied to a single element test which was larger than its tensile strength, after which displacement controlled increments of a shear force was loaded. The friction interface model used in further analyses behaves as would a brittle material shown in figure 3.16. This would be the same behaviour as a model with a shear resistance factor of zero.
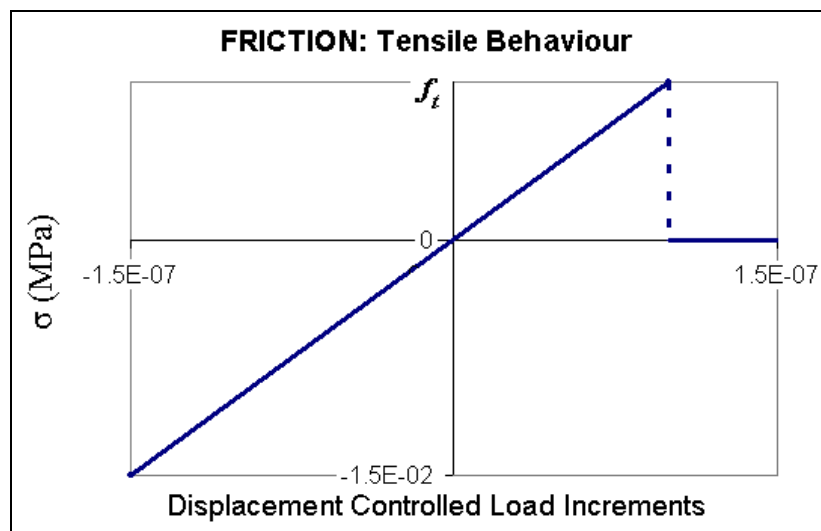
Figure 3.16: Tensile behaviour of the Friction interface model.
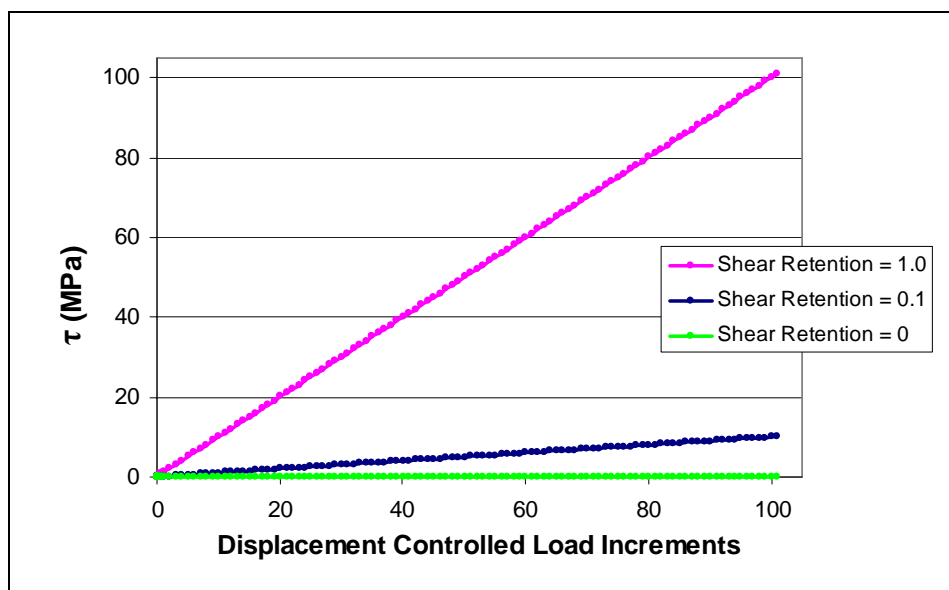
Figure 3.17: Shear behaviour after tensile strength exceeded for various shear retention values.

3.6   Chapter Summary

The described models and simple single element analyses results presented above serve to illustrate the capabilities, but also shortfalls of the three available interface models. The multi-surface plasticity model incorporates crushing, Coulomb-shearing and de-lamination/limited tensile resistance. However, the physical interaction between separation and shearing resistance is not directly incorporated. This is more directly considered in the friction model, at the cost of simplified modelling of tensile post-peak behaviour, the only possibility being brittle, abrupt loss of tensile strength. Also, crushing is not included in the friction model. The most simple of the three models, namely the nonlinear elastic model, does not consider friction (pressure-dependence), or coupling between de-lamination and shearing resistance. The effect of these simplifications will be shown in a later chapter by finite element analysis of the problem at hand with all three these interface models.

4. FOUNDTION ROTATIONAL RIGIDITY: Computational Response

4.1 Areas of Interest

Lateral displacement at the top of the column is undesired from a structural perspective. Larger steel beams are required to prevent movement and may significantly increase the cost of the structure. With a column height of eleven meters, a small rotation of the foundation will cause a large deformation at the top of the column. A one degree rotation to the foundation yields a 192 mm horizontal deflection, as calculated below:

$$\delta = L \cdot \tan\theta, \quad \text{where } L = 11\,\text{m and } \theta = 1°$$
$$= 11 \cdot \tan(1)$$
$$= 0.192\,\text{m}$$
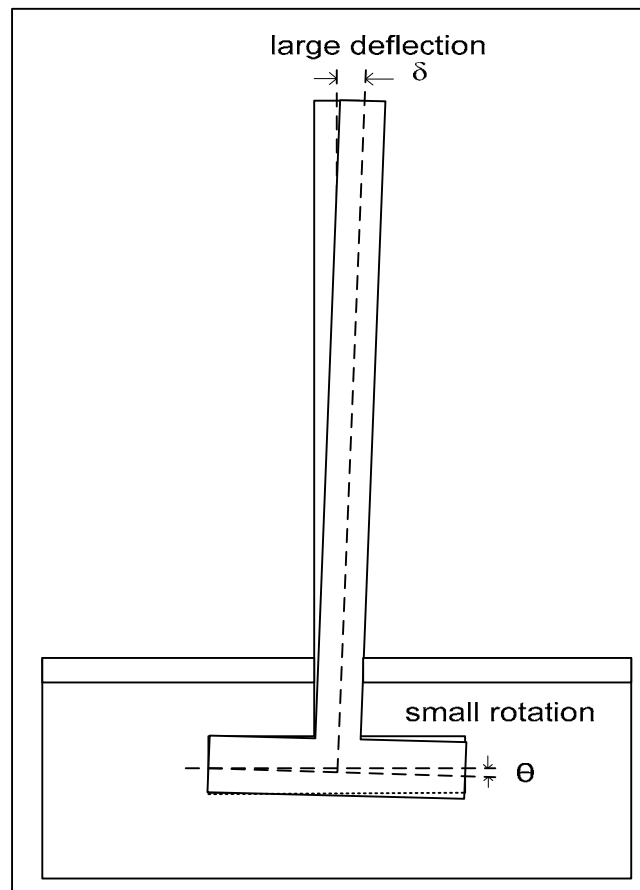
Figure 4.1: The effect of rigid foundation rotation on lateral deflection of tall column.

To not be influenced by the bending of the column when deformed, the rotation of the foundation is not determined from the relative displacements of the foundation corners but instead in the area of the foundation below the column. Exaggerated deformations are found in the modelled portion of the column. The overstated deformations that cause concern are

Elsje S. Fraser   University of Stellenbosch

those where the foundation and column meet. The model is simplified to have only enough volume above the slab which to apply loads to, leaving the possibility that the small local inaccuracies may occur directly around the loaded areas. The more probable cause for higher deformations where the column and foundation meet is however not inadequacies of the finite element model, but because of enormity of the foundation itself relative to the column section. From preliminary tests it is concluded that for this particular set of structural dimensions, the column will fail at the connection to the foundation before toppling of the foundation occurs. Note that this is a column design matter, which must be dealt with by the designer. To overcome the exaggeration of foundation rotation due to such local deformation, measurements are taken at increasing depths through the column until the effect of the column is no longer felt in the foundation. This would thus be when the rotation remains constant for increasing depths of the column. This method is illustrated and labelled in figure 4.2 below.
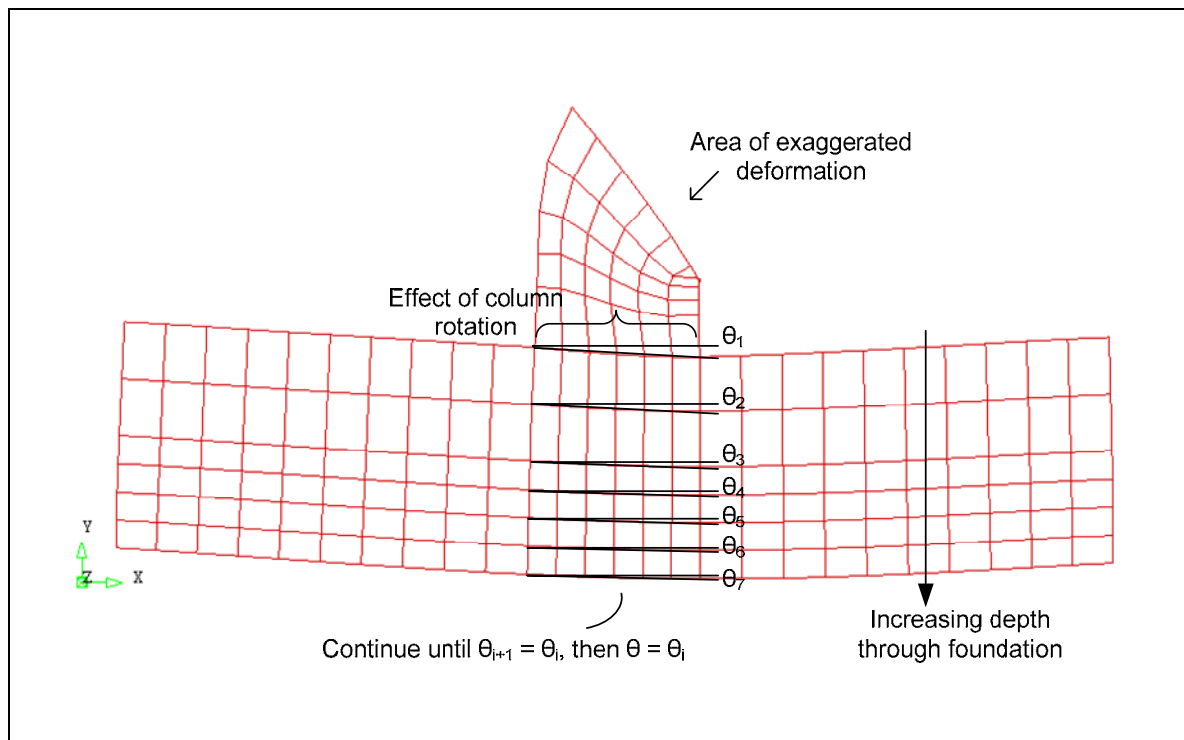
Figure 4.2: Method to exclude effect of column when determining foundation rotation.

4.2 The Conversion from Three- to Two-Dimensional Analyses

As reflected in table 2.3, the drop in analysis time from three- to two-dimensional models is of such significant proportions that further investigations are made into evaluating the differences between the models to find a bridging method from three- to two-dimensional modelling.

4.2.1   Shortcomings of the Two-Dimensional Model

Without specific detailing in a third direction, it is not possible to accurately represent a three-dimensional problem with a two dimensional analysis. This because all components of the column-foundation-soil system viewed from in a two-dimensional perspective, as in figure 2.5, are assigned an in-plane depth. These depths vary from component to component. The depth of the column for example is only six hundred millimetres while the soil and slab are ten meters deep. Material can be piled, from an in-plane view, in front and behind the column by defining elements on top of each other. The stiffness and self weights of these materials will be added correctly but no eccentricity can be modelled. All additions will be centred along the middle plane and not be off-set in the thickness direction. This will however not allow the two-dimensional model to govern the interaction between the foundation and soil in these areas using the interface material law. This is because the interface elements are not on the surface of the column and slab adjacent to the piled on materials and is unaware of behaviour it should be defining. The same applies for the areas in front and behind the foundation (see figure 4.3).
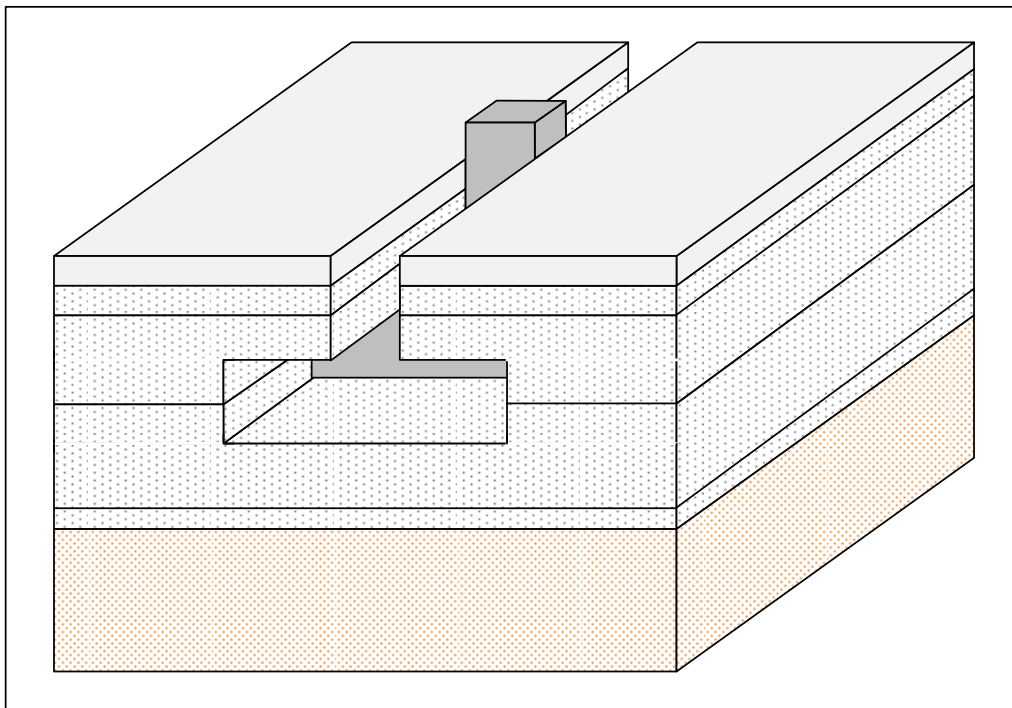
Figure 4.3: Omission of soil and slab masses in the two-dimensional model.

The shortage of soil mass directly around the focal areas of the model along with reduced interface stiffness may cause the two-dimensional model to be overly conservative or un-conservative, producing more expensive structural designs than would be necessary or structures that will fail sooner than anticipated. These soil and slab masses are included in the

three-dimensional model and the effects of complete contact surface between them and the structure is therefore included in the results. The three-dimensional model is consequently considered a realistic and accurate representation of the entire physical body of material and will hence be used as a reference model in the development of a more representative two-dimensional model.

4.2.2   A Conversion Method

As the rotation of the foundation is the main concern in this study, the most important areas to find correlation of results between models are the foundation and interface surrounding it. The aim is therefore to find similar deflections in the foundation and surrounding soil for both models. If comparatively higher deformations occur in the lower subgrades it should be of little concern as this is not the focal area. Deformations in the soil and slab directly around the column and foundation should however not be less than those of the three-dimensional results. This would make the investigation unconservative and could lead to structural failure due to inadequate structural design.

To compensate for missing soil volumes, the missing percentage is calculated per soil level and the depth of the relevant soil was increased by that percentage. The original depth of soil one for example is ten meters. The omitted percentage of this soil for a column of a 600 mm depth and foundation of 3.5 meters is 5.6 percent. Therefore the new soil depth is 10.56 meters. The balance of lost soil is therefore distributed evenly across the model avoiding any concentrated stiffness or stress that may occur if the material is lumped upon the model instead. The same method is used to recover the absent slab. Table 4.1 below shows the new depths of the slab and soil levels affected.

Table 4.1: Revised slab and subgrade depths, for the given structural dimensions, to accommodate for missing material masses.

	Slab	Soil 1	Soil 2	Soil 3
Original Depth (m)	10	10	10	10
Revised Depth (m)	10.564	10.564	11.859	10.674

To account for the lost stiffness in the subgrade directly around the foundation the soil stiffness is increased in the mesh elements bordering the foundation and column. All slab and soil elements in contact with the column have their stiffness increased. Only the soil elements along the top and bottom of the foundation have their stiffness altered. This is done to

prevent a "stiff box" of soil surrounding the foundation which would prevent the natural rotation of the foundation. By using strips of a higher stiffness instead of a box, elements at the corner edges of the foundation are not subjected rotational constraints that would effectively form in the latter case. This constraint is proved to be a valid concern in earlier trials to find an effective yet simple solution. The elements that are stiffened are done so proportionately to their size and that of the column and foundation. The amount of contact area lost in the two-dimensional model between the concrete and subgrades is calculated and the stiffness of the most local element to the void is increased by the missing factor. The blue elements in figure 4.4 along side the column for example contain their own stiffness and that of three of the column elements beside them. In the case of the corner where the column and foundation meet, coloured red in figure 4.4, elements contain their own stiffness, that of the neighbouring column, the foundation directly below, and the area diagonally across from it as shown by the dashed line.
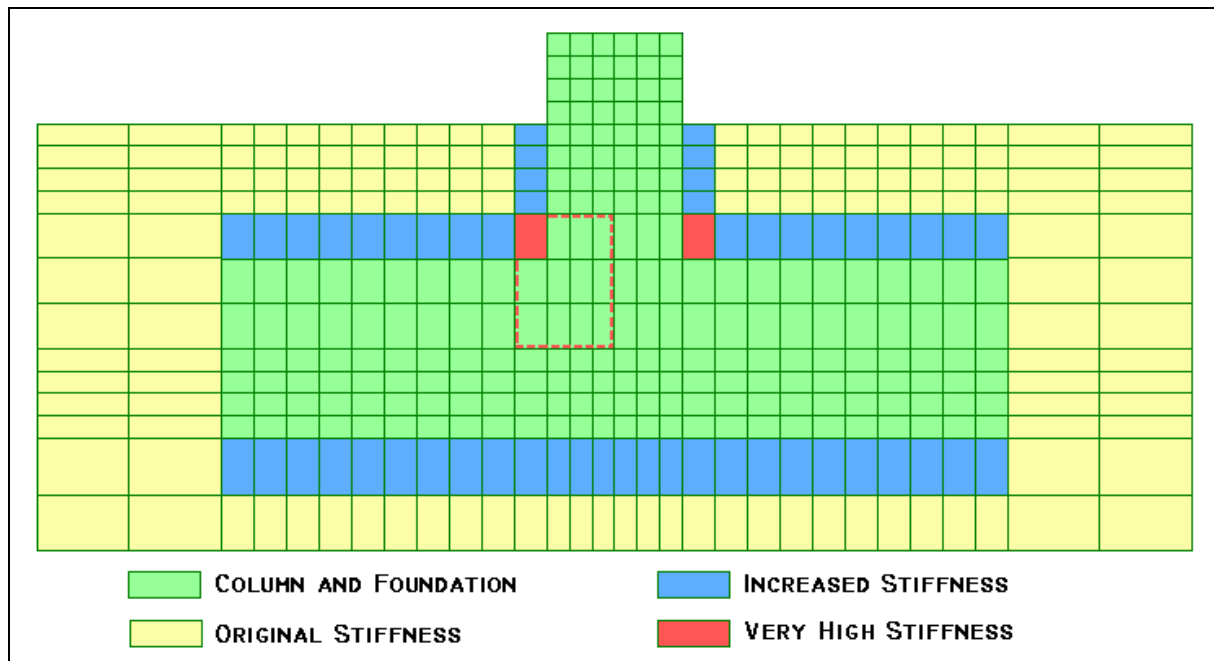
Figure 4.4: Diagram of adjusted stiffness values of two-dimensional model.

In later investigations when the dimensions of the foundation are changed, the above steps need to be revised in order for the new two-dimensional models to yield credible results.

4.2.3   The Evaluation of the Conversion Method

As it is of utmost importance that the two-dimensional model closely resembles the behaviour of its reference three-dimensional model and that future results can be trusted, results delivered by the conversion method are scrutinized to be sure that the method is reliable. As

the rotation of the foundation is considered the main threat to structural failure, this correlation between models is the most important measure by which the conversion method is evaluated.

Two- and three-dimensional models with identical boundary conditions, loads, mesh division and material properties are compared. An alteration to the stiffness of certain elements as discussed in the previous section is done in the two-dimensional model. Points of maximum deflections in elements in each level of soil, the slab, column, foundation and interface are inspected. The two-dimensional model provided more conservative results, particularly in the lower levels of subgrade. Fortunately these areas are not of great interest and results similar to the reference three-dimensional model are found in areas that are. Table 4.2 shows an average deflection percentage of the two-dimensional model relative to that of the reference model. The average is determined from various points investigated in each area.

Table 4.2: The percentage of two-dimensional deflections in terms of the reference model.

2D Model	Column	Foundation	Slab	Interface	Soil1	Soil2	Soil3	Soil4	Soil5	Soil6
Old	121	172	141	151	150	160	160	160	162	121
New	100	125	103	110	110	115	125	140	140	120

The reason for the large difference between the foundation deflections in the revised two-dimensional model versus the three-dimensional model is because even though the omitted soil masses have been added to the model and the stiffness of some elements increased, it is still only a method to approximate the physical problem. It is not a true representation of the structure. The alterations to the model have greatly improved the agreement between the models, as reflected in table 4.2, but there will always be shortcomings when moving from a three- to a two-dimensional analysis, for example, the higher percentage difference between the two models when comparing the deflections of the foundation. This is due to higher displacement in the lower lying subgrade levels, namely soils four to six. This causes the higher deflections found in soil three and the foundation and is an inadequacy of the conversion method used. The deflection patterns of the foundation for both models are however similar. An image of the deflected two-dimensional model in figure 4.5 shows the foundation ends curving upward as does the deflected three-dimensional model, shown in a similar image in figure 4.5.
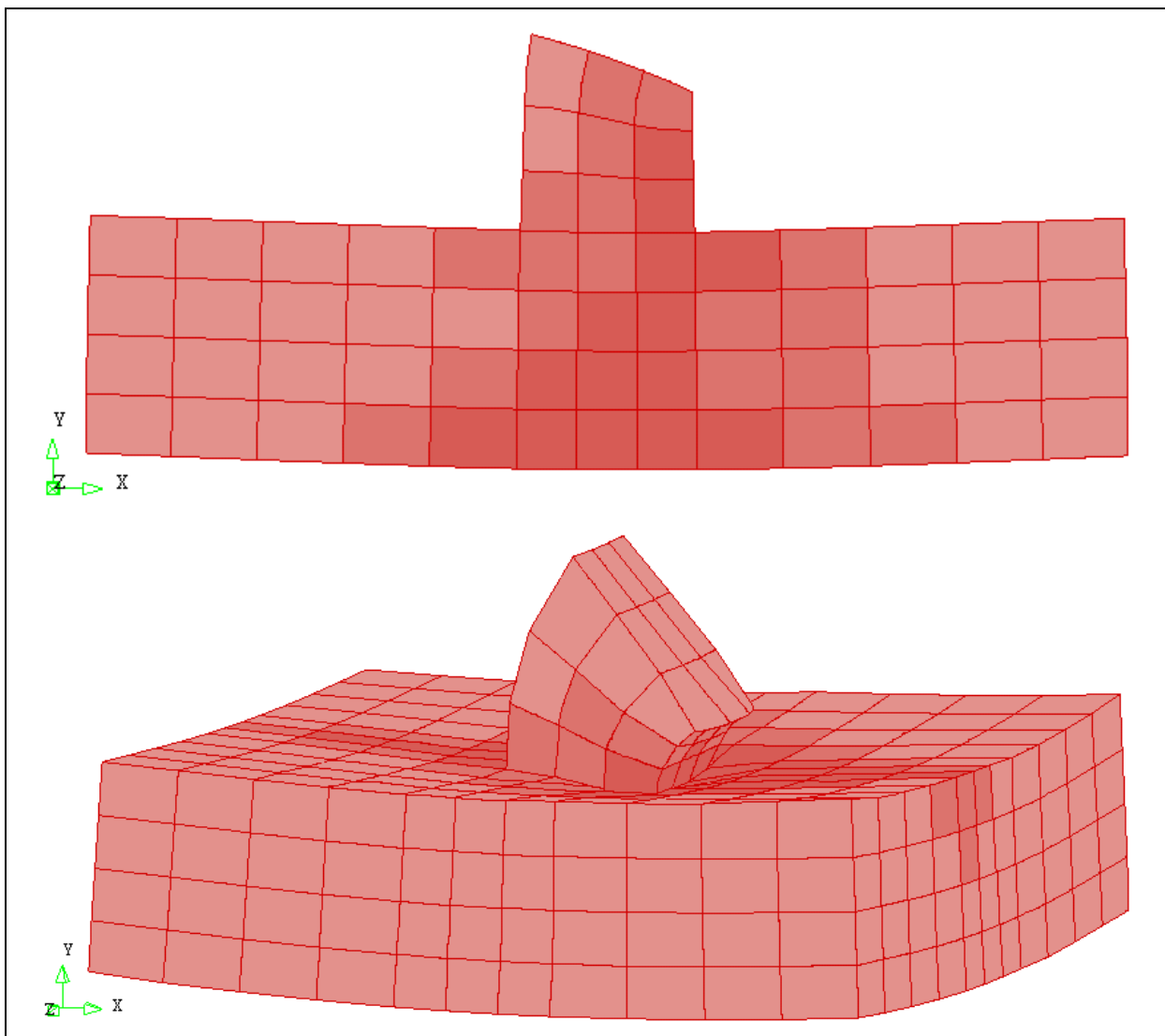
Figure 4.5: The deflected two- and three-dimensional model of the column and foundation under ultimate loading.

It is found that for the suggested method of stiffness modification, rotation of the foundation is of near identical amounts. The two-dimensional model gives a rotation estimation three percent more conservative than the reference three-dimensional model. As rotation is the main focus and primary concern, this is considered a satisfactory outcome for the proposed conversion method.

Overall the method suggested has greatly improved the compatibility of the model results. The two-dimensional model is in all cases the more conservative alternative and given the immense reduction in analysis time and that behaviour in areas of interest is found to be very similar, the goals of the conversion method are achieved.

4.3   Confirmation of Modelling Decisions

Before continuing with further investigations, some assumptions made in the modelling of this structure are verified next. The decision to exclude soil and subgrade settlement and plasticity is scrutinized in this section to be sure that their absence would not affect the accuracy and reliability of this study. This section contains the findings of either more complex analyses or the complete examination of current models in the quest to validate the assumptions made.

4.3.1   Phased Analysis

A phased analysis of the structure is performed to scrutinize the assumptions of the described boundary conditions described in chapter two. The settlement of soil and subgrade prior to the presence of a wind load is investigated to determine the effect, if any, on the rotation of the foundation. In this analysis the loading on the finite element model is divided into three phases. An initial settlement of the soil is allowed without the restriction of vertical displacements. In phase one the boundary conditions of edges one and three illustrated in figure 2.19, are therefore only pinned against translation in the x-direction. In the second phase all edges of the model are again pinned against all translations. The dead weight of the structure and own weight of the slab and foundation are applied in this phase. In the third and final phase the boundary conditions remain as in phase two and the loads and moments caused by wind are imposed on the model.

As can be seen in figure 4.6, a large amount of settlement takes place in the absence of the vertical constraints. The settlement of soil directly above the foundation is fractionally less than towards the edges. This difference is due to the presence of the foundation, the self weight of which is only included in the second phase. If there is soil in place of the concrete, uniform displacement would be found. This inadequacy of the model is however negligible and is not of concern as the aim of the phased analysis is not to determine subgrade settlement, but rather the effect it has on foundation rotation. As this fractional difference remains symmetrical about the column, it will have no effect on the rotation of the foundation.
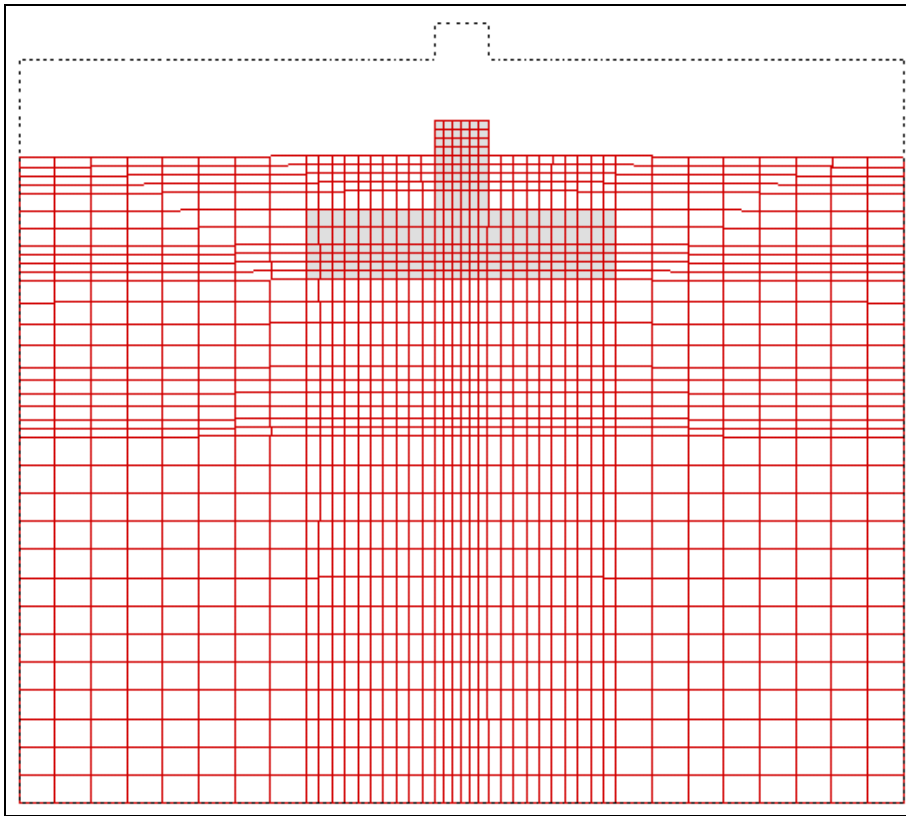
Figure 4.6: The total deformation of the model for phase one at a magnification factor of 100.

In phase two the own weight of the structure is added to the model and the deformation of the foundation-column system is illustrated in figure 4.7. The delamination of the interface in a phased analysis will not be comparable to that of a single phase analysis, that is, an analysis of one set of boundary conditions. This is due to entirely different deformation patterns between models, as will later be seen in figure 4.9. In the single phased analysis the pinning of the edges of the model causes a "pulling away" effect of the foundation from the soil at its top corners. This does however not effect the rotation of the foundation.
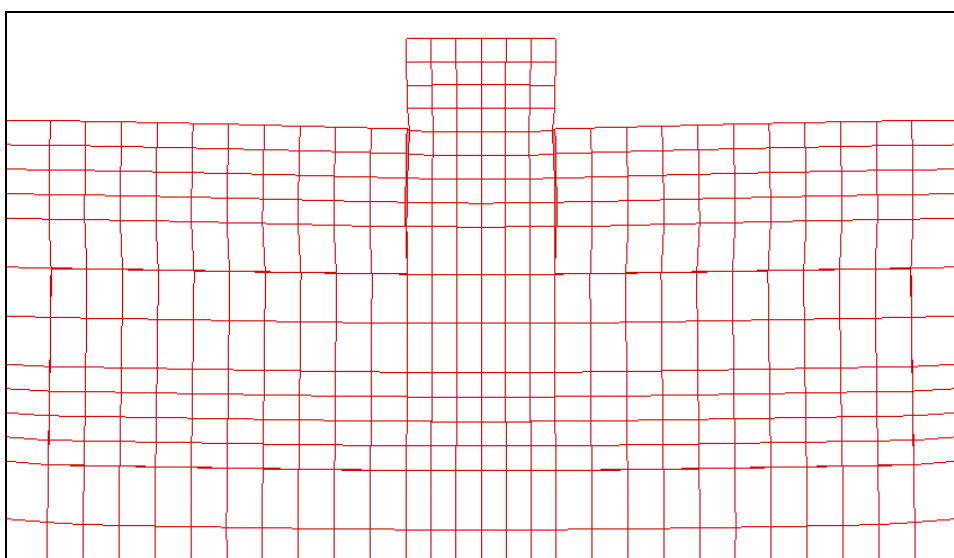
Figure 4.7: The delamination of the interface elements for phase two at a magnification factor of 500.

In the third phase it can be seen in figure 4.8 that the rotation of the foundation, despite different delamination of the interface elements, remains very similar to that of a single phase analysis later shown in figure 4.10.
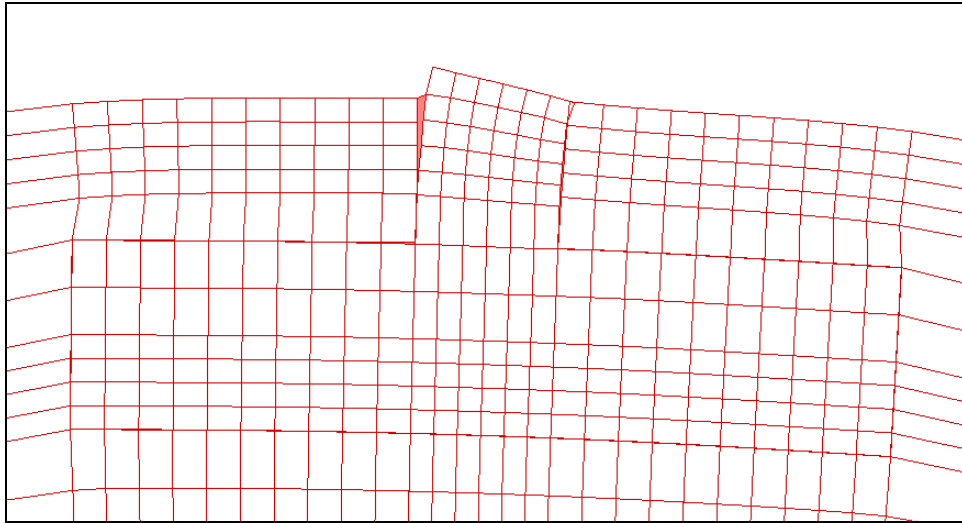
Figure 4.8: The delamination of the interface elements for phase three at a magnification factor of 500.

With a difference in rotation of between two and three percent between a three-phased and single phase analysis, the latter being the more conservative, it can be concluded that the settlement of soil plays no significant role in the mechanics that prevent or cause rotation of the foundation. As the phased analysis is considerably more time consuming due to convergence difficulties, the single phase analysis of the model described in chapter two will be used for all further investigations.

4.3.2   Testing of Soil Capacity

The decision to use linear elastic modelling for the soil is validated here by confirming that the bearing capacity of the soil is not exceeded. If a slip plane were to develop, the rotation of the foundation could potentially increase drastically. As the heavy structure offers more downward pressure on the subgrades, it would test the bearing capacity of the soil more severely than the lighter structure and is therefore the model used in the examinations in this section. The bearing capacities of the materials used in the model are given in table 4.3 below (Craig, 2004).

Table 4.3: Bearing capacities of materials used.

	Concrete	Cemented Gravel (C3)	Compacted Gravel (G7)	In-situ Clay
Bearing Capacity (kPa)	40000	2000	200-600	75-150

In the case of the compacted gravel and in-situ clay where there is a large difference between the upper and lower limits, the more conservative value is used. Contours of compressive stresses with values up till the bearing capacity of the compacted gravel are illustrated in figure 4.9. Values in the legend are negative as they are given in terms of global σ_y in Mega Pascal. From the sketch it is seen that for the ultimate limit load the bearing capacity of the compacted gravel is never exceeded except for local high stresses in the direct vicinity of the rotating column. This failure will however not be able to induce slip failure due to its local confinement. The overestimation of lateral resistance by linear elastic modelling in this regime is considered negligible, especially in the light of the presence of the significantly stiffer concrete floor. In figure 4.10, contours in the range of the bearing capacity of the in-situ clay are sketched and it can be seen that at no point is this capacity exceeded.
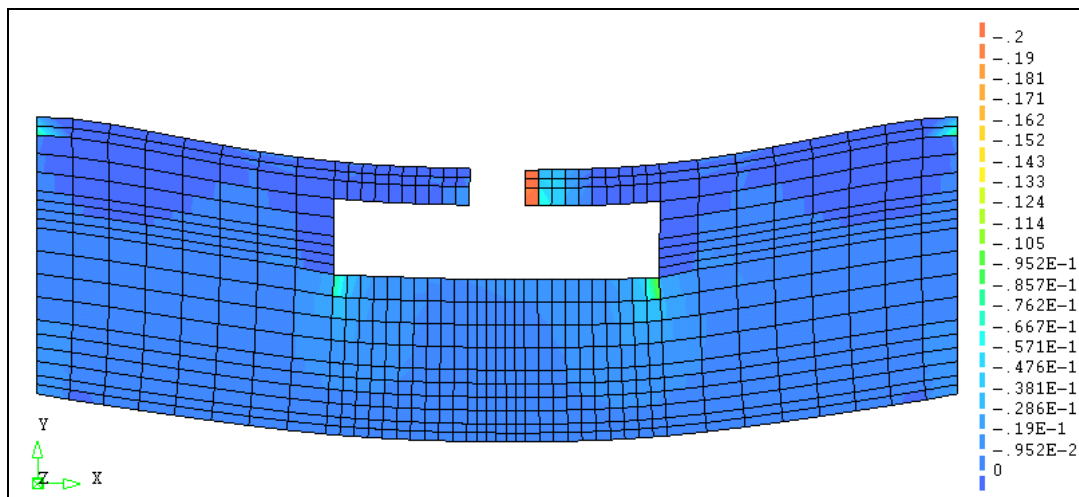
Figure 4.9: The vertical pressure (MPa) on the C3 and G7 materials at load factor one.
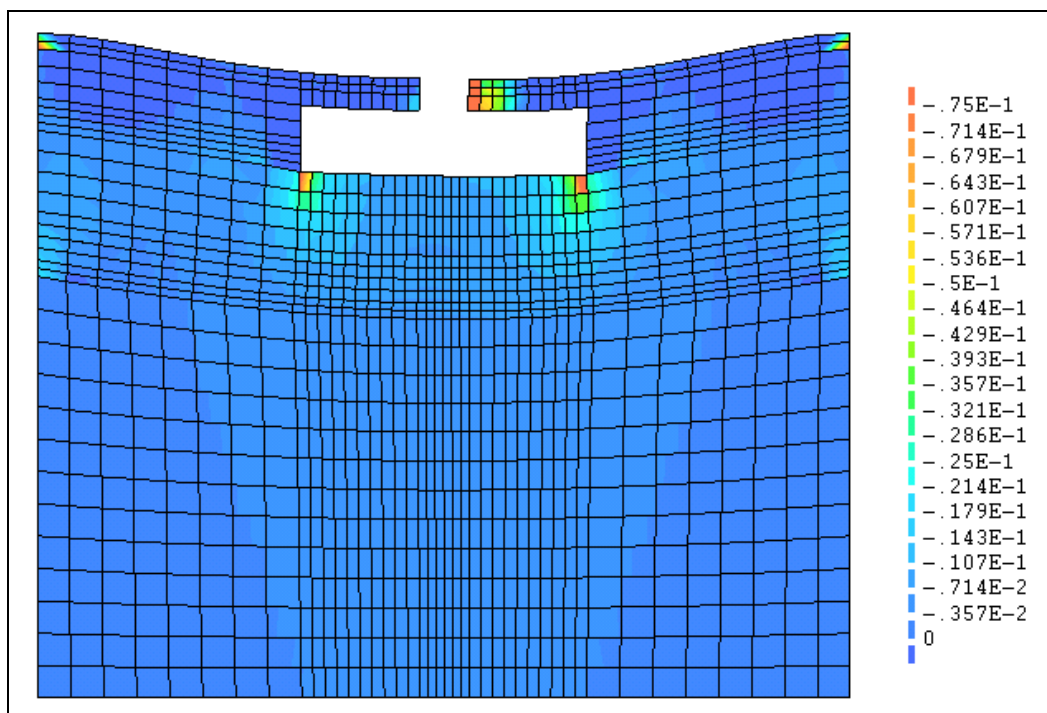
Figure 4.10: The vertical pressure (MPa) on all subgrade materials at load factor one.

At twelve times the ultimate limit load the bearing capacity of the soil is not yet exceeded. In the following chapter, various combinations of subgrade materials are investigated. The bearing capacity of the subgrade with the lowest stiffness is not exceeded for one times the ultimate load and only at seven times the ultimate load is the upper limit exceeded. As will be explained in the next chapter, this subgrade combination is an extreme case and is not commonly found in reality. All other subgrade combinations were confirmed capable of bearing the loaded foundation for twelve times the ultimate limit load.

It is therefore concluded that the decision to exclude the plasticity of the soil in investigations is acceptable for the purposes of this study.

4.4   Ultimate Limit Loading on the Heavy Structure

In this section the results are shown for the finite element model described in chapter two using interface elements as described by a multi-surface plasticity, under the loading assigned in chapter one. In figure 4.11 a contour diagram is shown of total displacements in millimetres of elements at one times the ultimate limit factor. The deformed shape of the model is shown at a factor two-hundred times that of actual displacement. The highest deformations take place in the vicinity of compression by the column overturning.
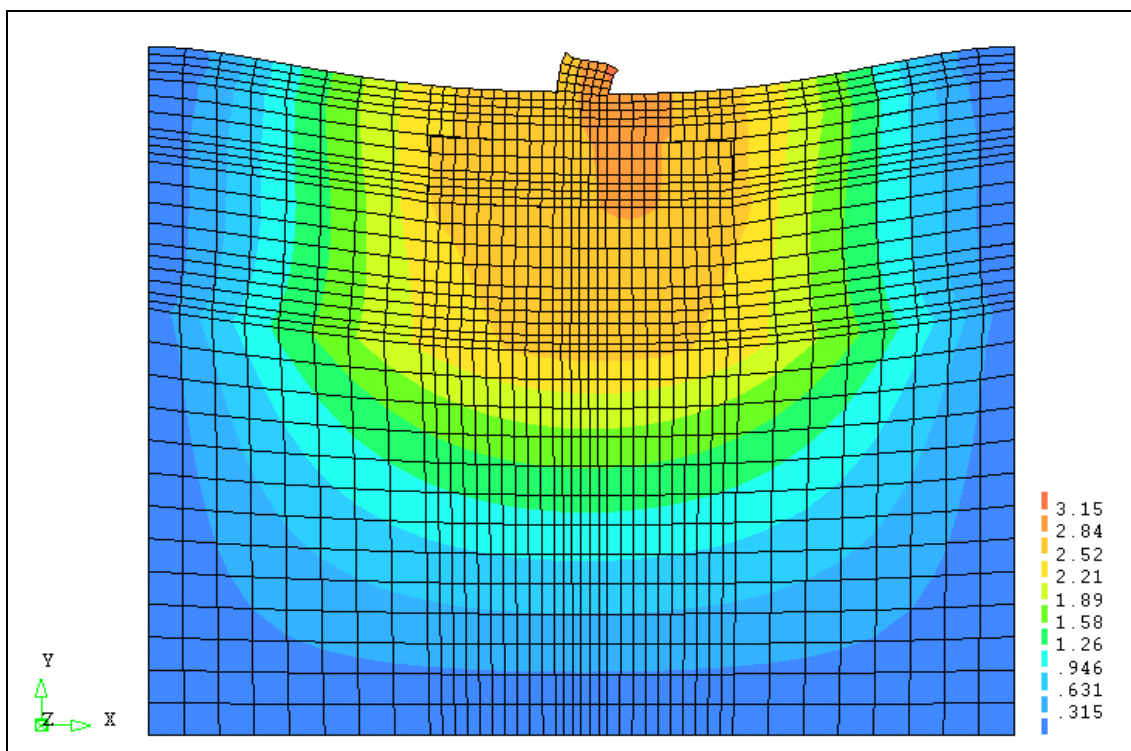
Figure 4.11: Total deformation for an ultimate limit load at a magnification factor of 200.

Elsje S. Fraser   University of Stellenbosch

These high values are a local occurrence and global values decrease incrementally around and beneath the foundation. The delamination of the interface is shown for increasing steps of the limit load in figure 4.12. The total dead load and self weight of the foundation are applied in an initial load step and the wind load is enforced in load step increments. The portion of the ultimate wind load applied is indicated in the diagrams below. No rotation can be seen in the foundation before the inclusion of the wind forces. Once the effect of the wind has been imposed on the structure the foundation starts to rotate. This rotation increases as the load factor increases, as can be seen in figure 4.12 at a magnification factor of 500.
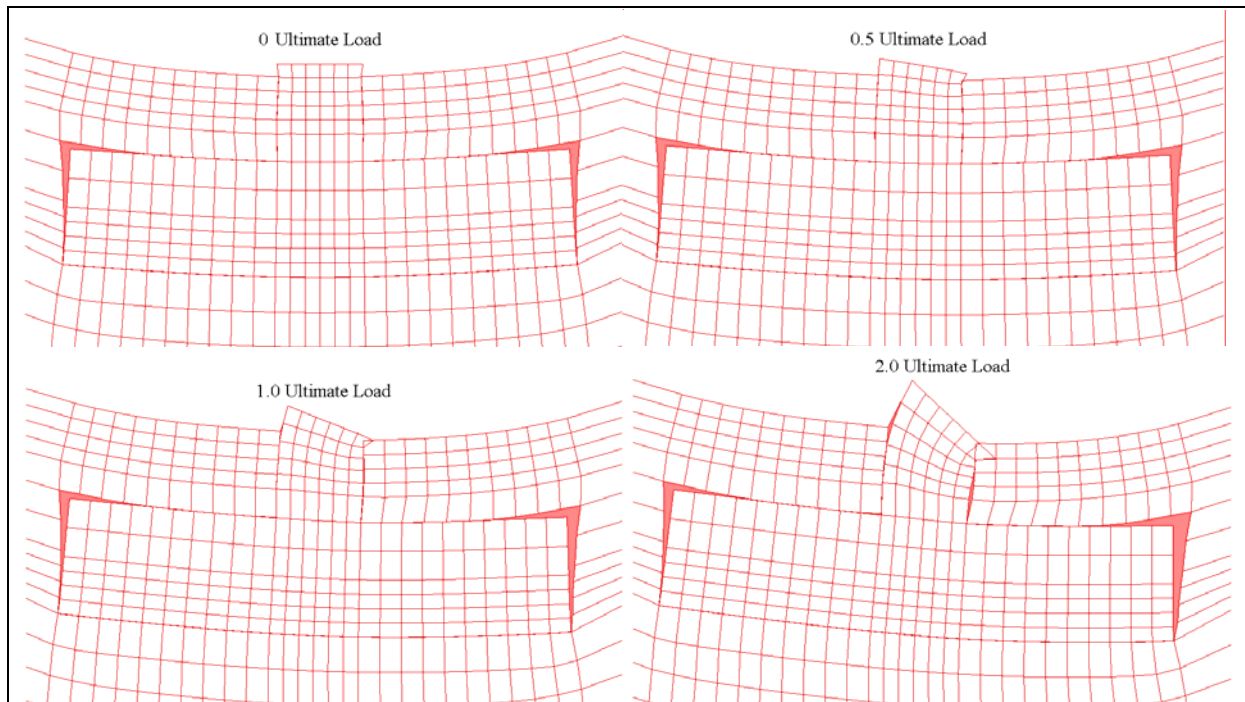
Figure 4.12: The delamination of the interface elements at a magnification factor of 500.

The wind load is applied to the structure up to twelve times that of the ultimate load. The rotation of the foundation is plotted against the corresponding load factor in figure 4.13.
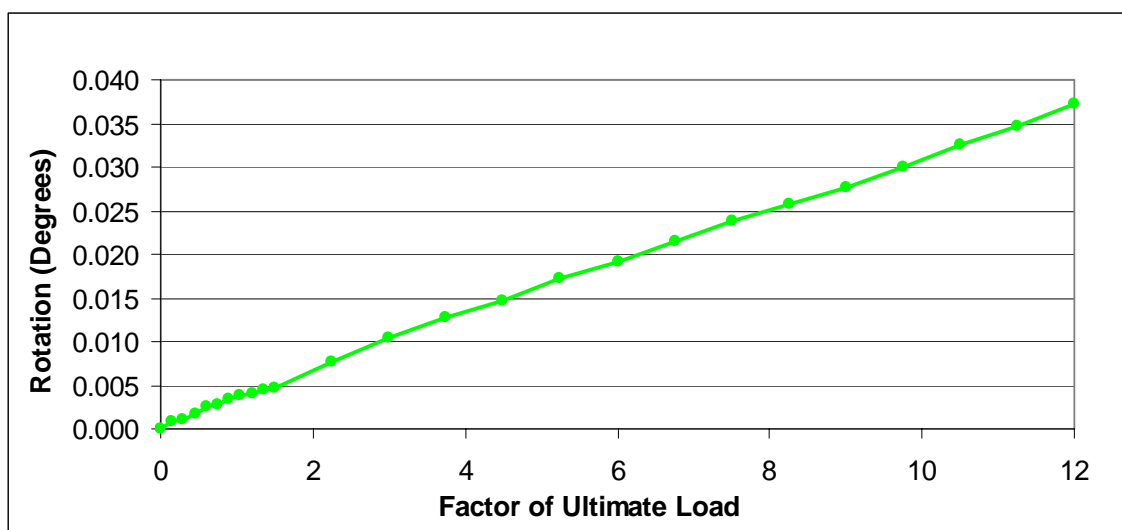
Figure 4.13: Rotation of foundation versus ultimate load factor for the heavy structure.

If failure of the structure were to occur due to the rotation of the foundation, the gradient of the rotation-load plot would start to increase rapidly as the foundation would become unstable. The uniform gradient of the line indicates that this state has not been reached, even at twelve times the wind load for this particular foundation size. It can therefore be concluded that this structure will not fail due to foundation rotation. The lateral displacement at the top of the column due to the rotation of the foundation causes no concern at the low levels of rotation experienced here. For one times the ultimate limit load the column is expected to translate laterally by less than a millimetre, as shown below.

$$\delta = L \cdot \tan\theta, \quad \text{where} \ \ L = 11\,\text{m} \ \ \text{and} \ \ \theta = 3.66 \times 10^{-3}$$
$$= 11 \cdot \tan(3.66 \times 10^{-3})$$
$$= 0.7027\,\text{mm}$$

4.5 Ultimate Limit Loading on the Light Structure

As for the heavy structure above, results for the light structure model described in chapter two using interface elements of a multi-surface plasticity under normal loading, are shown in this section. Figure 4.14 shows a contour diagram of total displacement for the ultimate load at a factor two-hundred times that of actual displacement.
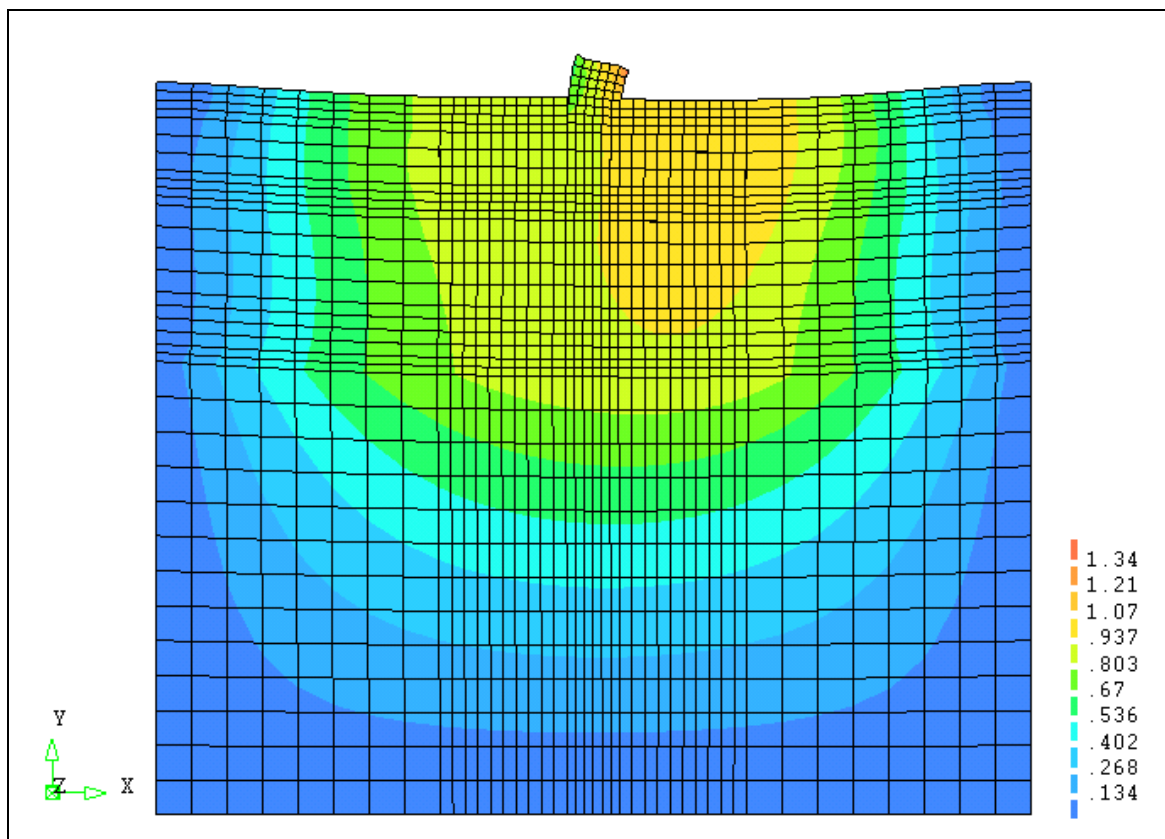
Figure 4.14: Total deformation for an ultimate limit load at a magnification factor of 200.

Elsje S. Fraser   University of Stellenbosch

The delamination of the interface is shown for increasing steps of the limit load in figure 4.15. As was done for the heavy structure, the total dead load and self weight of the foundation are applied in an initial load step and the wind load is enforced in load step increments, causing rotation. This rotation increases as the load factor increases, as can be seen in figure 4.15 at a magnification factor of 500.
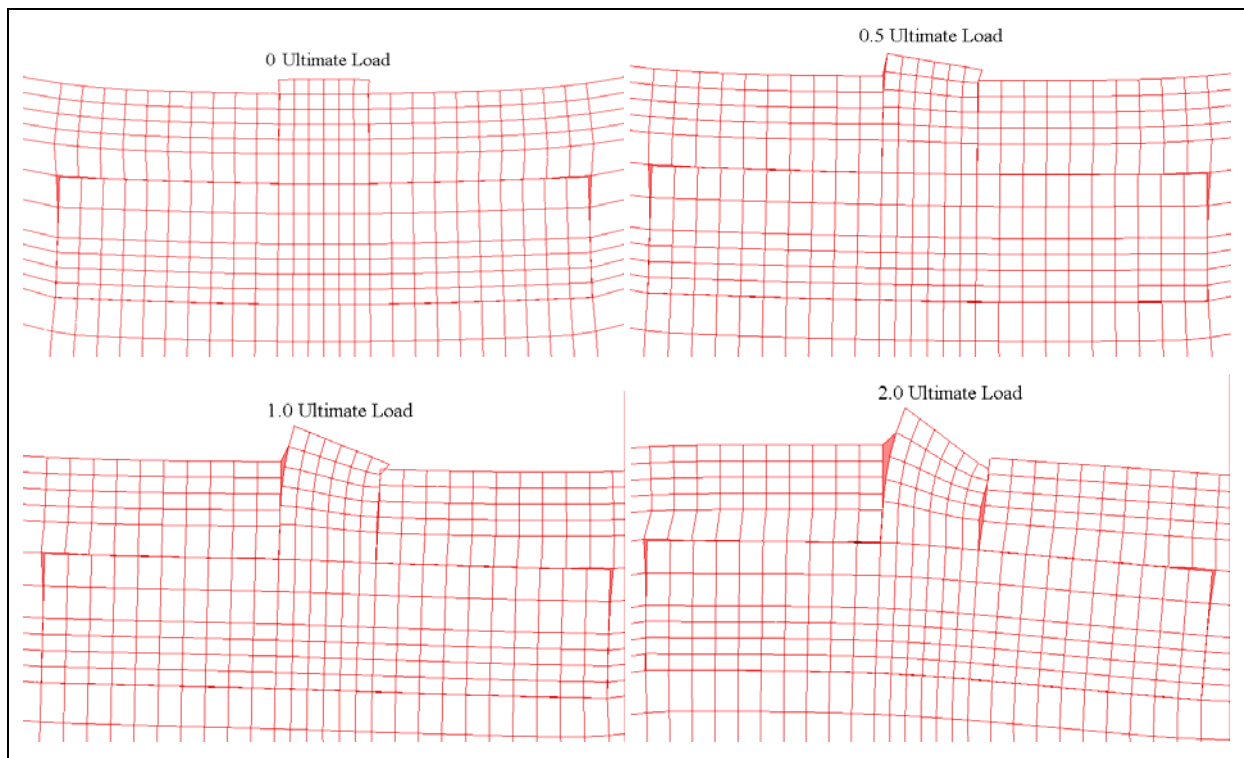
Figure 4.15: The delamination of the interface elements at a magnification factor of 500.

Under the application of the dead loads, no rotating of the foundation takes place. The foundation experiences compression into the subgrade below. Once wind forces are included, the foundation begins to experience both rotation and uplifting. The effect of this uplifting does not surpass the dead weight of the structure until twice the ultimate wind load. When this happens, the foundations starts to lift up off the subgrade below itself and starts pressing upwards causing undesirable stresses on the slab. The wind load is applied to the structure up to nine times that of the ultimate load. The rotation of the foundation is plotted against the corresponding load factor in figure 4.16. As there are no interface elements between the slab and soil, the finite element model is not adequate to represent the uplifting of the foundation and slab at excessive upward wing loading. This is because once the foundation starts to press against the slab, the slab elements will not be able to pull away from the soil beneath it, as would be the true sequence of events. This causes inaccurate results for the load-rotation plot outside this critical area. This phenomena does however fall outside the scope of this thesis, as described in chapter one, as this presents a whole new failure criterion and is the

responsibility of the design engineer to ensure that the self weight of the foundation is sufficient restraint against uplifting.
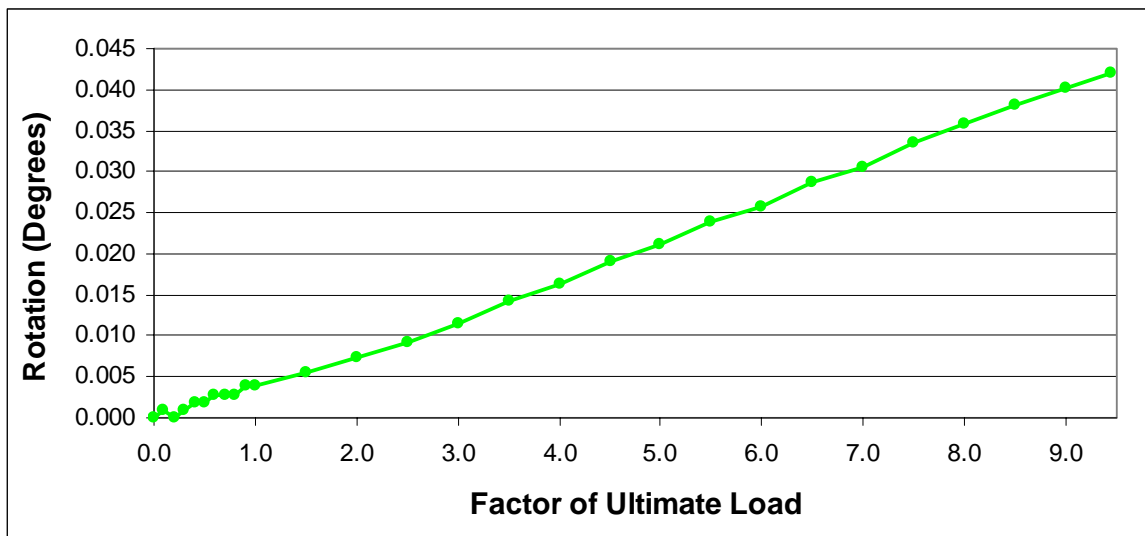
Figure 4.16: Rotation of foundation versus ultimate load factor for the light structure.

As the rotations from figure 4.16 can be trusted only up to twice the amount of the ultimate limit load (equalling the total downward structural self weight), figure 4.17 details a closer inspection of the valid area. The same foundation will rotate less if it formed part of a heavy structure, seen in figure 4.17. These rotations are still very low and less than a millimetre of lateral displacement will occur at the top of the column for the ultimate load and is therefore not a threat to structural stability.
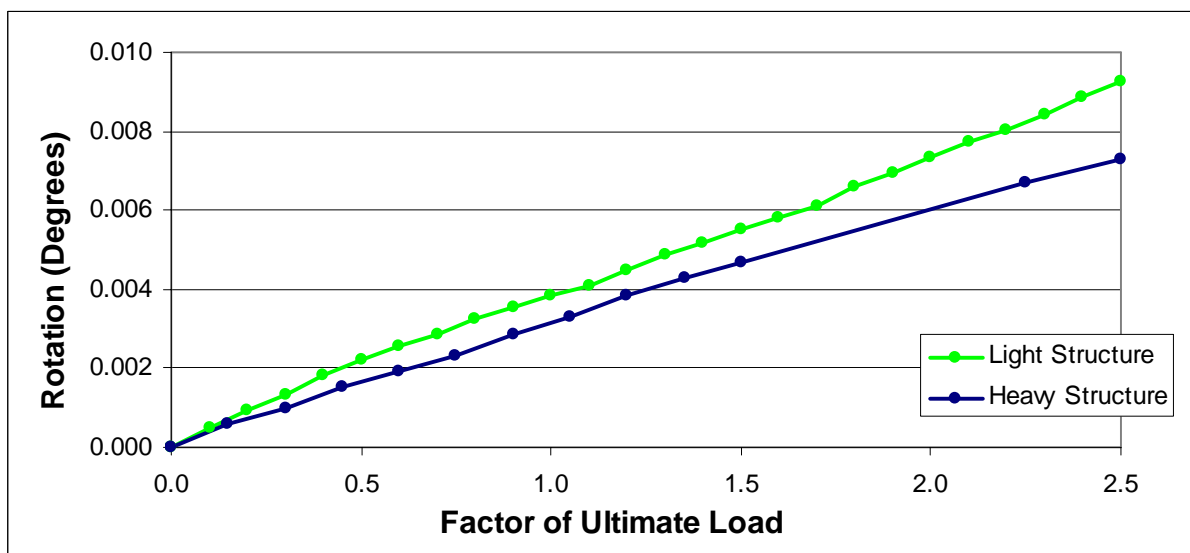
Figure 4.17: Rotation of foundation versus ultimate load factor for both structures.

5.   FACTORS CONTRIBUTING TO FOUNDATION ROTATION

As seen in the previous chapter, for the given loading conditions, foundation size, soil types and concrete strengths, neither the heavy or light structures are nearing instability due to the rotation of the foundation. The results are however the outcome of a specific case study. This chapter aims to generalise the behaviour of such structures by investigating factors that effect the rotation of the foundation. Such factors included the material properties of the subgrades present, the size of the foundation, and more that will be discussed in the sections to follow. Investigations in this chapter are carried out on the heavy structure using the multi-plastic interface element, unless otherwise stated, and the behaviour found is confirmed briefly for the light structure for some factors studied.

5.1   A Variation of Subgrade Materials

Few elements of a foundation-soil system would effect deformations and displacements as much as the material properties of the subgrade. Three alternatives to the subgrade layout previously described and illustrated in figure 2.5, are chosen and are discussed in this section. Two models with considerably higher or lower soil stiffness are considered. The case of lower stiffness is illustrated in figure 5.1. In this case there is no G7 compacted gravel present but instead only the in-situ clay subgrade. The C3 cemented layer directly below the slab is still considered for this case.
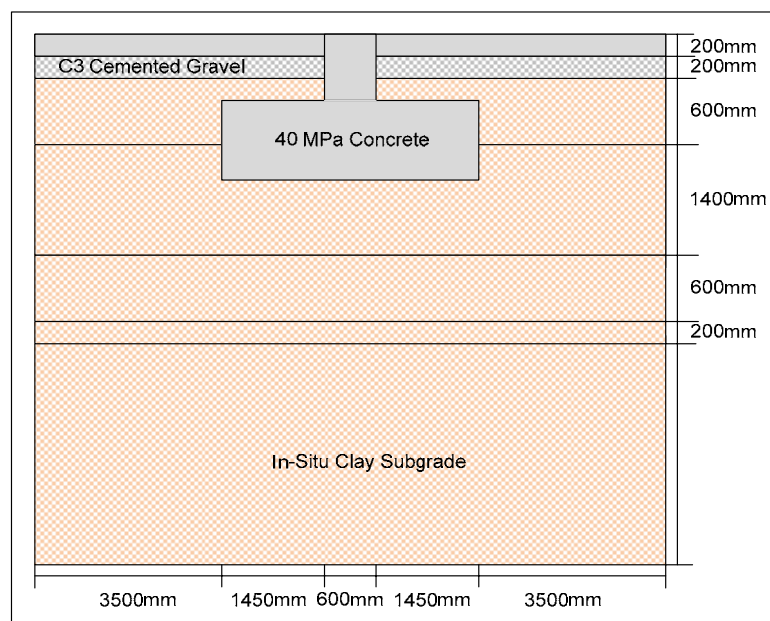
Figure 5.1: Layout and dimensions of subgrade with low stiffness.

The case of a higher stiffness is illustrated in figure 5.2 Again there is no G7 compacted gravel present, but in this case the void is filled with C3 cemented gravel which lies three meters deep starting directly below the slab. The actual construction of such a subgrade would be very expensive but the purpose of the investigation is to consider the effect of a more stiff material than currently prescribed.
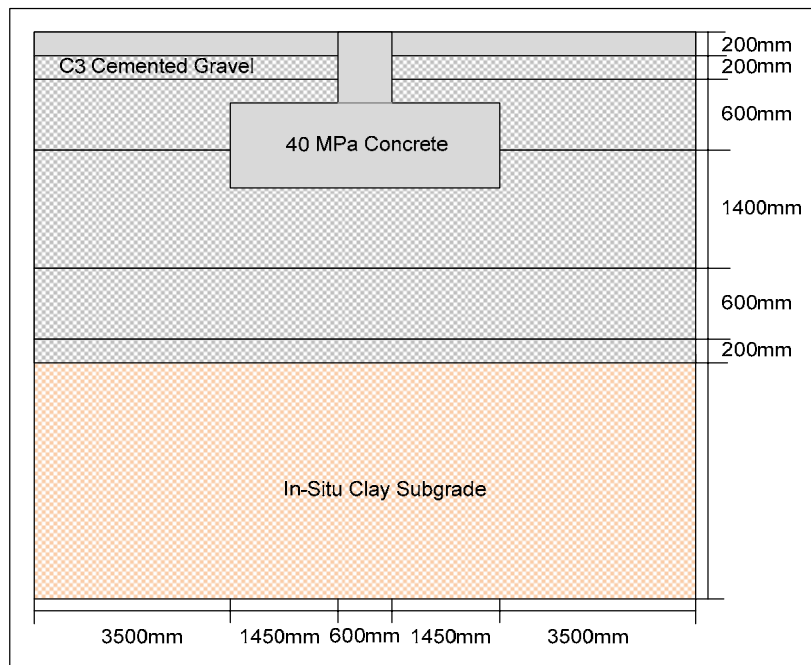
Figure 5.2: Layout and dimensions of subgrade with a high stiffness.

The third alternative investigated has subgrade specifications similar to the original subgrade specifications, but with an additional 200 mm layer of C3 cemented gravel directly beneath the foundation.
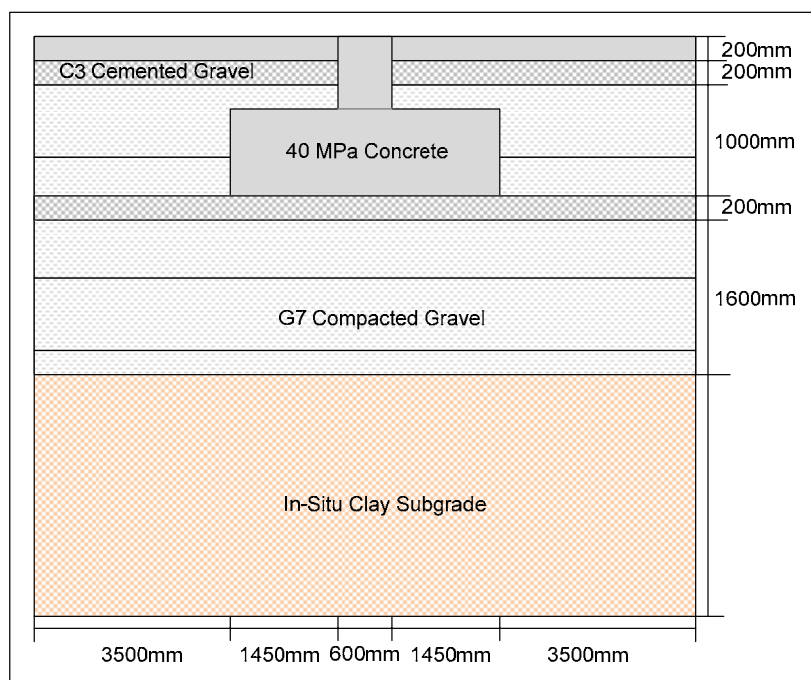
Figure 5.3: Layout and dimensions of an alternative subgrade stiffness.

The wind load is applied to structure up to nine times that of the ultimate load. The rotation of the foundation is plotted against the corresponding load factor in figure 5.4 for all the subgrade variations discussed. The most apparent change in foundation behaviour in terms of rotation is the enormous increase in rotation found when replacing the G7 compacted gravel with in-situ clay. This drop in stiffness causes rotation of the foundation that is five times higher than that of the original soil stiffness. By adding a layer of C3 cemented gravel to lie directly below the foundation, the rotation of the foundation is halved. With the expensive alternative of using only C3 cemented gravel instead of G7 compacted gravel, the rotation can be reduced six times. It can be concluded that in a case where rotation of the foundation may lead to structural instability, a thin layer of stiff material directly below the foundation is a cost-effective way to significantly reduce rotation.
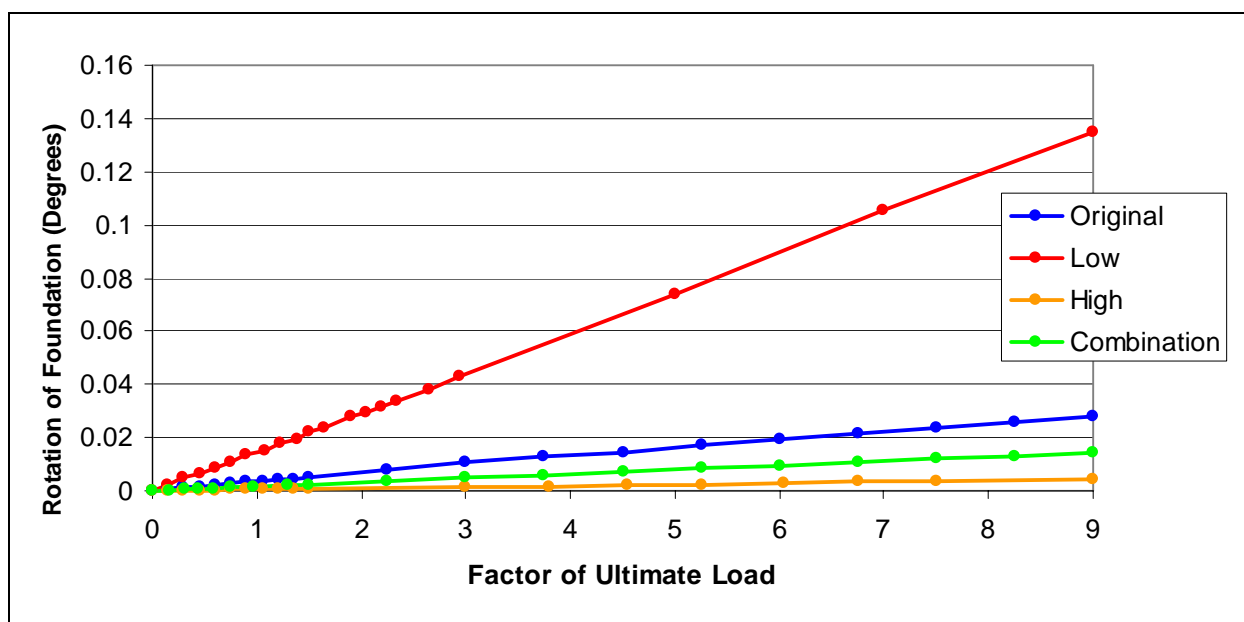
Figure 5.4: Rotation versus ultimate load factor for a variation of subgrade stiffness.

Further investigations in this chapter will show results for the original subgrade composition and the compositions of subgrade alternatives. In all cases the type of composition will refer to those described in this section.

5.2　　Changes in Foundation Size

One of the factors influencing the rotation of the foundation under a constant load is its size. A smaller foundation is expected to rotate more than a larger one. This is due to the decrease in the contact area between the concrete and soil providing less frictional resistance, and the reduction of resistance to a constant moment carried to the foundation via the column. The latter can be

illustrated by means of a simple calculation and is shown in figure 5.5. A moment is applied to a column and in a very simplified approximation of the problem, the soil resists against the moment at the two corners shown. It is deduced here that if the foundation width are halved, resistance forces at the corners will need to be larger to prevent more rotation than before. As the subgrade is not infinitely stiff, larger deformations than before will be a result and more rotation will therefore occur.

$$M = \frac{1}{2} L_1 \cdot F_1 \cdot 2 = L_1 F_1$$

$$\text{if} \quad L_2 = \frac{1}{2} L_1,$$

$$\text{then} \quad M = L_1 F_1 = \frac{1}{4} L_2 \cdot x \cdot 2$$

$$\therefore \quad F_2 = 2 F_1$$
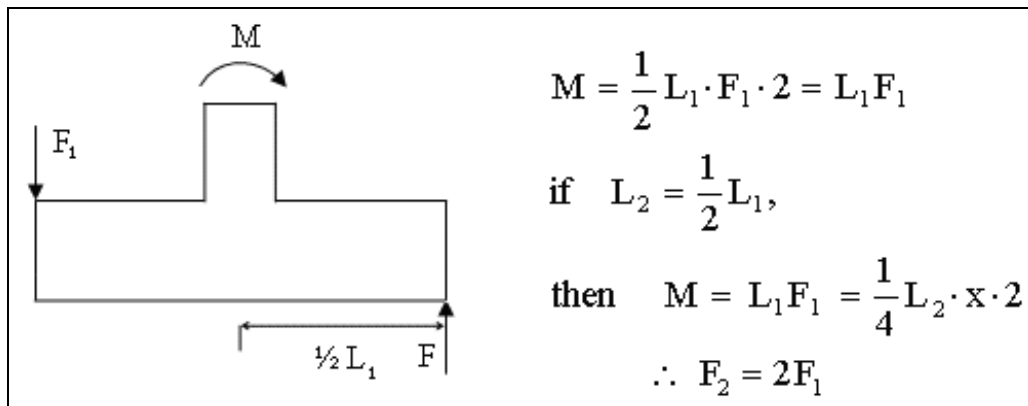
Figure 5.5: A simple rotation resistance problem for a changing foundation width.

5.2.1 Original Subgrade

The theoretical calculation above is confirmed by examining figure 5.6. It can clearly be seen how the delamination of the interface elements increases from a foundation of a four meter width to one of one-point-seven-five meters. The increase in delamination of the interface is due to a larger vertical downward displacement of the foundation under the compressive dead weight of the structure above, and less resistance to rotation as the foundation decreases in size.
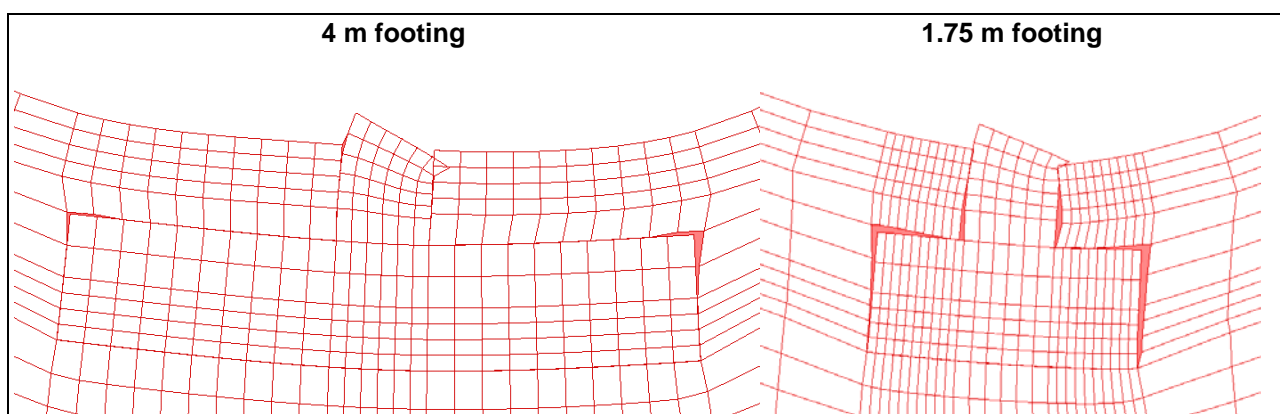
Figure 5.6: Delamination of interface elements for the ultimate load viewed at a factor of 500.

The rotation angle versus factor of ultimate limit loading is plotted in figure 5.7 for the original foundation width of 3.5 meters, and is accompanied by the plots of a 4 meter and a 1.75 meter foundation. For every new width of the foundation chosen, a new set of soil depth dimensions

and locally increased stiffness around the foundation, as described in section 4.2.2, has to be determined. In addition, a new finite element model boundary perimeter has to be calculated for each new foundation using equation 2.1.

Heavy Structure
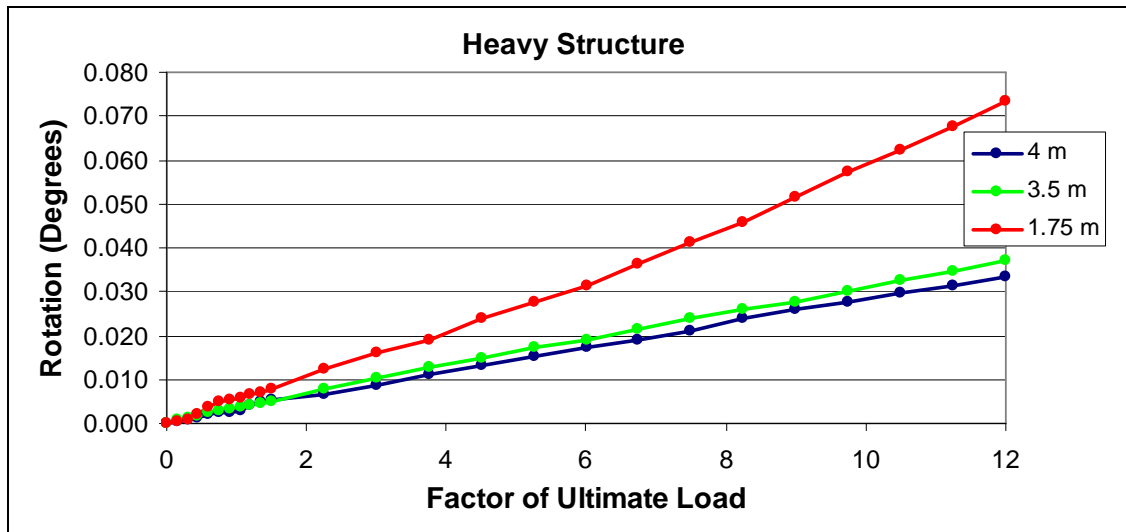
Figure 5.7: Rotation versus ultimate load factor for a variation of foundation widths.

It can clearly be seen how the rotation decreases for a larger foundation and increases for a smaller one. The upward curling plot of the smallest foundation shows that it increases more rapidly than the larger foundations with linearly increasing plots. This behaviour is confirmed for the light structure as a rotation-load plot similar to that of the heavy structure, shown above, is constructed using test results for foundations of various sizes under uplifting wind forces. The factor of the ultimate load is limited to the region just after the foundation starts to lift up off the subgrade below, indicated by the black dots on the plot in figure 5.8. The finite element model in not sufficiently designed to consider uplifting and further results would be inaccurate. It is also a scenario which must be prevented by the designer; the footing weight together with other permanent loading must provide sufficient anchorage to prevent uplift.

Light Structure
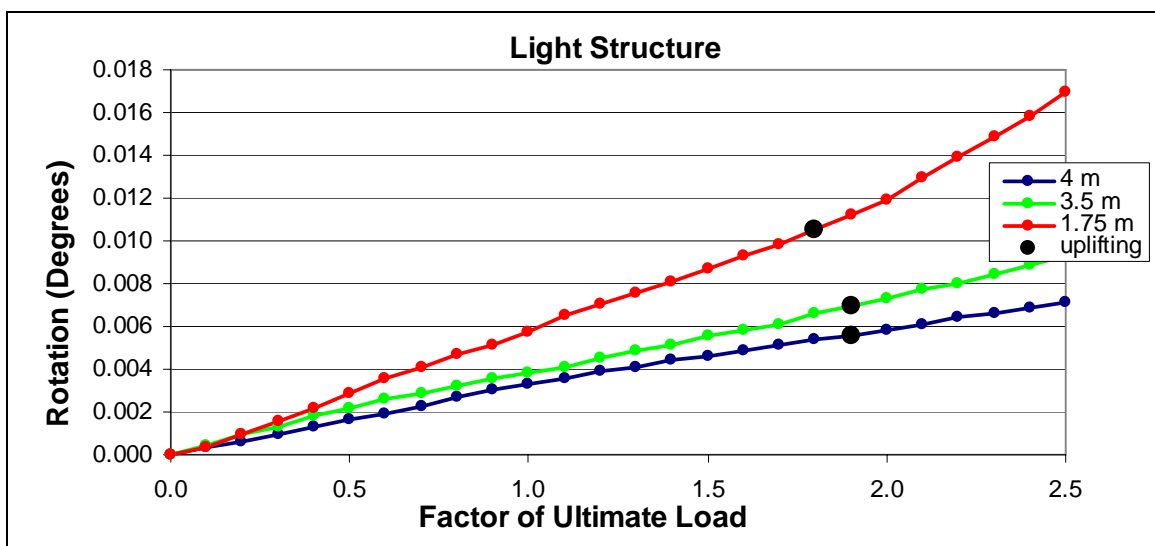
Figure 5.8: Rotation versus ultimate load factor for a variation of foundation widths.

It can also be concluded that not only does a smaller foundation rotate more; it will lift up earlier under an uplifting wind load, as can be seen in the figure 5.8. The opposite is also true for a compressive load where it was found that the smaller foundation sinks into the subgrade sooner than a larger one. This could be seen in figure 5.6 above judging from the delamination of the interface and gradient of the slab.

The effect of the foundation sizes is investigated for all three types of interface models discussed in chapter three. The amount of rotation for each foundation at one times the ultimate wind load is plotted in figure 5.9. The effect of a difference in the material laws of nonlinear elastic interface element versus the combined crushing-shearing-cracking and friction interfaces can clearly be seen in the graph shown in figure 5.9. The reasonable agreement between the responses predicted by the friction model and those predicted by the crushing-shearing-cracking graphs can be attributed to the fact that both capture the main mechanisms. The sudden drop in tensile and shear resistances of the friction model versus the softening curves of the crushing-shearing-cracking model would cause small dissimilarities as the fracture energies under the softening curves are small and resistances drop to zero very quickly. The absence of a compression strength limit in the friction model should also not come into play as the limit prescribed to the other interface models is never reached. The predictions by the simpler nonlinear elastic model differ significantly from the other two models. The major deficiency of this model is that it does not incorporate pressure-dependent friction increase. For the investigations done in this study, the nonlinear elastic interface has proven capable of inexpensively predicting trends in behaviour of the structure as it does resemble, though inaccurately, the results of the other two interface types.
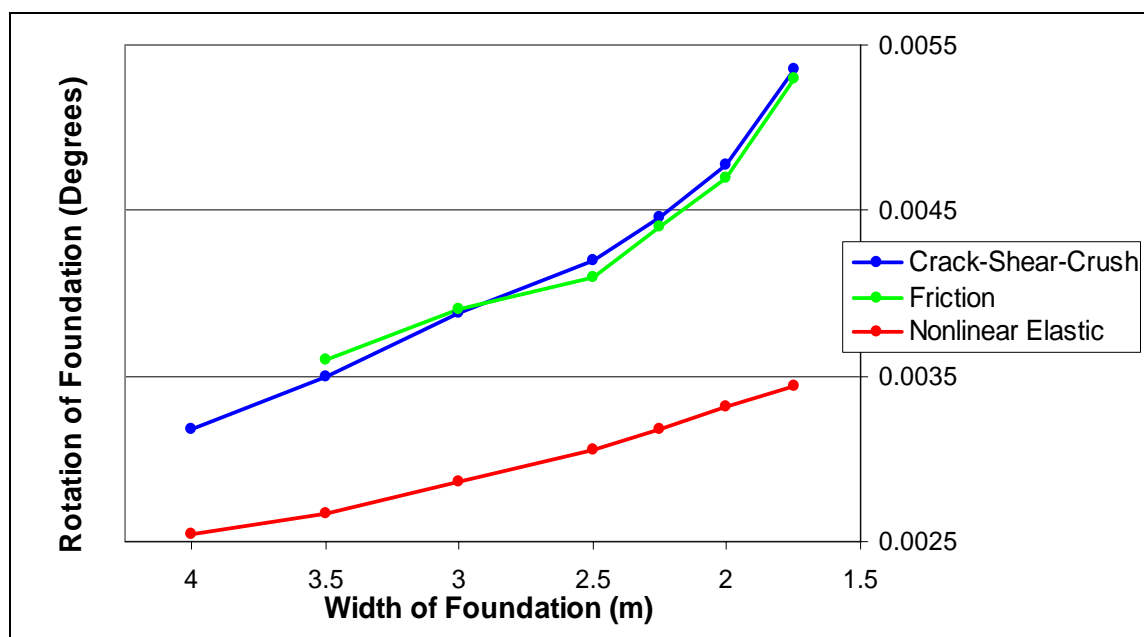
Figure 5.9: Rotation of various foundation sizes for all three interface elements.

From the above it is clear that the foundation rotation increases more rapidly as the foundation size decreases. It is therefore concluded that the reduction of foundation size causes more and more rapid rotation and that a smaller foundation will rotate sooner and more extensively as the ultimate load is increased.

5.2.2   Other Subgrade Combinations

The same tests of varied foundation size, described in the above section, are done for the other soil subgrade combinations identified in section 5.1. For these analyses the inaccurate nonlinear elastic interface model is used to predict structural behaviour and these tests are followed by the problem prone convergence of the crushing-shearing-cracking and friction interface models. The same behaviour is found for all other subgrade combinations as for the original subgrade. A reduction in foundation size means an increase in the rotation of the foundation. Smaller foundations rotate sooner and more rapidly and the reduction of foundation size leads to speedier rotations. The difference between subgrade combinations for the accurate interface models are only as a result of the soil stiffness used in each case. As shown by figure 5.4, a foundation surrounded by soil of a low stiffness will rotate more than one in soil of a higher stiffness. Therefore a small foundation in soil of low stiffness will rotate several times more than a large foundation in stiff soil. The rotation of each individual foundation at one times the ultimate load is given in table 5.1 for all subgrade combinations for the combined crushing-shearing-cracking model. It can be determined from this table what the relation between foundation rotation is for all variations investigated. This is done in table 5.2 where rotations of all foundations are given as a percentage of that of the original foundation size and subgrade.

Table 5.1: Rotation of all foundations investigated at one times the ultimate load.

(Degrees)	Soil Stiffness Types			
	High	Combination	Original	Low
4 m	4.46×10^{-04}	1.46×10^{-03}	3.01×10^{-03}	1.15×10^{-02}
3.5 m	4.77×10^{-04}	1.56×10^{-03}	3.66×10^{-03}	1.50×10^{-02}
1.75 m	6.37×10^{-04}	2.23×10^{-03}	5.44×10^{-03}	3.49×10^{-02}

Table 5.2: Rotation of all foundations investigated as a percentage of the original rotation.

(Percentage)	High Stiffness	Combination	Original	Low
4 m	12.19	39.89	82.24	314.21
3.5 m	13.03	42.62	100	409.84
1.75 m	17.40	60.93	148.63	953.55

Plots for all the other subgrade combinations are given in Appendix B.1. This includes plots of rotation versus foundation width for one times the ultimate load and rotation versus an increasing factor of the ultimate for various foundation sizes, as shown in figures 5.7 and 5.9.

5.3   Changes in Elasticity Modulus and Presence of the Slab

The elasticity modulus used for the slab, as given in table 2.1, is in many cases much lower as designers may use concrete of a lower strength than that of structural elements, for economical reasons. The elasticity modulus of the slab is reduced for the original subgrade combination and foundation dimensions and the new rotation plotted on the graph in figure 5.10.
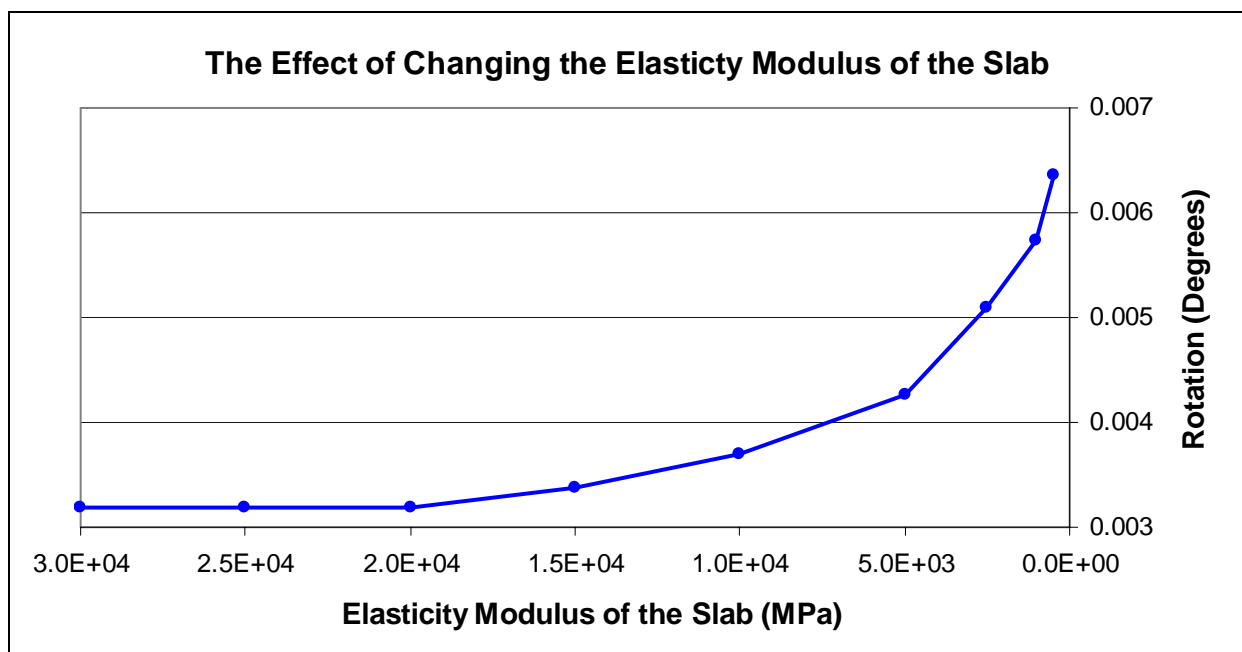
Figure 5.10: The effect of changing the elasticity modulus of the slab on rotation.

Halving the elasticity modulus of the slab only increased the rotation of the foundation by six percent. Using a layer of C3 cemented gravel instead of concrete increased rotation by 160 percent. A further reduction of the elasticity modulus to that of G7 compacted gravel increased rotation twofold. A slab of this type of material does start to become unrealistic as it would not be used in practice. The influence area of the slab and C3 cemented layer under most stress shown in figure 4.9 on rotation is investigated. The total absence of a slab and C3 cemented layer is also considered. These results are shown in figure 5.11. The complete absence of the slab and C3 cemented layer causes rotations four times higher than the original model. The partial removal results in a 260 percent increase. This large increase of the latter is because of the resistance the slab gives against the overturning column. By removing this part of the slab,

greater column rotation leads to higher levels of foundation rotation. This information will prove to be valuable in the next chapter when modelling the subgrades and supporting components with springs instead of continuum elements.
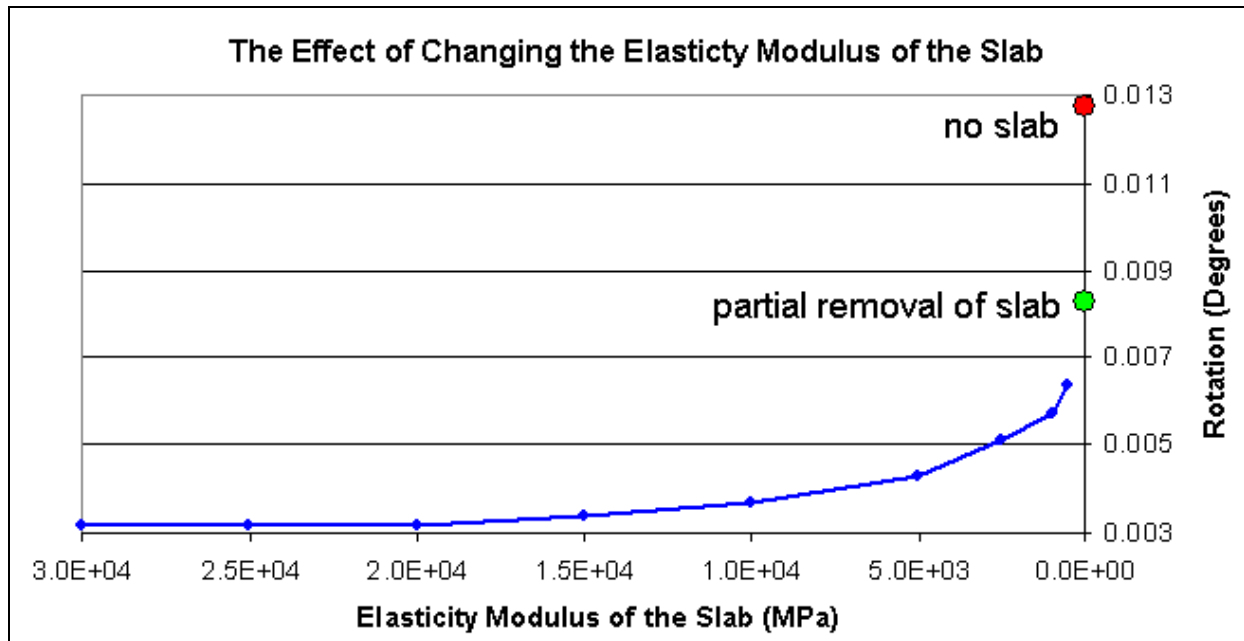
Figure 5.11: The effect of total and partial removal of the slab on rotation.

The same tests are done for the other subgrade combinations. The same behaviour described above is found for the all subgrade combinations (see figure 5.12). An initial decrease in stiffness of the slab does not effect the rotation of the slab. Halving the elasticity modulus of the slab influences the rotation by a fraction. Slabs of lower stiffness are not commonly used in practice. It can therefore be concluded that by using a concrete of a lower grade will not drastically increase rotation of the foundation. The absence of the concrete material or slab entirely could however cause structural instability as large increases in rotation are found.
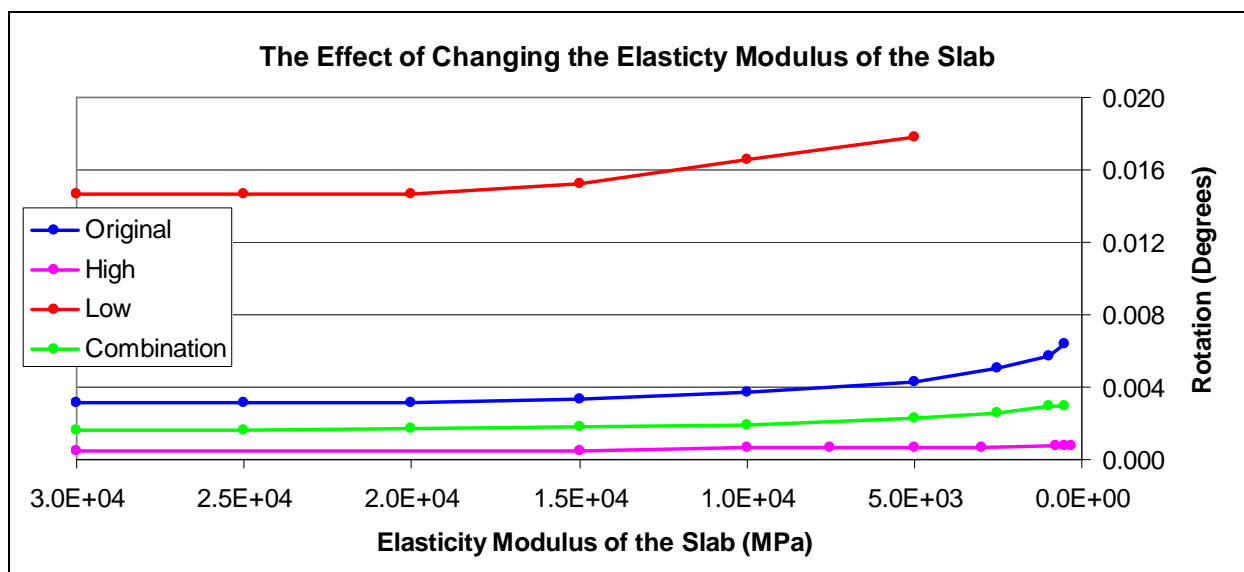
Figure 5.12: The effect of changing the elasticity modulus of the slab for alternative subgrades.

5.4 The Presence of Expansion Joints

The presence of relatively small gaps at the base of the column to allow for expansion joints, commonly used in the industry, have the potential to significantly effect the rotation of the foundation. These joints are filled with material of relatively low stiffness which can effectively be considered as zero. This would mean that should the filler material be compressed, its thickness would deform from typically ten millimetres, to zero; its presence can be ignored and only a physical gap between column and slab need be included in investigations to study its effect. Provided the soil surrounding the foundation is sufficiently stiff to prevent the foundation from "drifting away", it is assumed the foundation will rotate about its centre of gravity. In a worst case scenario, an infinitely stiff column-foundation element, allowing no bending or local deformations, is used to determine the upper limit of the rotation possibilities due to a gap. This allows for maximum rotation and therefore lateral displacement at the top of the column. This displacement would be in addition to that caused by the deformations due to loading. Figure 5.13 shows how to determine this rotation.

$$\theta = \tan^{-1}(b/\ell)$$
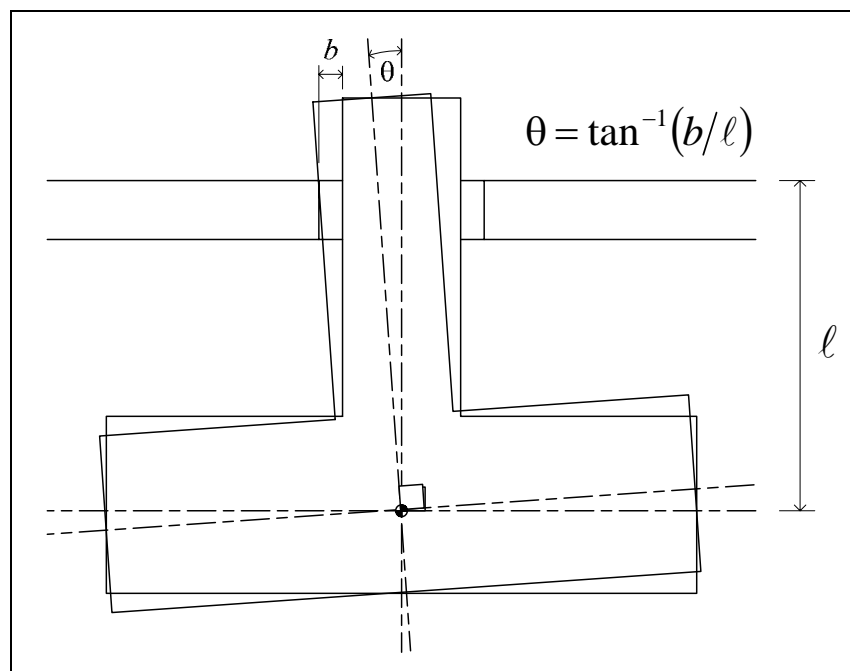
Figure 5.13: The rotation of a stiff column-foundation system in the presence of joints.

$$\theta = \tan^{-1}(b/\ell) \qquad 5.1$$

where ℓ = distance from the top of the slab to the centroid of the foundation,

and b = thickness of the gap of rubber.

In the case of the originally prescribed foundation and model dimensions, the following is found:

Elsje S. Fraser University of Stellenbosch

b = 10 mm, ℓ = 1000mm

$\therefore \theta = 0.573°$

$\therefore$ lateral displacement at the top of the column = 110 mm

If however the centre of gravity of foundation is shallower, say half the depth of the case study above, it is found the lateral displacement increases to 220 mm.

ℓ = 500mm, $\therefore$ lateral displacement = 220 mm

If the thickness of the gap is also halved, the lateral displacement will remain at 110mm.

ℓ = 500mm and b = 5 mm, $\therefore$ lateral displacement = 110 mm

It is therefore concluded from the simple geometrical study above that for an infinitely stiff column-foundation element, the depth of the foundation below the slab and the width of the expansion joint may be the biggest factors contributing to rotation of the foundation and ultimately the cost of the structure.

As an infinitely stiff column-foundation element is neither likely nor possible, a rubber is included in the finite element model and its presence is investigated. The material and geometrical properties are given in table 5.3.

Table 5.3: Material and geometrical properties of the joint filler material.

Elasticity Modulus	Normal Modulus (k_n)	Shear Modulus (k_s)	Bond strength	Thickness
0.5 GPa	50 N/mm^3	5 N/mm^3	0.01 N/mm^2	10 mm

These values indicated a much lower stiffness for the filler material than that of the interface or slab materials. The bond strength however remains the same as in table 3.1. This means that to represent the joint behaviour with the nonlinear elastic model the gradient of the compression-tensile curve between the compressive and tensile strengths, shown in figure 3.14, will be much lower. The nonlinear elastic interface model is again used to initially indicate the behaviour of foundation. For neither the combined crushing-shearing-cracking nor the nonlinear elastic models is there any significant difference in the rotation of the foundation over increasing increments of the ultimate wind load when the expansion joint is included in the design (see figure 5.14). The same is found for the subgrade of a higher stiffness and the combination alternative. Their plots are given in Appendix B.2.
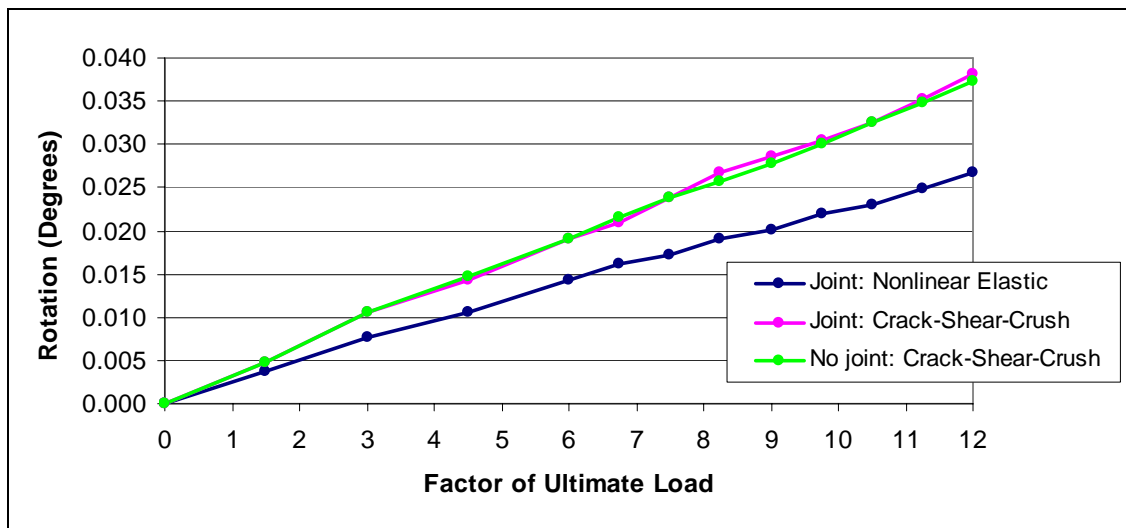
Figure 5.14: Rotation versus the factor of ultimate load for the inclusion of an expansion joint.

It can be concluded that for the given column-foundation material properties, an expansion joint of ten millimetre thickness will not cause the increase in rotation as predicted by the worst-case scenario or the order of rotation in the partial absence of the slab as found in the previous section. This is due to the column not being infinitely stiff; instead the column rotation increases locally (see figure 5.15). With the remainder of the slab still present in addition to the whole C3 cemented layer as in figure 5.11, there is ample resistance to prevent further overturning of the column. The addition of a ten millimetre rubber around the column will therefore not affect structural stability unless the conditions start to approach those of a worst-case scenario.
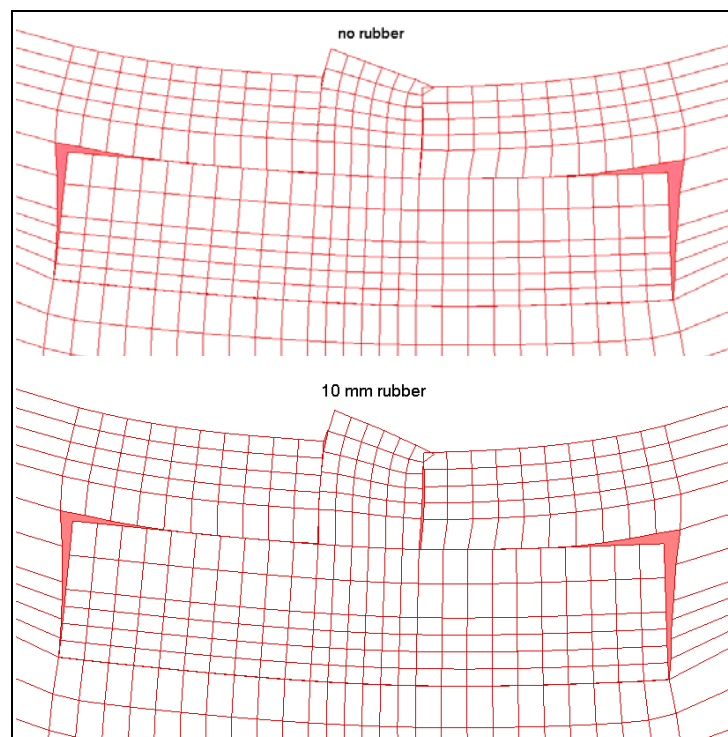
Figure 5.15: The delamination of the interface at a magnification factor of 500 with and without expansion joints.

5.5   The Effect of Connection Joints

In a structure of the magnitude as for this case study with floor spans 100 by 80 metres, the slab is made up of smaller segments which are practically possible to build, but also allow expansion/shrinkage movement. These units are connected at movement joints by metal joints or other forms of shear interlocking which are meant to transfer stresses from one to another (see figure 5.16).
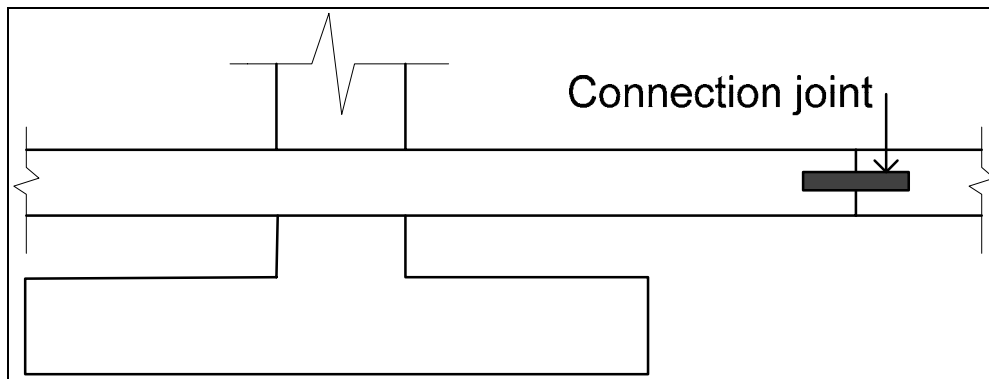
Figure 5.16: Structural connection joint used to combine segments of the slab.

The event of failure of the connection joints to transfer stresses or hold the slab in place is investigated in this section. To simulate this phenomenon, the boundary conditions of both edges slab of the slab were released and the slab set free to move in all directions without translational constraint. It is therefore assumed that such joints are located far from areas experiencing compression or rotation while the structure is under ultimate loading. The original foundation and subgrade combination is used in this investigation. The ability of the slab to move freely at the edges can be seen in the deformed view of the model in figure 5.17.
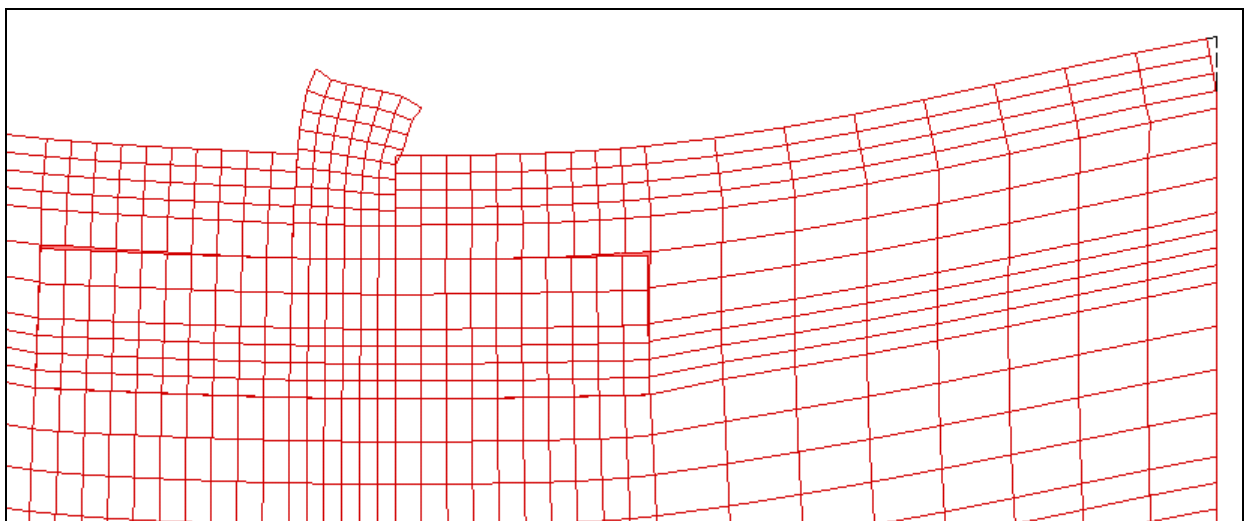
*Figure 5.17: A deformed view of the free ended slab for ultimate limit loading at a
              magnification factor 500.*

Although the slab edges are free from constraints and the connection joints had therefore failed, there is no increase found for the rotation of the foundation. It is concluded that if connection joints are positioned in non-critical areas, their failure will not affect structural stability.

5.6   Conclusions

It can be concluded from the investigations carried out in this chapter that several factors can greatly influence the behaviour of the structure while others do not at all.

As expected, subgrade materials of a higher stiffness offer more resistance to the displacements of foundations than materials of a lower stiffness. This means that higher levels of rotation will occur in a subgrade comprised of clay than would have in compacted or cemented gravel. Changing the size of the foundation has the same effect on the behaviour of the foundation where a small foundation rotates more than a large one under the same loading. Combining these factors gives a whole range of behaviours. An example is that a small foundation of one1.75 meters with a thin layer of C3 cemented gravel directly beneath it rotates about the same as a large four meter foundation would without the presence of a stiff layer of subgrade material beneath it. Another example is that for the same loading a small foundation embedded in clay will rotate eighty times more than a large foundation surrounded by C3 compacted material.

The grade of concrete used for the slab need not be a high standard to prevent rotation but a slab must however be present to offer resistance to the overturning of the column. A concrete strength sufficient to carry this compression should be used.

Neither the use of expansion joints in close vicinity of the column nor movement joints to allow free movement of slab segments will cause a significant increase of the rotation of the foundation, provided they are used sensibly.

6. DESIGNING A TWO-DIMENSIONAL LINEAR SPRING MODEL

Ultimately the goal of this study is to design a two-dimensional linear spring model that can be assembled using software commonly available in engineering design offices. This model must provide the user a simple method to predict, with reasonable accuracy, the rotations that can be expected from a foundation under various loading or subgrade conditions. This chapter details the method recommended to the user to craft such a spring model.

6.1 Literature Study

Several methods exist which makes it is possible to represent the soil mass with linear springs. A method which includes soil properties, the composition of the subgrade structure, the dimensions of the foundation and the depth of the foundation below the surface is considered in this study. This method makes use of the modulus of subgrade reactions.

6.1.1 The Modulus of Subgrade Reaction

The modulus of subgrade reaction is widely used in the structural analysis of continuous footings, mats and pilings. Here it is applied to the foundation members investigated in this study. It is the conceptual relationship between soil pressure and deflection and is defined by the basic equation $k_S = q/\delta$, where q is the average measured pressure and δ the average measured displacement under a load P for a stacked plate test. A direct relationship between E_S and k_S, where E_S is the elasticity modulus of the soil, can be found and is given in equations 6.1 to 6.3. The discussion of this process can be found in chapter 9.6 of *Foundation Analysis and Design* (Bowles, 1996).

$$k_s = \frac{q}{\delta} = \frac{\Delta q}{\Delta H} \qquad\qquad 6.1$$

with
$$\Delta H = q_0 B' \frac{1-\mu^2}{E_S}\left(I_1 + \frac{1-2\mu}{1-\mu}I_2\right)I_F \qquad\qquad 6.2$$

where q_0 = intensity of contact pressure in units of E_S

  B' = least lateral dimension of contributing base area in units of ΔH

Elsje S. Fraser   University of Stellenbosch

I_i = influence factors, which depend on L/B, thickness of stratum H,

Poisson's ratio μ, and base embedment depth D

$E_S, μ$ = elastic soil parameters.

From equations 6.1 and 6.2, the stiffness of a spring representing a soil mass is as defined in equation 6.3 below.

$$k_s = \frac{1}{BE_S' I_S I_F}$$ 6.3

with $I_S = I_1 + \dfrac{1-2\mu}{1-\mu} I_2$

where $I_1 = \dfrac{1}{\pi}\left[M \ln \dfrac{\left(1+\sqrt{M^2+1}\right)\sqrt{M^2+N^2}}{M\left(1+\sqrt{M^2+N^2+1}\right)} + \ln \dfrac{\left(M+\sqrt{M^2+1}\right)\sqrt{1+N^2}}{M+\sqrt{M^2+N^2+1}} \right]$

$I_2 = \dfrac{N}{2\pi} \tan^{-1}\left(\dfrac{M}{N\sqrt{M^2+N^2+1}} \right)$, $\tan^{-1}$ in radians

while $M = \dfrac{L'}{B'}$ and $N = \dfrac{H}{B'}$

for which $B' = \dfrac{B}{2}$ for centre ; = B for corner and $L' = \dfrac{L}{2}$ for centre ; = L for corner

and I_F can be obtained from figure 6.1:
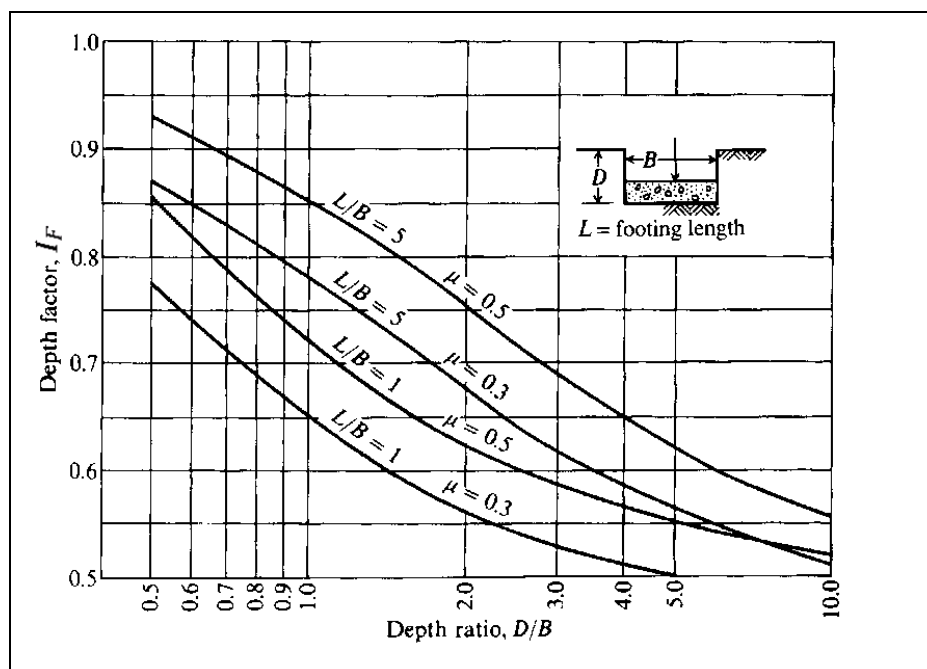
Figure 6.1: The influence factor I_F for footings at a depth D (Bowles, 1996).

Elsje S. Fraser   University of Stellenbosch

and $\quad E_S^{'} = \dfrac{\left(1-\mu^2\right)}{E_S}$

where $\quad E_S = \dfrac{H_1 E_1 + H_2 E_2 + \ldots + H_n E_n}{H}$ is the weighted average E_S at depth H for *n* layers.

As can be seen in figure 6.2, the substructure below the foundation does not contribute equal amounts of resistance. For the most of the substructure combinations discussed in chapter five, using a weighted average to determine E_S would give an overly conservative approximation of the soil stiffness. This is because the soil directly below the foundation, the soil offering the most resistance, according to figure 6.2 and as seen in figure 4.10, has a much higher elasticity modulus than the in-situ clay further below the foundation. To account for the larger contribution of the soil closer to the foundation base, the author proposes the modification of the stiffness by consideration of soil layer position according to equation 6.4. This equation uses figure 6.2 to determine the piecewise contribution of each layer of subgrade. The calculation of E_S for the original subgrade combination is given in Appendix C.

$$E_S = \dfrac{E_1 \left(\sum {q}/{q_0}\right)_1 + E_2 \left(\sum {q}/{q_0}\right)_2 + \ldots + E_n \left(\sum {q}/{q_0}\right)_n}{\sum {q}/{q_0}} \qquad 6.4$$
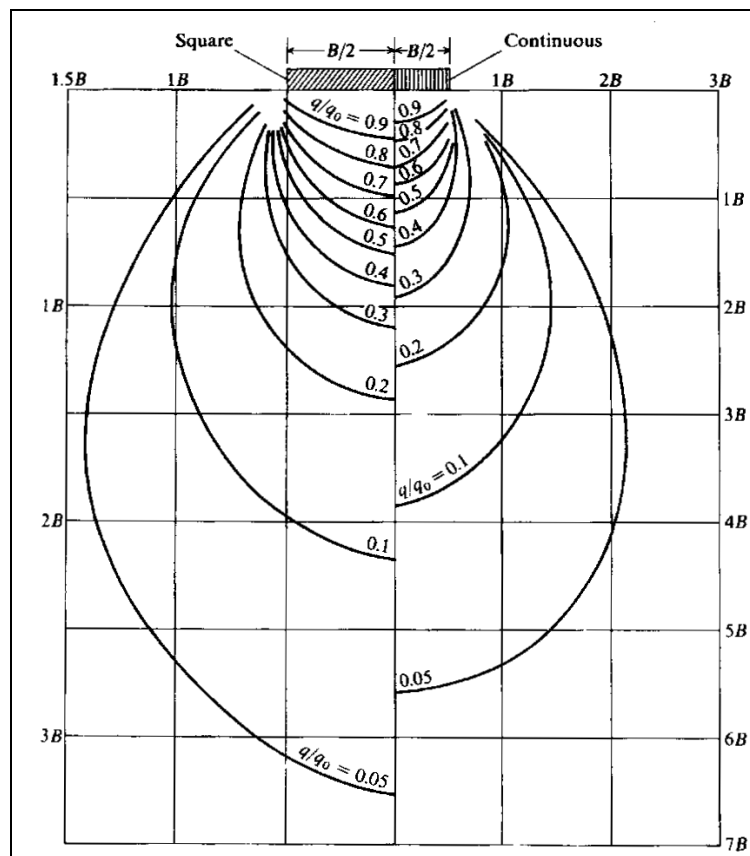
Figure 6.2: The pressure bulbs for square and long footings (Bowles, 1996).

6.1.2   Support of the Column

As seen in chapter four in figure 4.9, high stresses occur in the slab and C3 cemented layer adjacent to the overturning column. Figure 5.11 shows the importance of this area in preventing rotation of the foundation. Misinterpretations of contributions to the stiffness value for these two layers at this crucial point of rotation prevention can lead to inaccurate results. The area of slab resisting the deforming of the column is not considered as merely a straight strip from the column edge to the model boundary, but instead as a larger area as shown in figure 6.3. This area depends on the angle θ chosen by the user.
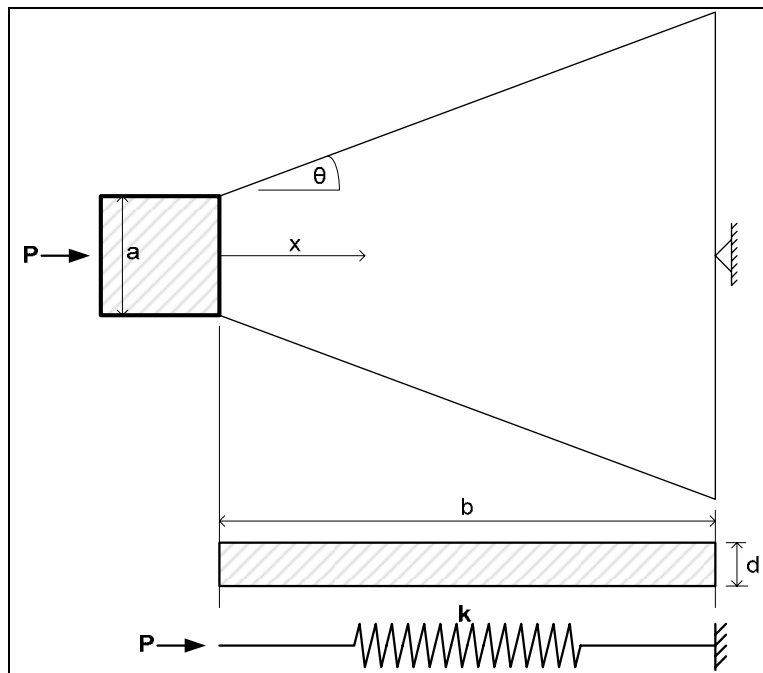
Figure 6.3: The plan view of a spring representing an area resisting the deforming column.

The deflection Δ of a spring representing an area loaded under an overturning force P, for dimensions given in figure 6.3, can be determined for a constant strain ε as follows:

$$\Delta = \int_0^b \varepsilon \, dx \qquad = \int_0^b \frac{P}{AE} \, dx \qquad = \frac{P}{E} \int_0^b \frac{1}{A(x)} \, dx$$

$$= \frac{P}{E} \int_0^b \frac{dx}{d(a + 2x \tan \theta)}$$

$$= \frac{P}{dE} \left(\frac{1}{2 \tan \theta} \cdot \ln|(a + 2x \tan \theta)|_0^b \right)$$

$$= \frac{P}{2dE\tan\theta} \cdot \ln\left(\frac{a + 2b\tan\theta}{a} \right)$$

$$= \frac{P}{k}$$

From this the stiffness k of this area is given in equation 6.5 below.

$$k = \frac{2dE\tan\theta}{\ln\left(1 + \dfrac{2b}{a}\tan\theta \right)} \qquad\qquad 6.5$$

6.2   Calculation and Application of Stiffness Values

The springs representing the soil masses are connected to the edges of the column and foundation. As discussed above, the stiffness values can be determined for each side, centres and corners, of the foundation. A layout of these areas is given in figure 6.4. The end zones (corner areas) are taken as B/6 as done in chapter nine of *Seismic Design for Buildings* (HQUSACE, 1998).
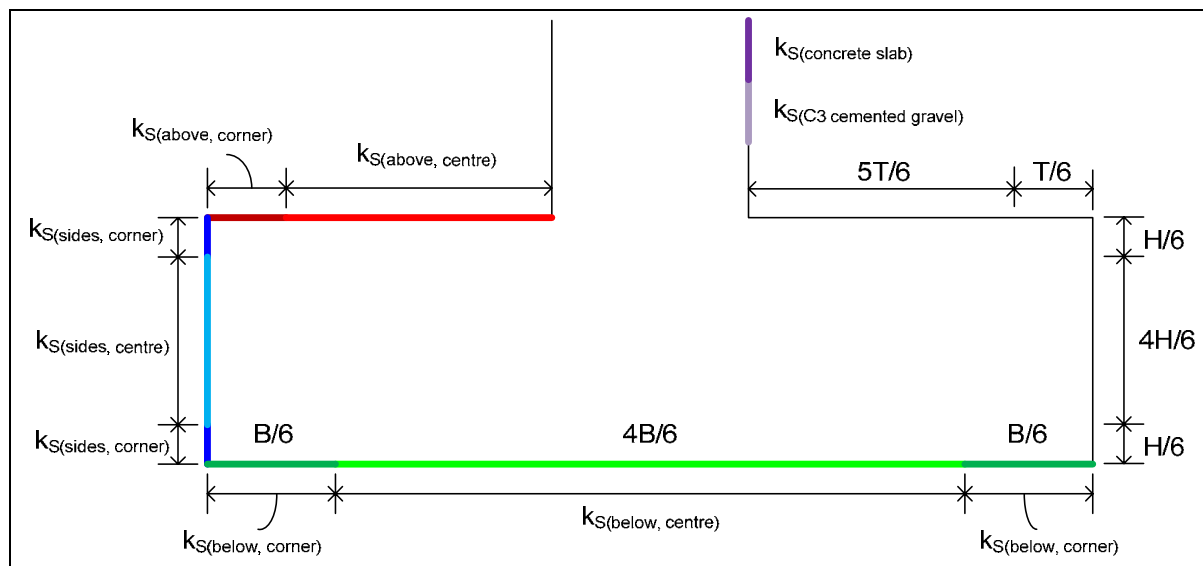
Figure 6.4: Layout of spring stiffness areas.

The stiffness values for the areas above, on the side and below the foundation are calculated using equations 6.1 and 6.2 and the values of the original subgrade combination are given in table 6.1. Note that these values are per cubic millimetre and they are multiplied by the

contact area they represent. Detailed calculations of these stiffness values are given in Appendix C.

Table 6.1: Stiffness values of springs connected to the foundation.

| k_S	Above	Sides	Below
Centre	9.2276 x10^5 N/mm^3	8.788 x10^4 N/mm^3	6.5793 x10^4 N/mm^3
Corners	1.1096 x10^6 N/mm^3	1.0568 x10^5 N/mm^3	7.9118 x10^4 N/mm^3

The stiffness values of the slab and C3 cemented gravel are calculated using equation 6.3. For areas with a sudden drop in horizontal displacement with an increase in distance from the source, a parameter γ which represents the rate of decrease of the displacement, the stiffness of that area can be increased by a factored γ (Badie, 1995). The factor γ can be determined using figure 6.5.
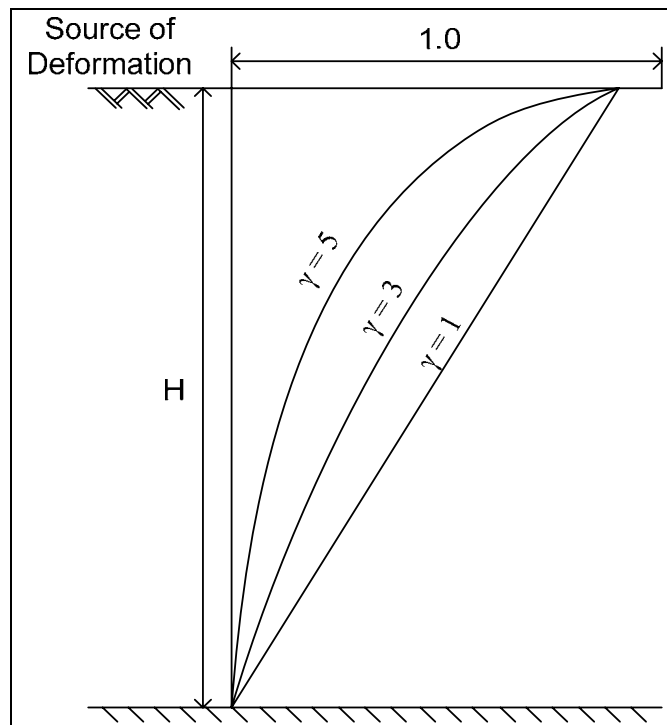
Figure 6.5: The rate of decrease γ of horizontal displacement (Badie, 1995).

Displacements are different for each combination of subgrade materials. Horizontal displacement decreases more rapidly for soils of a higher stiffness than for low stiffness soils. The parameter γ representing the rate of decrease will therefore be a higher value when C3 cemented gravel is present and lower in the case of in-situ clay. Judging from the deformation in the x-direction of the original subgrade combination, shown in figures 6.6 and 6.7 for the slab and C3 cemented gravel respectively, parameter value five is chosen for the slab a value of three for the cemented gravel layer. The final stiffness values of these layers for the original subgrade combination are given in table 6.2.
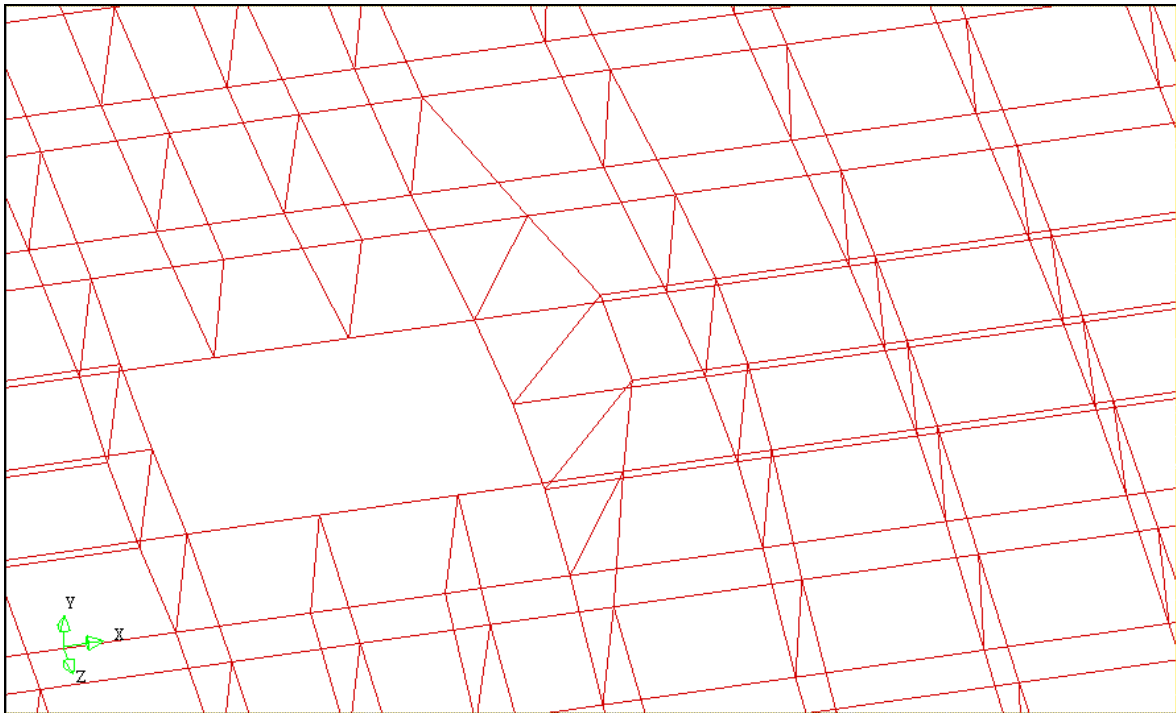
Figure 6.6: Deformed shape of the slab in the x-direction at a magnification factor of 1000.
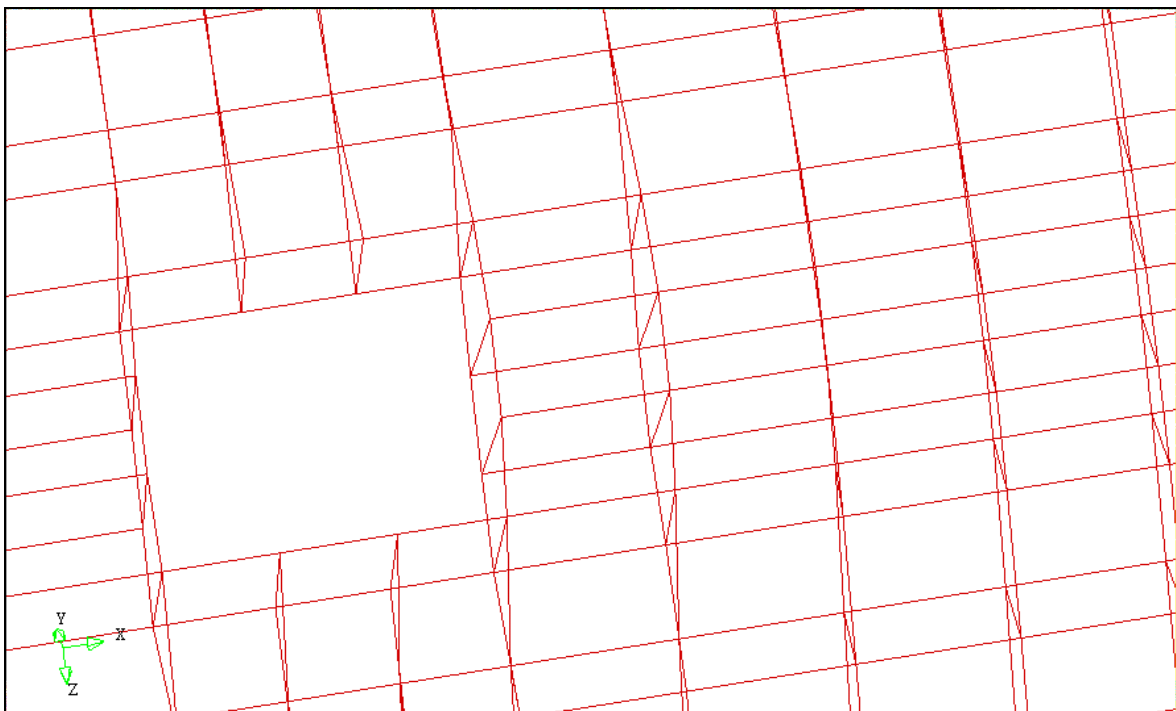
Figure 6.7: Deformed shape of the C3 cemented gravel in the x-direction at a magnification factor of 1000.

Table 6.2: Stiffness and parameter γ values of column support springs for the original model.

	Concrete Slab	C3 Cemented Gravel
γ	5	3
k_S	$2.133 \cdot 10^7$ N/mm	$8.531 \cdot 10^5$ N/mm

6.3   Modelling Strategies and Limitations of the Spring Model

To capture the behaviour of a foundation-soil system under loading patterns expressed in chapter one, a nonlinear spring is needed that has zero resistance in tension but will offer immediate resistance when the spring is compressed, even if the spring is at that point elongated past its original length. This material law is shown in figure 6.8.
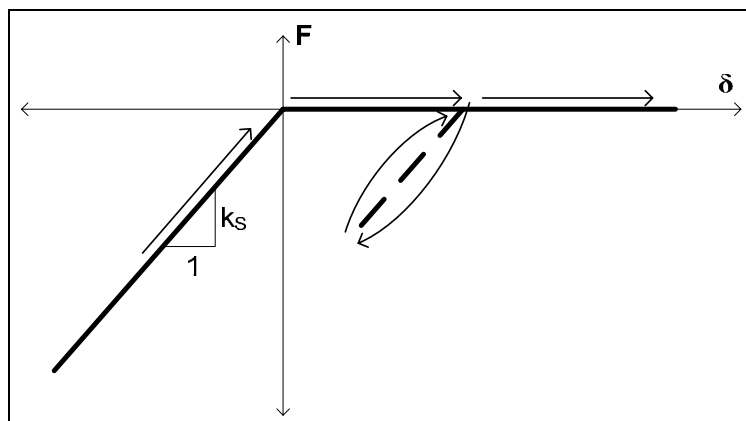
Figure 6.8: The displacement/force behaviour of a nonlinear spring.

This law is applicable when soils settle under the self weight of the structure, at first offering no resistance, but once the wind loads are applied, these soils do resist rotation. A linear spring is however not able to model this behaviour. As it is the aim of this study to model a foundation-soil system using the simplest method capable of yielding accurate results, and considering that many widely available analysis packages do not offer nonlinear springs, further investigations are done using linear springs only. This means though that springs will resist displacements whether in tension or compression. To overcome this liberal prevention of rotation, an initial analysis can indicate all springs in tension and their stiffness can be turned to zero in a second, more accurate analysis. The effect of a dead load elongating certain springs, which consequents zero stiffness, is still felt as some of these springs represent soil that offers resistance to rotation. In the absence of the dead load, purely rotating wind forces cause compression in areas that do in reality offer resistance and tension in areas that do not. This is in exception to the springs along the base of the foundation in the case of the heavy structure, and along the top of the foundation for the light structure.

It is therefore concluded that to predict the rotation of a foundation only the wind loads are applied to the model and springs in tension receive a zero stiffness value. In the case of a heavy structure all the springs along the base of the foundation retain their calculated stiffness values, as do the spring elements along the top of the foundation in the case of a light structure. The two-dimensional linear spring model is therefore unable to predict the vertical

and horizontal displacements of the foundation. The linear model is purely designed to deliver reliable values of foundation rotation. The user may use superposition to predict a complete rotation-translation pattern of the foundation. A spring model that can predict the effect of dead loads is however not investigated or assembled in this study.

6.4   Results

A two-dimensional linear spring model is assembled using stiffness values as calculated using equations 6.1 to 6.3. Five springs models are investigated. This includes models of a heavy and light structure loading pattern for the original subgrade combination, and a heavy loading pattern for the high stiffness, low stiffness and combination subgrade compositions described in chapter five. No investigations into the role of the foundation size are done in this chapter. Factors influencing rotation are discussed in chapter five. Here the two-dimensional linear spring model is verified.

6.4.1   DIANA Spring Model

The possibility to model a foundation-soil system using two-dimensional linear springs is confirmed here judging from the results obtain using the stiffness values prescribed and modelling strategies explained in the sections above. The results of the five models discussed above, are given in table 6.3 along with the rotations found for each similar model using continuum and interface elements. In all cases the spring models yield more conservative rotation figures than the continuum-interface element models. The spring model results are written as a percentage of the original results in table 6.3.

Table 6.3: Rotations obtained from the spring models and the percentage of the spring model in terms of the reference two-dimensional model.

Rotation (Degrees)	Original Stiffness		High Stiffness	Combined Stiffness	Low Stiffness
	Heavy Structure	Light Structure			
2D Model	3.66×10^{-03}	3.72×10^{-03}	4.77×10^{-4}	2.34×10^{-3}	1.5×10^{-2}
Spring Model	4.57×10^{-03}	4.20×10^{-03}	5.10×10^{-4}	2.61×10^{-3}	1.78×10^{-2}
% of Reference Result	124	113	107	117	119

The deformation pattern of the foundation for the heavy structure of the spring model, shown in figure 6.9, closely resembles that found in figure 4.8 where the delamination of the

interface elements for phase three is shown. In the case of phased analysis, the dead loads did not leave a convex bending pattern on the foundation as in figure 4.12 as a result of the chosen boundary conditions for the phased analysis. The absence of a dead load in the spring model therefore gives a similar deformation outline. The deformation of the light structure spring model resembles the delaminated interface elements in figure 4.15 and is shown in figure 6.10.

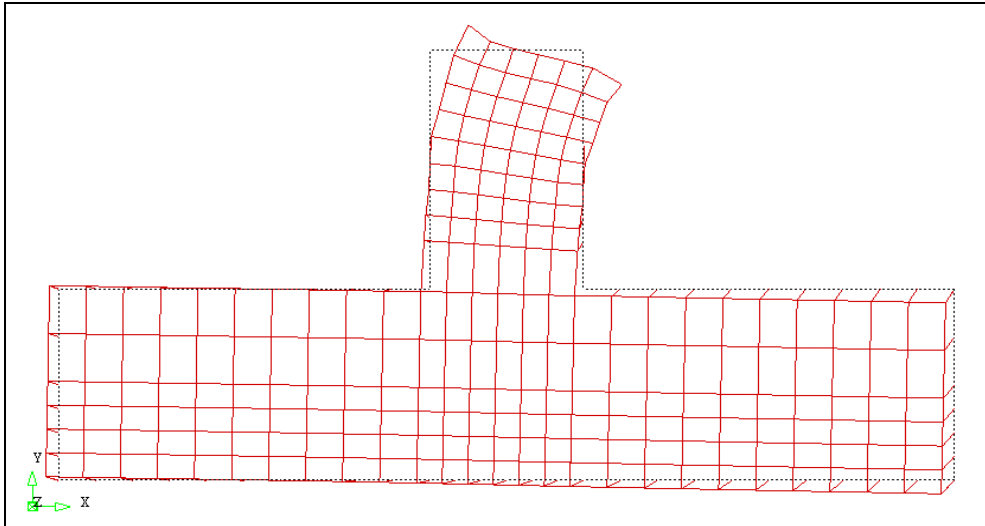*Figure 6.9: The deformed shape of the heavy structure spring model at a magnification factor of 500.*
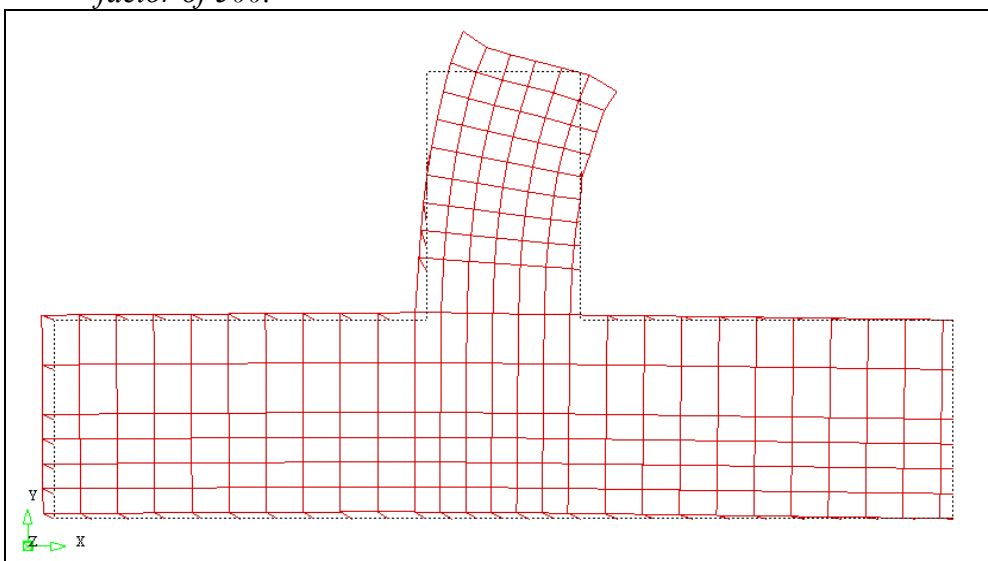
Figure 6.10: The deformed shape of the light structure spring model at a magnification factor of 500.

6.4.2   PROKON Spring Model

The results found in DIANA are confirmed using software available in most engineering offices. A well known design and structural analysis package, namely PROKON, is used for this purpose.

A two-dimensional spring model is assembled using stiffness values for the original subgrade combination and the loading pattern of the heavy structure is applied to the model. All dimensions, material properties, load and stiffness values remain as they are for the DIANA models. The two-dimensional spring model is shown in figure 6.11.
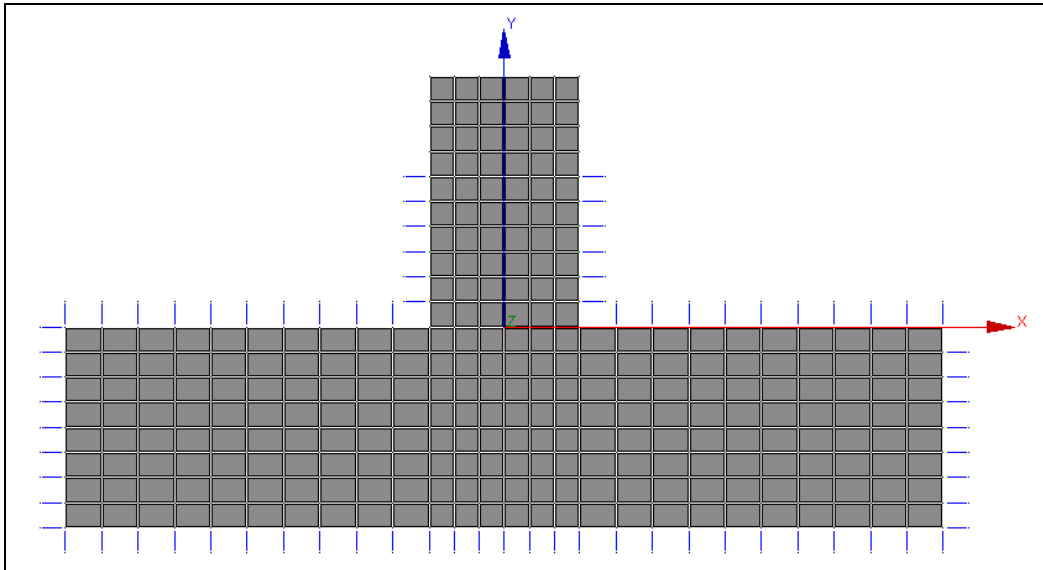
Figure 6.11: The two-dimensional spring model assembled in PROKON.

As for the DIANA spring models, the stiffness of springs in tension is turned to zero after an initial trial analysis. The deformation pattern closely resembles that of the DIANA model shown in figure 6.9. The rotation value differs by a percentage and is accounted to the larger number of elements used in the PROKON model. The PROKON model therefore gives a rotation value 123 percent of that obtained from the continuum-interface element model.
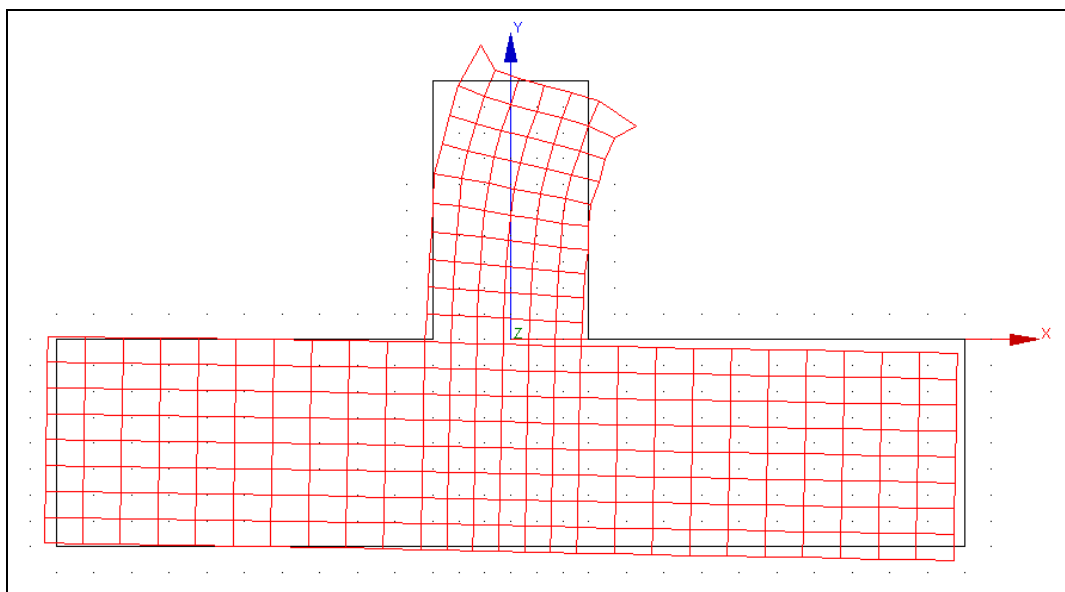
Figure 6.12: The deformed shape of the PROKON spring model at a magnification factor of 200.

6.5   Conclusion

Under the application of only the wind loads and by following the modelling strategies described in the sections above, two-dimensional linear spring models can offer a simple modelling approach to obtain reasonably accurate rotation predictions. The stiffness values obtained from equation 6.1 to 6.3 resemble the present soil masses with enough accuracy to obtain realistic results from an analysis testing for foundation rotation. A two-dimensional linear spring model can be assembled using a widely available structural analysis package, such as PROKON, with reasonable accuracy. A simple alternative to complex nonlinear analyses is available to predict the rotation of foundations provided the user is certain the bearing capacities of the subgrades are not exceeded.

7. CONCLUSIONS AND RECOMMENDATIONS

The aim of this research is to use comprehensive numerical investigations to predict and detail the behaviour of large foundations under loading and the interaction with its soil surroundings. The case study used in this study and the alterations made to the structure in further investigations are concluded to be relevant and the results useful to common engineering practice. The software used for the nonlinear finite element analysis, namely DIANA, proved adequate to simulate nonlinear material behaviour. The outcomes of this study and conclusions drawn are described in this chapter along with several recommendations made to the user.

7.1 Finite Element Modelling Strategies

Material properties and foundation size can be used to determine adequate finite element model boundaries. If the user finds that the bearing capacity of the subgrade defined by the model is exceeded, the use of nonlinear soil models is recommended. The model boundaries must also be reconsidered according to the type of failure event, such as the possible development of a slip-plane. In this study the bearing capacities of the subgrade materials are never exceeded except when several times the load factor is applied to a subgrade compilation of exceptionally low stiffness.

A reduction in mesh size can reduce analysis times tenfold without a significant loss in accuracy, if the reduction process is considered carefully. Elements in areas of less interest can have a side length to side length aspect ratio of 1:4 while regions more closely scrutinized retain elements closer to a 1:1 side ratio. The reduction in analysis time from the fine to very coarse mesh investigated in this study is apparent for the three-dimensional models, and especially so when converting from three- to two-dimensional models. It is recommended to the user to plan the finite element mesh carefully before undertaking complex analyses. The design of an efficient mesh layout can repay the user several times over if many analyses are planned.

The reduction in load step sizes and the use of arc-length control may lead to faster convergence in complex models. Tolerances can also be increased if convergence failure

reoccurs, but it is suggested that this action be cautiously used as too great a decrease in tolerance values may lead to inaccurate solutions.

7.2　　　Interface Material Law

The software used in this study, DIANA, offers the user several possible approaches to define the concrete-soil interface material law. Of the three models investigated in this study, the multi-surface plasticity interface model which combines material behaviours in crushing, shearing and cracking states is considered the most accurate representation of actual occurrences along this contact surface. The physical interaction between separation and shearing resistance is considered in the friction model. This model does however define a simplified post-peak tensile behaviour as this interface is considered to be brittle resulting in an abrupt loss of tensile strength. The simplest of the three models, the nonlinear elastic model, does not consider friction resulting from pressure, or coupling between de-lamination and shearing resistance. The differences between these interface models are apparent when comparing the results under the application of each to a single case study. The user is recommended to consider which interface model best defines the material law at hand before assigning one or the other. Each interface element is unique and will describe the same physical behaviour of a structure in different ways. However, for concrete footing-soil interaction along interfaces as considered in this study, pressure dependence, included in the crushing, shearing, cracking model as well as the friction model, is essential. In this particular series of analyses the incorporation of accurate tensile softening or coupling between shear and cracking does not have significant influence on the global results. Thus, the most convenient of these two mentioned models may be chosen by the analyst.

7.3　　　The Computational Response of the Foundation-Soil System

The rotation of the foundation is of particular interest in this study. In this case study tall columns are present making large lateral displacements at the top of the column possible as a result of a small foundation rotation.

It is possible to assemble a two-dimensional model that corresponds closely with the displacement values of an accurate three-dimensional model. A method by which to include

the presence of the volume and stiffness of otherwise omitted soil and slab masses, has been developed and is deemed successful. This conversion method enables the user to model nonlinear interactions between the soil and concrete materials far more economically than when using the three-dimensional alternative. This is as a result of a reduction in both assembly and analysis times.

It is found through the use of phased analysis that the uniform settlement of soils prior to the application of wind loads or after, does not influence foundation rotation. The subgrade found in the case study is sufficient to carry the foundation in excess of twelve times the ultimate limit load and at no point is the stability of the structure threatened. Of course, if orthogonal wind loads must be considered, three-dimensional modelling may be required. However, for design purposes it may be sufficient to evaluate the responses in one-direction at a time and select appropriate footing dimensions and/or subgrade and cemented layer layouts to prevent excessive slab rotation. It must be born in mind that, due to nonlinear behaviour (delamination and slip) these responses may not be superposed. This means that, a conservative approach will be required, or else a full three-dimensional modelling must be performed.

7.4   Generalization of the Case Study

It is concluded from investigations carried out that some factors can greatly influence the behaviour of the structure and others do not.

Variations in the stiffness of the subgrade materials and the size of the foundation can have significant impacts on the foundation response to ultimate loading. Less rotation occurs in subgrade materials of a higher stiffness than in materials of a lower stiffness. Increasing the size of the foundation has the same effect on the behaviour of the foundation. A large foundation rotates less than a small one under the same loading. Combining these factors gives the user a range of alternatives to ensure structural stability. The user might find that designing a larger foundation will offer sufficient stability and expensive soil-works and compactions will not be necessary to prevent rotations. The user might also find that a smaller foundation is adequate for his/her current subgrade compilation.

Realistically lower grades of concrete for the slab will not noticeably effect the rotation of the foundation, but a slab must be present to prevent overturning of the column. The user must take note of the forces acting on the column at the level of the slab. If crushing of the column or slab may occur at this level it is the responsibility of the designers to take adequate action to prevent this phenomenon.

The sensible use of expansion joints in close vicinity of the column or movement joints to allow free movement of slab segments, will not cause a significant increase of the rotation of the foundation. The user should however confirm the design of these joints if they differ significantly from those investigated in this study. In addition, it is also the responsibility of the designer to prevent the uplifting of the foundation under wind loads, provided sufficient shearing capacity to prevent the forming of hinges in the structure, and to be sure that the foundation is stable against toppling over.

7.5 The Use of Spring Elements

The user is able to predict foundation rotations with reasonable accuracy when following the modelling strategies described by the author. The method suggested includes soil properties, the composition of the subgrade structure, the dimensions of the foundation and the depth of the foundation below the surface. It is possible to attain these results using a widely available structural analysis package, such as PROKON, to assemble a two-dimensional linear spring model. The user is therefore provided with a simple alternative to complex nonlinear analyses to predict the rotation of foundations provided the bearing capacities of the subgrades are not exceeded.

A possible extension of the simplified modelling strategy is to allow full three-dimensional analysis when orthogonal loads and moments act simultaneously. The same principles as applied in the case of the two-dimensional model will prevail, but three-dimensional modelling of the footing, and three-dimensional arrangement of springs representing soil structure interaction will be required. This falls beyond the scope of the current study, but may be confirmed in a follow-up study.

REFERENCES

BAŽANT, Z.P. (1998) *Fracture and Size Effect in Concrete and Other Quasibrittle Materials*, CRC Press, New York.

BADIE, S.S. (1995). *Computers & Structures, 65(2), pp. 213-224*. Elsevier Science Ltd.

BOWELS, J.E. (1996). *Foundation Analysis and Design, Fifth Edition*. The McGraw-Hill Companies, Inc.

COOK, R.D. (2002). *Concepts and Applications of Finite Element Analysis.* John Wiley & Sons, Inc.

CRAIG, R.F. (2004). *Craig's Soil Mechanics, Seventh Edition*, Spon Press, London and New York.

DIANA. (2008). *Diana Finite Element Software Version 9.3.* TNO Diana BV, www.tnodiana.com

HQUSACE. (1998). *Seismic Design for Buildings, Report TI 809-04.* The U.S. Army Corps of Engineers, Huntsville Engineering and Support Centre.

LOURENSCO, P. B., AND ROTS, J. G. (1997). *J. Struct. Eng., ASCE 123*, 7 pp. 660-668. A multi-surface interface model for the analysis of masonry structures.

PROKON. (2007). *Prokon Finite Element Software Version W2.2.11*, Prokon Software Consultants, www.prokon.com

ROSOCHACKI, S. (2007). *Finite Element Modeling & Analysis of Fixed Foundations for Slender Reinforced Concrete Columns*. Paper presented in partial fulfilment of the requirements for the degree of Bachelor of Civil Engineering at the University of Stellenbosch.

SCOTT, C.R. (1980). *An Introduction to Soil Mechanics and Foundations, Third Edition*, Applied Science Publishers LTD, London.

TRH 4 (1996). *Structural Design Of Flexible Pavements For Interurban And Rural Roads* – Department of Transport, South Africa.

WALRAVEN, J. C. AND REINHARDT, H. W. (1981). *Heron 26*, *1(a), pp. 5-68*. Theory and experiments on the mechanical behaviour of cracks in plain and reinforced concrete subjected to shear loading.

APPENDIX A

As discussed in chapter four, the primary areas of interest lie with the rotational behaviour of the foundation and the materials directly surrounding it. It can therefore be said that the deformation of the interface model needs to be considered in conjunction with the rotation of the foundation. As results can be produced rapidly in two-dimensional analyses, the comparison of results between the mesh density alternatives is done with the use of the two-dimensional models only. This is justified in chapter two.

The maximum and minimum displacements of the interface, slab, C3 cemented gravel, column and foundation elements are measured. In addition, displacements in focal areas are measured and the rotation of the foundation is calculated. This is done for all the mesh densities at increasing load steps for the original and high stiffness subgrade combinations (as described in chapter five). The weighted average of these measured points and rotations is used to determine a percentage of deviation between results. These are the results given in figures 2.22 and 2.23. Figure A.1 details the points in focal areas that are used to determine the weighted average. These points are indicated on the deformed column and foundation of the fine mesh. These nodes occur in all the mesh density layouts and are therefore good reference points. The effect of column rotation and the reason for the importance of this effect is discussed in section 4.1.
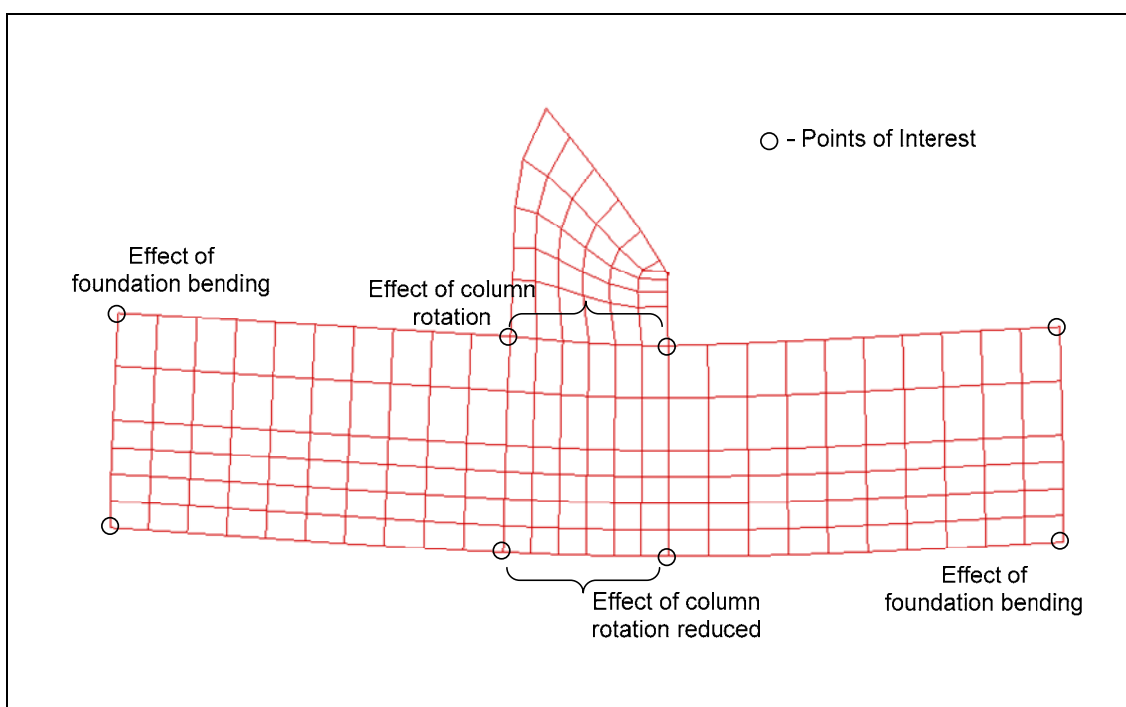

Figure A.1: Areas of interest in determining the average percentage of deviation between mesh densities.

Small differences are found between the results of the various mesh densities. Their deformation patterns are also very similar, as can be seen in figure A.2 where the interface delamination of each mesh is shown for one times the ultimate load at a magnification factor of 250. These differences are however significant enough to cause possible concern in later investigations at several times the ultimate load. The most conservative of the mesh densities, the fine mesh, is therefore used in further investigations. For two-dimensional analyses the increase in analysis time is small and trivial in comparison with the reassurance the user receives from a more accurate solution.
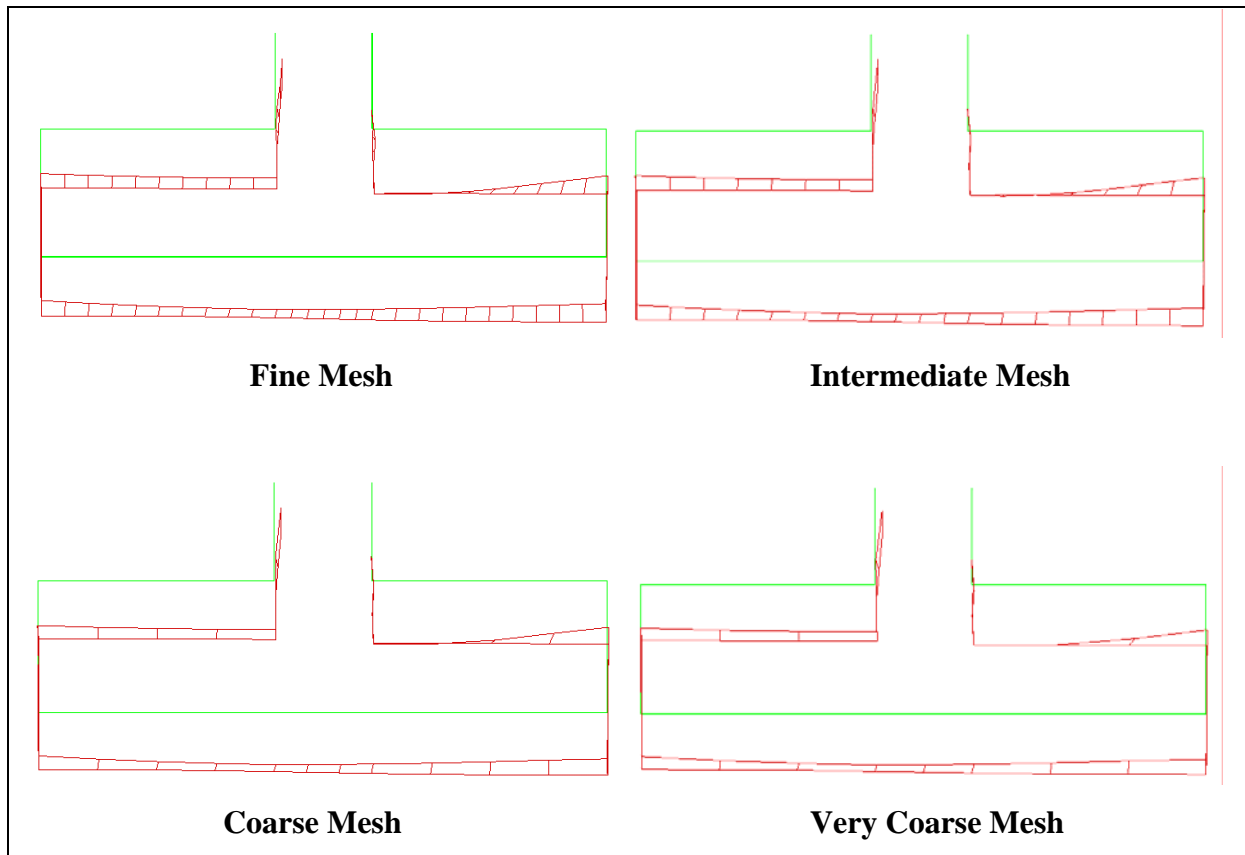

Fine Mesh　　　　　　**Intermediate Mesh**

Coarse Mesh　　　　　　**Very Coarse Mesh**

Figure A.2: The interface delamination of each mesh at one times the ultimate load at a magnification factor of 250.

APPENDIX B

The amount of rotation for each foundation size at one times the ultimate wind load is plotted in figures B.1, B.3 and B.5 below for the various subgrade combinations. Figures B.2, B.4 and B.6 show the rotation versus factor of ultimate limit loading plots for these subgrade combinations.
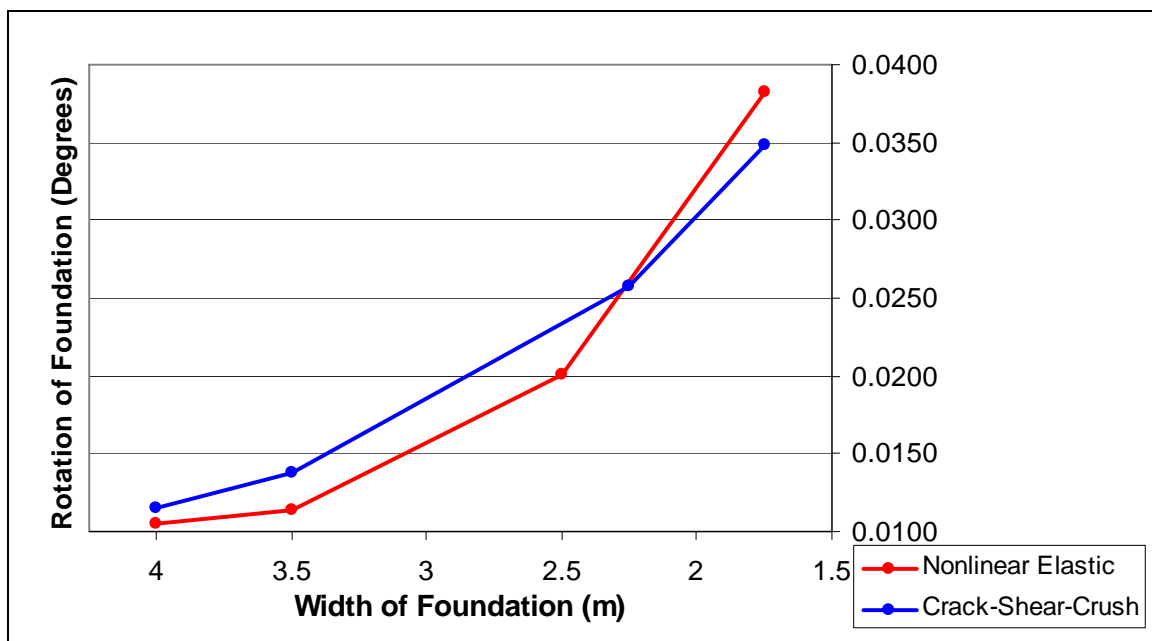
B.1 Plots for the Low Stiffness Subgrade Compilation

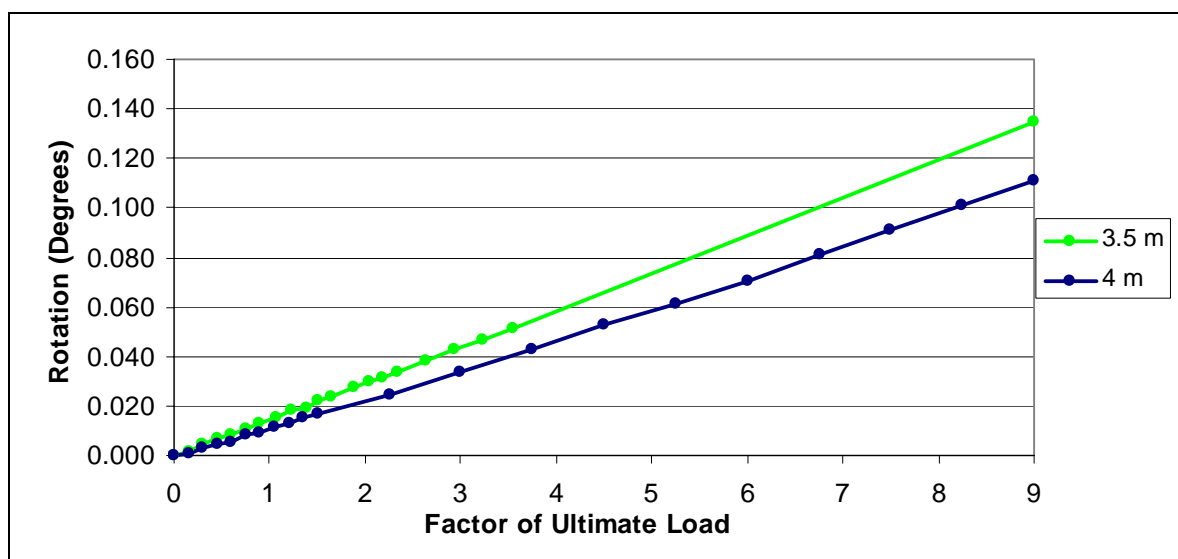*Figure B.1: Rotation of various foundation sizes for two interface elements (low stiffness).*

Figure B.2: Rotation versus ultimate load factor for a variation of foundation widths (low stiffness).

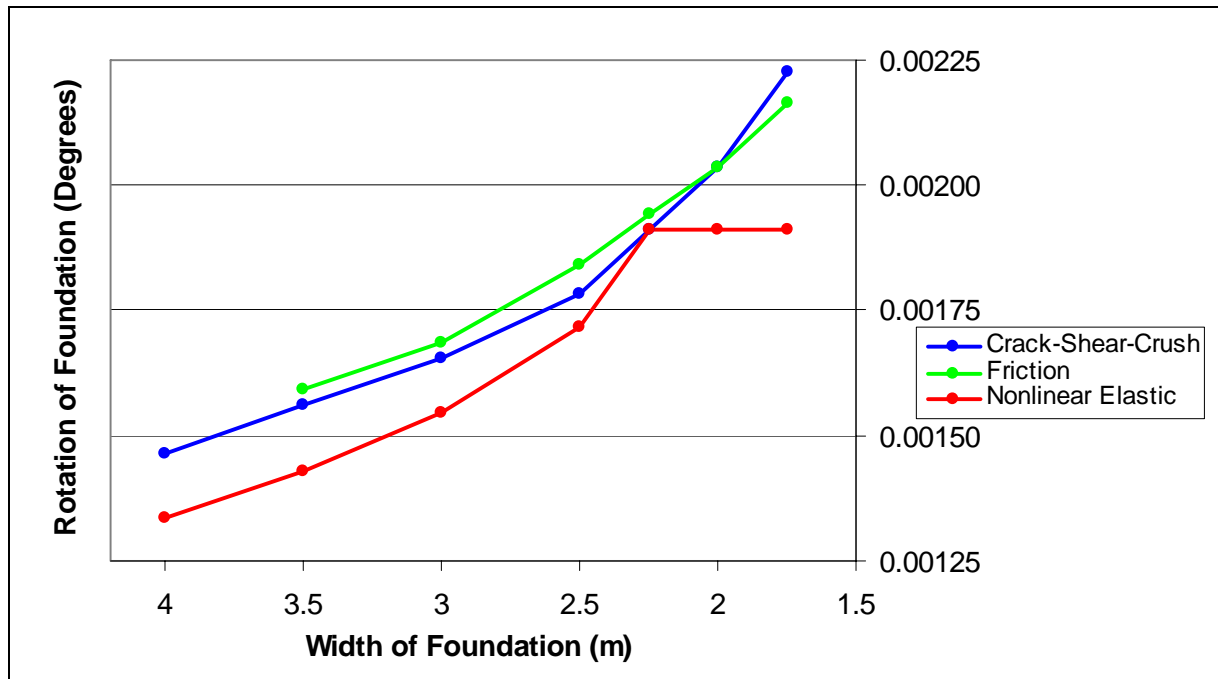## B.2   Plots for the Combined Stiffness Subgrade Compilation

Figure B.3: Rotation of various foundation sizes for all three interface elements (combination stiffness).
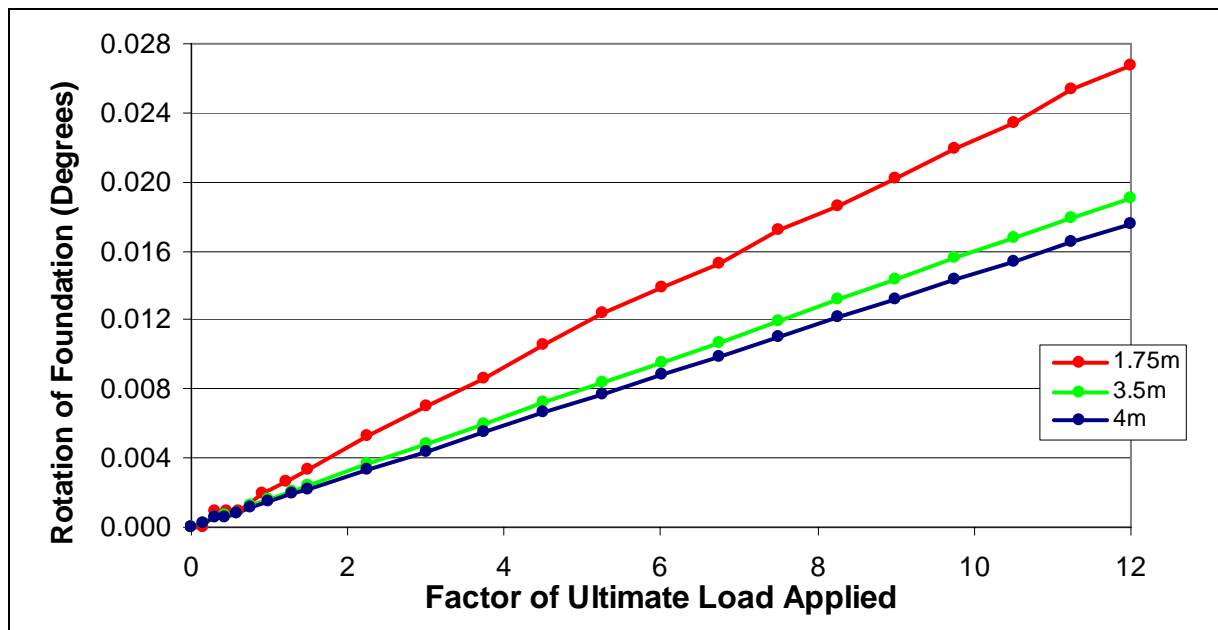

Figure B.4: Rotation versus ultimate load factor for a variation of foundation widths (combination stiffness).

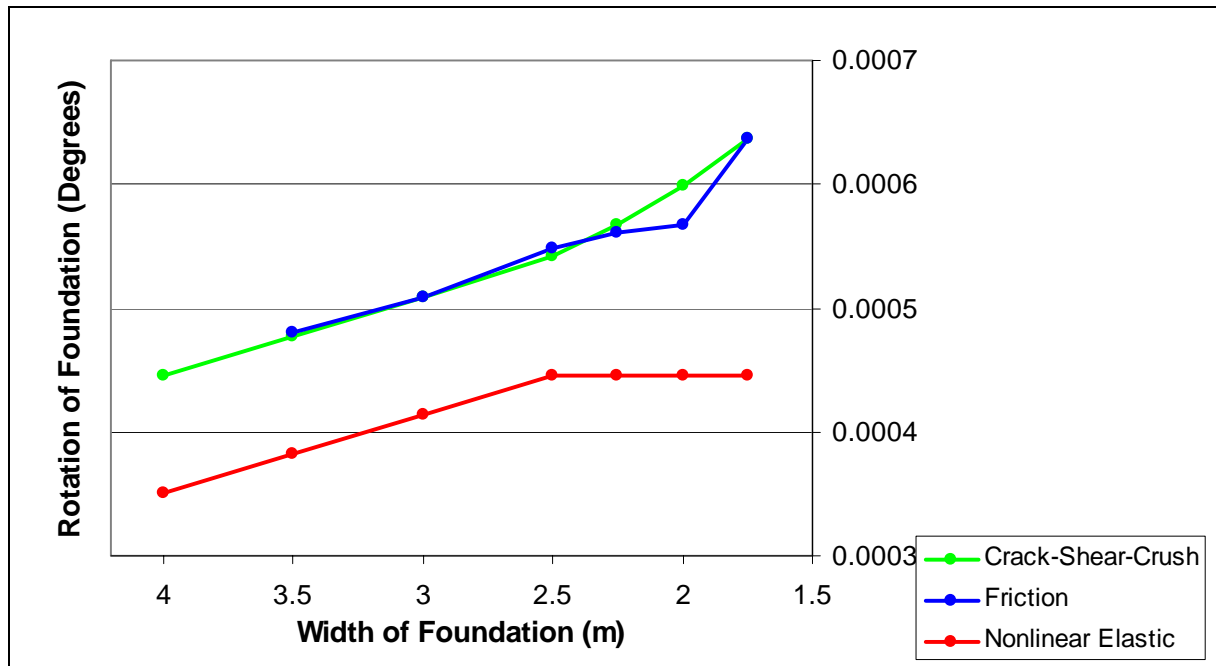## B.3   Plots for the High Stiffness Subgrade Compilation

Figure B.5: Rotation of various foundation sizes for all three interface elements (high stiffness).
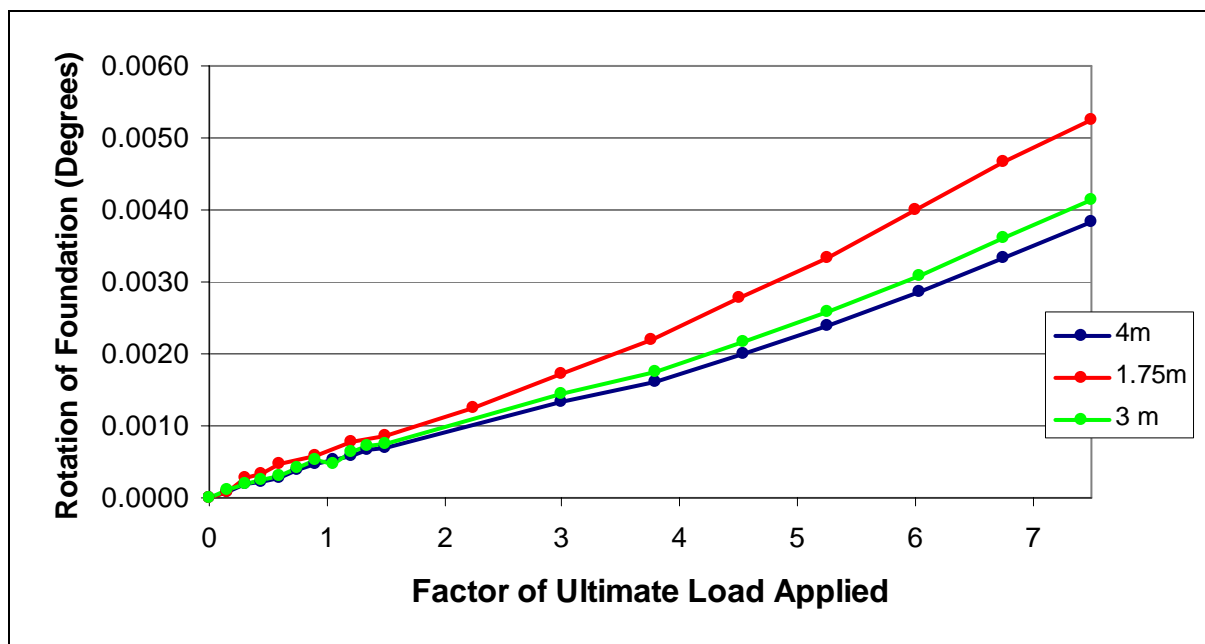

Figure B.6: Rotation versus ultimate load factor for a variation of foundation widths (high stiffness).

APPENDIX C

The stiffness of the springs used in the DIANA and PROKON two-dimensional models for the original subgrade combination, is calculated as follows using the equations discussed in chapter six:

$$k_s = \frac{1}{B E_S' I_S I_F}$$

6.1

B = 3.5 m

Determining E_S

$E_{S1} = 2000$ MPa $H_1 = 0.2$ m

$E_{S2} = 100$ MPa $H_2 = 1$ m above; $H_2 = 1.8$ m below

$E_{S3} = 10$ MPa $H_3 = 1.5 \cdot 3.5 - 1.8 = 3.45$ m

Above foundation:

$\therefore \; E_{S,avg} = \dfrac{0.2 \cdot 2000 + 0.2 \cdot 100}{0.4} \;=\; \mathbf{1050}$ MPa   (The slab excluded in resistance to rotation)

Sides of foundation:

$E_S = \mathbf{100}$ MPa

Below foundation (using equation 6.2):

$E_S = \dfrac{100(1.0 + 0.9 + 0.8 + 0.7 + 0.6) + 10(0.5 + 0.4 + 0.3 + 0.2 + 0.1 + 0.05)}{(1.0 + 0.9 + 0.8 + 0.7 + 0.6 + 0.5 + 0.4 + 0.3 + 0.2 + 0.1 + 0.05)} \;=\; \mathbf{74.865}$ MPa

$\therefore E_{S(above)}' = \dfrac{(1 - 0.35^2)}{1050} = \mathbf{8.3571 \cdot 10^{-4}}$

$E_{S(sides)}' = \dfrac{(1 - 0.35^2)}{100} = \mathbf{8.775 \cdot 10^{-3}}$

$E_{S(below)}' = \dfrac{(1 - 0.35^2)}{74.865} = \mathbf{1.1721 \cdot 10^{-2}}$

Elsje S. Fraser   University of Stellenbosch

Determining I_S

$$B = 3.5 \text{ m} \qquad L = 3.5 \text{ m} \qquad H = 3.25B$$

For centres:

$$N = \frac{3.25B}{B/2} = 6.5 \qquad M = \frac{L/2}{B/2} = 1$$

$$\therefore I_1 = 0.464$$

$$I_2 = 0.024$$

$$\therefore I_S = 0.464 + \frac{1 - 2 \cdot 0.35}{1 - 0.35} \cdot 0.024 \quad = \quad \mathbf{0.475}$$

For corners:

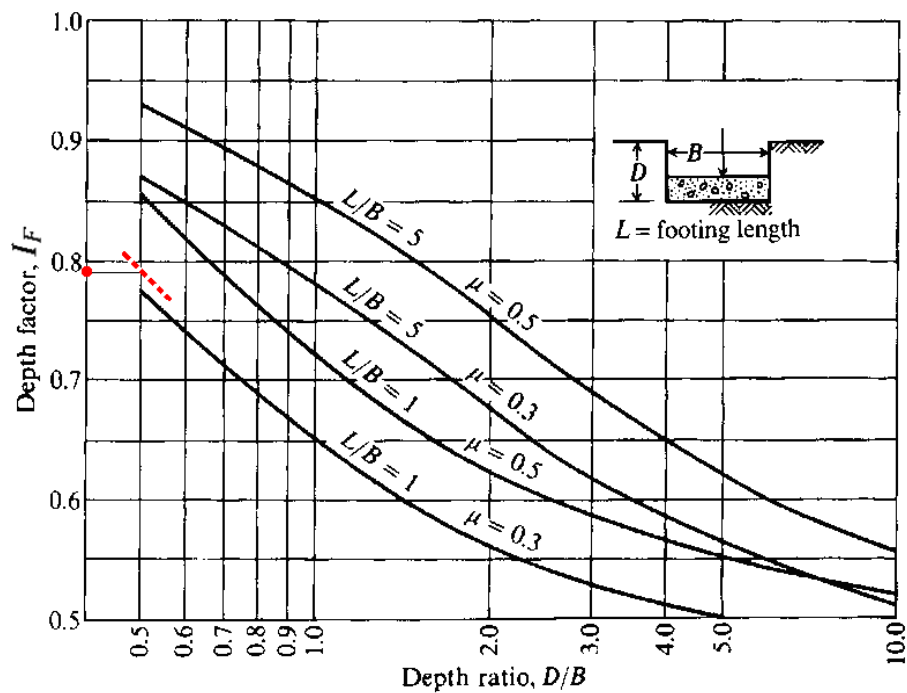$$N = \frac{3.25B}{B} = 3.25 \qquad M = \frac{L}{B} = 1$$

$$\therefore I_1 = 0.37425$$

$$I_2 = 0.04525$$

$$\therefore I_S = 0.37425 + \frac{1 - 2 \cdot 0.35}{1 - 0.35} \cdot 0.04525 \quad = \quad \mathbf{0.395}$$

Determining I_F

$$B = 3.5 \text{ m} \qquad L = 3.5 \text{ m} \qquad H = 1.4 \text{ m} \qquad \mu = 0.35$$

$$\therefore D/B = 1.4/3.5 = \mathbf{0.4} \qquad L/B = \mathbf{1}$$

So from the figure above, $I_F = \mathbf{0.78}$

Now, using the variables above, the stiffness of springs of each area is given as follows:

$$k_{S(above,\,centre)} = \frac{1}{3.5 \cdot 8.3571 \cdot 10^{-4} \cdot 0.475 \cdot 0.78} \quad = \quad \textbf{922.76 MN/m}^{3}$$

$$k_{S(above,\,corner)} = \frac{1}{3.5 \cdot 8.3571 \cdot 10^{-4} \cdot 0.395 \cdot 0.78} \quad = \quad \textbf{1109.64 MN/m}^{3}$$

$$k_{S(sides,\,centrer)} = \frac{1}{3.5 \cdot 8.775 \cdot 10^{-3} \cdot 0.475 \cdot 0.78} \quad = \quad \textbf{87.88 MN/m}^{3}$$

$$k_{S(sides,\,corner)} = \frac{1}{3.5 \cdot 8.775 \cdot 10^{-3} \cdot 0.395 \cdot 0.78} \quad = \quad \textbf{105.68 MN/m}^{3}$$

$$k_{S(below,\,centre)} = \frac{1}{3.5 \cdot 1.7121 \cdot 10^{-2} \cdot 0.475 \cdot 0.78} \quad = \quad \textbf{65.793 MN/m}^{3}$$

$$k_{S(below,\,corner)} = \frac{1}{3.5 \cdot 1.7121 \cdot 10^{-2} \cdot 0.395 \cdot 0.78} \quad = \quad \textbf{79.118 MN/m}^{3}$$

These values are multiplied by the amount of surface area of soil that comes into contact with the foundation that each individual spring represents.

The springs supporting the column are calculated as follows using equation 6.3:

$$k = \frac{2dE\,\tan\,\theta}{\ln\left(1 + \dfrac{2b}{a}\,\tan\,\theta\right)} \qquad \qquad 6.3$$

$$\text{for} \quad \theta = 45°:$$

$$k_{slab} = \frac{2 \cdot 0.2 \cdot 30000 \cdot \tan 45}{\ln\left(1 + \dfrac{2 \cdot 4.7}{0.6}\tan 45\right)} \quad = 4265.3\,\textbf{MN/m}$$

$$k_{C3\,Cemented\,Gravel} = \frac{2 \cdot 0.2 \cdot 2000 \cdot \tan 45}{\ln\left(1 + \dfrac{2 \cdot 4.7}{0.6}\tan 45\right)} \quad = 284.35\,\textbf{MN/m}$$